

BEST AVAILABLE COPY

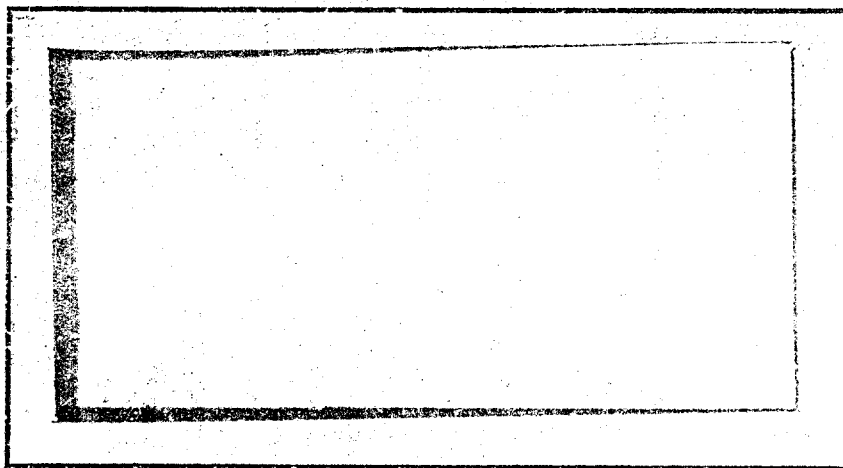
AD A 0 4 8 8 9 8

# AIR FORCE INSTITUTE OF TECHNOLOGY



AIR UNIVERSITY  
UNITED STATES AIR FORCE

AD NO. \_\_\_\_\_  
DDC FILE COPY



DDC  
PERMITTEE  
JAN 23 1976  
RECEIVED

## SCHOOL OF ENGINEERING

WRIGHT-PATTERSON AIR FORCE BASE, OHIO

DISTRIBUTION STATEMENT A  
Approved for public release;  
Distribution Unlimited

12

D D C  
RECEIVED  
JAN 23 1976  
LIBRARY

9 Master's thesis,

8 AN AERODYNAMIC INVESTIGATION OF A  
FORWARD SWEEP WING.

14 AFIT/GAE/AA/77D-14 THESIS 10 Kenneth L. Sims  
Captain USAF

11 Dec 77

12 115 p.

Approved for public release; distribution unlimited.

012 225

JB

AFIT/GAE/AA/77D-14

AN AERODYNAMIC INVESTIGATION OF A  
FORWARD SWEPT WING

THESIS

Presented to the Faculty of the School of Engineering  
of the Air Force Institute of Technology  
Air University  
In Partial Fulfillment of the  
Requirements for the Degree of  
Master of Science

By

Kenneth L. Sims, B.S.

Captain USAF

Graduate Aeronautical Engineering

December 1977

SEARCHED for	INDEXED	FILED
W	90	
1977		
DISTRIBUTION/AVAILABILITY STATEMENTS		
A		

Approved for public release; distribution unlimited.

## Preface

The purpose of this study was to experimentally and analytically determine certain aerodynamic characteristics of a recently proposed high subsonic, forward swept wing, with a new supercritical airfoil section. It was my intention to evaluate the effectiveness of this section and to compare the aerodynamic characteristics of a forward swept wing to a similar aft swept wing. The root chord, tip chord, wing span, and wing area was held constant for each wing.

I wish to thank my thesis advisor, Major Steve Koob, of the Aeronautical Engineering Department of the United States Air Force Institute of Technology. Without his able assistance, this study would not have been possible.

I am particularly grateful to Major Roger A. Crawford, for his guidance and encouragement during the early stages of this study.

I wish also to acknowledge the outstanding craftsmanship of Mr. Russ Murry, Mr. Jack Tiffany, and Mr. John Brohas, of the AFIT Model Fabrication Division, for the superb model which they produced. I must also thank Dr. Tom Weeks of the External Aerodynamics Branch of the Air Force Flight Dynamics Laboratory for his technical advice and support throughout this study.

Finally, I wish to thank my wife, Mary, and my two

sons, Kerry and Keith, for tolerating me in my moments of despair while accomplishing this research effort.

Kenneth L. Sims

TABLE OF CONTENTS

	Page
Preface . . . . .	ii
List of Figures . . . . .	vi
List of Tables . . . . .	ix
List of Symbols . . . . .	x
Abstract . . . . .	xii
I. Introduction . . . . .	1
Background . . . . .	1
Problem . . . . .	1
Scope . . . . .	4
Approach . . . . .	4
Materials and Equipment . . . . .	5
II. Facility and Model Description . . . . .	6
Facility Used For Testing . . . . .	6
Models Tested . . . . .	9
III. Experimental Procedures . . . . .	13
Force Measurements . . . . .	13
Test Procedures . . . . .	14
IV. Analytical Procedures . . . . .	16
Woodward's USS Aero Program . . . . .	16
V. Results . . . . .	21
Lift . . . . .	21
Drag . . . . .	25
Pitching Moment . . . . .	30
Predictions . . . . .	36
Pressure Distribution . . . . .	49
Oil Visualization . . . . .	49
VI. Conclusions and Recommendations . . . . .	58
Conclusions . . . . .	58
Recommendations . . . . .	59

	Page
Bibliography . . . . .	61
Appendix A: Model Stress Analysis . . . . .	63
Appendix B: Aerodynamic Characteristics Presented in Graphical Form . . . . .	73
Vita . . . . .	99

## LIST OF FIGURES

Figure		Page
1	Schematic of Aft Swept Model . . . . .	2
2	Schematic of Forward Swept Model . . . . .	3
3	Aft Swept Model used for Wind Tunnel Test. .	10
4	Forward Swept Model used for Wind Tunnel Test . . . . .	10
5	Aft Swept Model used for USS Aero Prediction Program . . . . .	17
6	Forward Swept Model used for USS Aero Prediction Program . . . . .	18
7	Wind Axis Coordinate used for Aerodynamic Coefficients . . . . .	22
8	$C_L$ vs $\alpha$ for $M = 0.63$ . . . . .	23
9	$C_L$ vs $\alpha$ for $M = 0.93$ . . . . .	24
10	$C_D$ vs $\alpha$ for $M = 0.63$ . . . . .	26
11	$C_D$ vs $\alpha$ for $M = 0.93$ . . . . .	27
12	$C_D$ vs $C_L$ for $M = 0.63$ . . . . .	28
13	$C_D$ vs $C_L$ for $M = 0.93$ . . . . .	29
14	$L/D$ vs $\alpha$ for $M = 0.63$ . . . . .	31
15	$L/D$ vs $\alpha$ for $M = 0.93$ . . . . .	32
16	$C_D$ vs Mach at Constant $C_L = 0.25, 0.50, 0.75$ .	33
17	$C_M$ vs $\alpha$ for $M = 0.63$ . . . . .	34
18	$C_M$ vs $\alpha$ for $M = 0.93$ . . . . .	35
19	Theoretical $C_L$ vs $\alpha$ for the Forward Swept Model at $M = 0.7$ . . . . .	37
20	Theoretical $C_L$ vs $\alpha$ for the Forward Swept Model at $M = 0.8$ . . . . .	38
21	Theoretical $C_L$ vs $\alpha$ for the Forward Swept Model at $M = 0.9$ . . . . .	39



Figure	Page
22 Theoretical $C_D$ vs $\alpha$ for the Forward Swept Model at $M = 0.7$ . . . . .	40
23 Theoretical $C_D$ vs $\alpha$ for the Forward Swept Model at $M = 0.8$ . . . . .	41
24 Theoretical $C_D$ vs $\alpha$ for the Forward Swept Model at $M = 0.9$ . . . . .	42
25 Theoretical $C_L$ vs $\alpha$ for the Aft Swept Model at $M = 0.7$ . . . . .	43
26 Theoretical $C_L$ vs $\alpha$ for the Aft Swept Model at $M = 0.8$ . . . . .	44
27 Theoretical $C_L$ vs $\alpha$ for the Aft Swept Model at $M = 0.9$ . . . . .	45
28 Theoretical $C_D$ vs $\alpha$ for the Aft Swept Model at $M = 0.7$ . . . . .	46
29 Theoretical $C_D$ vs $\alpha$ for the Aft Swept Model at $M = 0.8$ . . . . .	47
30 Theoretical $C_D$ vs $\alpha$ for the Aft Swept Model at $M = 0.9$ . . . . .	48
31 $C_D$ vs $X/C$ for the Forward Swept Model at $M = 0.63$ . . . . .	50
32 $C_D$ vs $X/C$ for the Aft Swept Model at $M = 0.63$ . . . . .	51
33 $C_D$ vs $X/C$ for the Forward Swept Model at $M = 0.93$ . . . . .	52
34 $C_D$ vs $X/C$ for the Aft Swept Model at $M = 0.93$ . . . . .	53
35 Oil Flow of Forward Swept Wing at $M = 0.63$ , $\alpha = 4$ . . . . .	55
36 Oil Flow of Aft Swept Wing at $M = 0.63$ , $\alpha = 4$ . . . . .	55
37 Oil Flow of Forward Swept Wing at $M = 0.63$ , $\alpha = 10$ . . . . .	56
38 Oil Flow of Aft Swept Wing at $M = 0.63$ , $\alpha = 10$ . . . . .	56

Figure		Page
39	Oil Flow of Forward Swept Wing at $M = 0.93$ , $\alpha = 10$ . . . . .	57
40	Oil Flow of Aft Swept Wing at $M = 0.93$ , $\alpha = 10$ . . . . .	57
41	Force Diagram of Wing Section . . . . .	65
42	Schematic of Forward Swept Wing used for Stress Analysis . . . . .	67
43	Schematic of Aft Swept Wing used for Stress Analysis . . . . .	68
44	Wing Modeled as a Thin Beam . . . . .	69
45- 49	$C_L$ vs $\alpha$ for $M = 0.7$ , $0.8$ , $0.85$ , $0.87$ , $0.9$ . . . . .	74
50- 54	$C_D$ vs $\alpha$ for $M = 0.7$ , $0.8$ , $0.85$ , $0.87$ , $0.9$ . . . . .	79
55- 59	$C_D$ vs $C_L$ for $M = 0.7$ , $0.8$ , $0.85$ , $0.87$ , $0.9$ . . . . .	84
60- 64	$L/D$ vs $\alpha$ for $M = 0.7$ , $0.8$ , $0.85$ , $0.87$ , $0.9$ . . . . .	89
65- 69	$C_M$ vs $\alpha$ for $M = 0.7$ , $0.8$ , $0.85$ , $0.87$ , $0.9$ . . . . .	94

LIST OF TABLES

Table	Page
I. TGF Transonic Test Section Characteristics . . .	7
II. Model Geometry . . . . .	9
III. Pressure Tap Locations . . . . .	12
IV. Test Conditions . . . . .	15
V. Skin Friction Coefficients . . . . .	20

## LIST OF SYMBOLS

A	Aspect ratio
b	Wing span
c	Chord
$\bar{c}$	Mean aerodynamic chord
$C_D$	Drag coefficient
$C_{D_0}$	Drag coefficient at $\alpha = 0$
$C_F$	Turbulent skin friction coefficient
$C_L$	Lift coefficient
$C_{L_0}$	Lift coefficient at $\alpha = 0$
$C_M$	Pitching moment coefficient
$C_{M_0}$	Pitching moment coefficient at $\alpha = 0$
$C_r$	Root chord
$C_t$	Tip chord
$C_p$	Pressure coefficient
D	Drag
F	Degrees Fahrenheit
$F_a$	Axial force measured
$F_{ac}$	Axial force adjusted to zero base drag
FS	Factor of Safety
$F_{Su}$	Ultimate shearing stress
$F_{Sy}$	Yield shearing stress
$F_{Tu}$	Ultimate tensile stress
$F_{Ty}$	Yield tensile stress
$I_x$	Moment of inertia about x-axis

K	Ratio of specific heat of air at constant pressure to that at constant volume
L	Lift
L/D	Lift to drag ratio
L/D <sub>max</sub>	Maximum lift to drag ratio
M	Mach number
M <sub>DD</sub>	Drag divergence Mach number
N	Maximum normal force
P	Pressure
P <sub>b</sub>	Base pressure
P <sub>o</sub>	Total pressure
P <sub>s</sub>	Static pressure
q	Dynamic pressure
R	Reynolds number
S	Planform area
S <sub>b</sub>	Base area
psi	Pound force per square inch
psf	Pound force per square foot
T	Twisting moment
T <sub>o</sub>	Total temperature
X/C	Percent chord
$\alpha$	Angle of attack
$\lambda$	Taper ratio

Abstract

This study consisted of modeling and wind tunnel testing of a high speed, subsonic, low aspect ratio, forward swept wing with an advanced supercritical airfoil section for the purpose of determining its lift, drag, and pitching moment characteristics as compared to a similar aft swept wing. Tests were conducted at Mach numbers of 0.63 to 0.93 in the Air Force Flight Dynamics Laboratory's Trisonic Gasdynamic Facility located at Wright-Patterson Air Force Base, Ohio. Two wing configurations, forward and aft swept, were tested and compared to computer predictions provided by the Unified Subsonic-Supersonic Program (Woodward's Version B). The results indicated that the forward swept wing was capable of higher useable angles of attack while maintaining a lower drag coefficient for angles of attack below eight degrees. Wind tunnel test results are presented in graphical and tabular form for use in future design studies of similar aerodynamic configurations.

# AN AERODYNAMIC INVESTIGATION OF A FORWARD SWEEP WING

## I. Introduction

### Background

This study addresses the problem of determining aerodynamic characteristics of a forward swept wing vehicle proposed by the Air Force Flight Dynamics Laboratory (AFFDL). In the past, the use of a forward swept wing was generally ruled out due to the increased root loads requiring substantial increases in structural weight. With the advent of advanced composites, it is possible to negate these weight penalties (Ref 4:1-4). A study of a forward swept wing was needed to obtain a data base for use in the design of forward swept wing aircraft. The proposed wing design was generated to be compatible with an existing half-span fuselage from AFFDL. Plan and side view model schematics are shown in Figs 1 and 2.

### Problem

The AFFDL was particularly interested in the aerodynamic investigation of a highly cambered, supercritical airfoil on a forward swept wing design as compared to a similar aft swept wing design. To maintain similar geometry on each wing, the tip chord, root chord, wing span, and wing area were held constant. The following information was required:

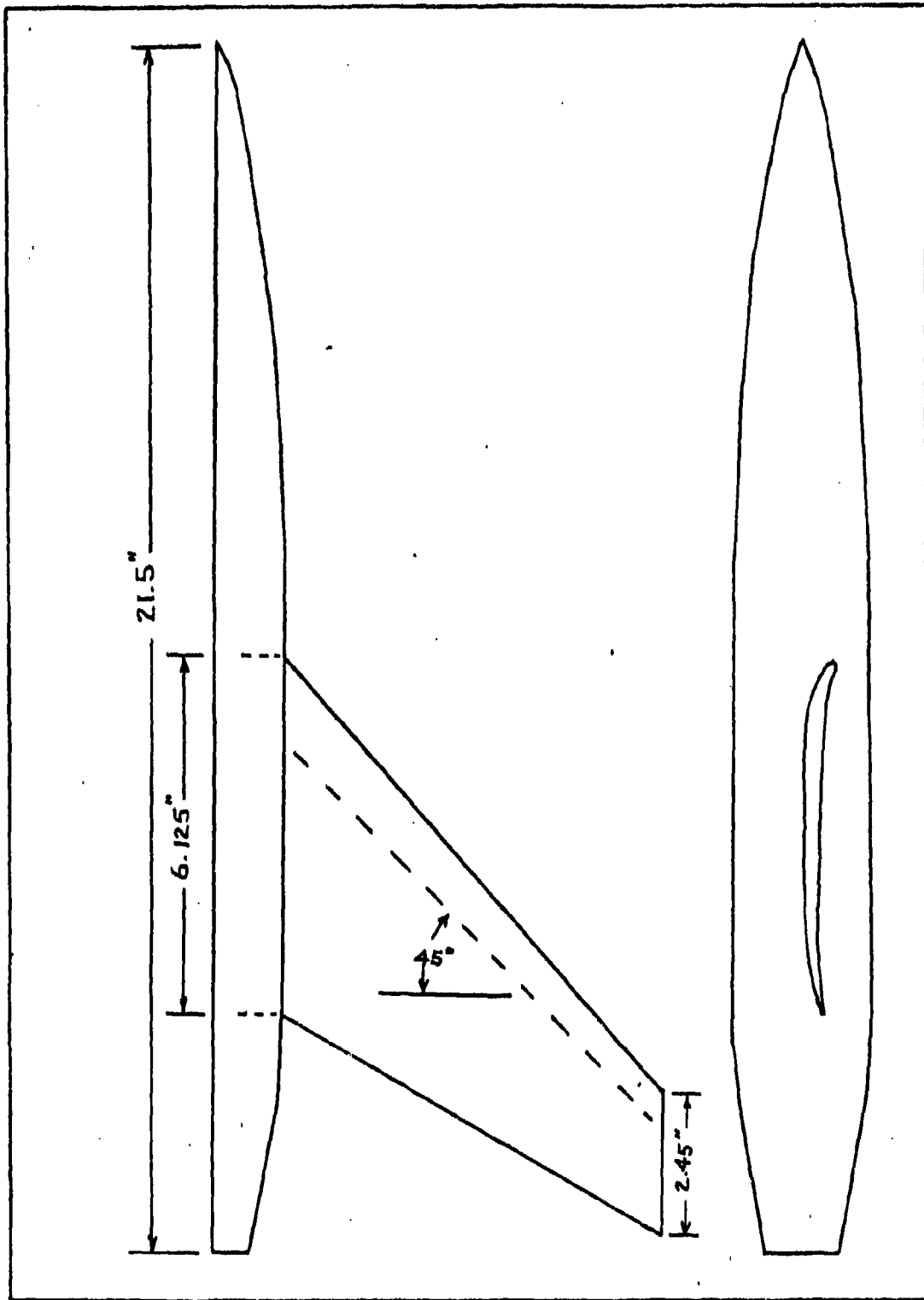


Figure 1. Schematic of Aft Swept Model



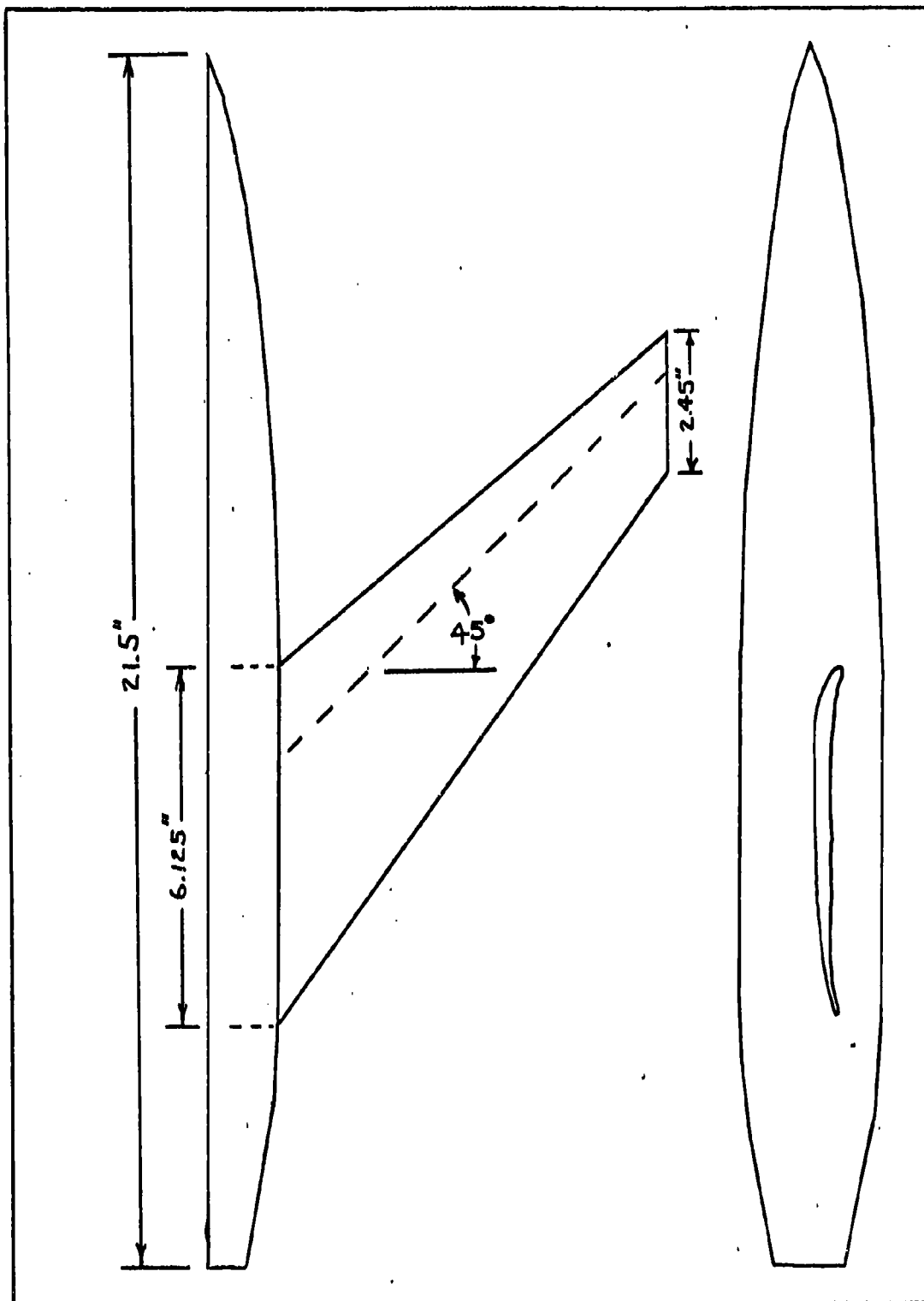


Figure 2. Schematic of Forward Swept Model

1. Determination of the effect of sweep on the aerodynamic characteristics.

2. Determination of the interference between the body and the swept wing.

The cambered wing was considered beneficial in improving the stalling characteristics of forward swept wings by delaying leading edge separation (Ref 6:11). The extent of the anticipated effect on lift and drag was to be determined.

### Scope

The forward swept wing was tested and compared to a similar aft swept wing over numerous high subsonic speeds. Each model was analyzed over an extensive range of angles of attack. The proposed model and test parameter ranges included:

Sweep at Quarter Chord	-45.0 and +45.0 (degrees)
Taper Ratio	0.4
Mach Number	0.63 to 0.93
Reynolds Number	2,000,000 (per foot)
Angle of Attack	-5.0 to +15.0 (degrees)

### Approach

Wind tunnel tests were the primary means of determining the lift, drag, and pitching moment coefficients on each model. The AFFDL's two foot, Trisonic Gasdynamic Facility (TGF), located at Wright-Patterson Air Force Base, Ohio, was selected for the tests. Data reduction was accomplished

simultaneously during the tests, via the Control Data Corporation (CDC) 6600 digital computer tied directly to the TGF. The force and moment data reduction program was provided by AFFDL.

The Unified Subsonic-Supersonic Aerodynamics Program (USS Aero) provided analytical predictions which were utilized in predicting the wind tunnel results. The computer results were used to estimate aerodynamic characteristics for each model for stress analysis purposes. The wind tunnel test data would be compared to the USS Aero Program predictions to indicate the accuracy of this program.

#### Materials and Equipment

For this study the AFFDL half-span fuselage section was used in conjunction with two swept wings. Each wing was mounted at the same root chord position on the fuselage and constructed using a 5.5 percent thick, cambered, supercritical airfoil provided by AFFDL. The geometry of each wing was kept as similar as possible to allow better comparison. Other modifications to the existing model included:

1. New center body for wing support.
2. New center fuselage section to allow for pressure lines.
3. Thirteen pressure taps in each wing.

## II. Facility And Model Description

### Facility Used for Testing

The Air Force Flight Dynamics Laboratory's Trisonic Gasdynamic Facility (TGF) was utilized for the wind tunnel tests. This facility was chosen for several reasons. The TGF is a closed circuit, variable density wind tunnel capable of continuous flow. It may be operated at subsonic, transonic, and supersonic speeds through a range of Mach numbers from 0.23 to 4.76. The facility's axial flow compressor was maintained at constant RPM with the use of two synchronized motors, capable of up to 11,500 horsepower. Hydraulically actuated stator blades controlled, instantaneously, the volume flow and pressure rise. Water cooled heat exchangers maintained a stagnation temperature of  $100\text{ F} \pm 1\text{ F}$ , while two dryer systems maintained a dew-point necessary to prevent liquefaction of water vapor in the test section. Quantitative data on test section turbulence levels were not available, but a honeycomb and screen arrangement located in the tunnel stagnation section were used to reduce turbulence in the test section. The variable density capability allowed for a constant high unit Reynolds Number, approximately 2.0 million per foot, to be used as the Mach number varied. The characteristics of the transonic test section are given in Table I.

Table I  
TGF Transonic Test Section Characteristics

Mach Number Range	0.30-1.20
q PSF (Max)	1,480
P <sub>0</sub> PSF (Max)	4,000
P <sub>8</sub> PSF (Max)	2,110
R/Ft (Max)	8,250,000
T <sub>0</sub> (F)	100
Cross Section (in.)	15 x 15
Density Altitude (ft.)	50,000
Number of Slots	56

(Ref 12:3)

An 11.426 inch diameter window in the test section permitted access to the model for rapid configuration changes as well as an unobstructed view of the model during testing. The window facilitated the use of oil flow photography as a flow visualization method.

The model was supported by the General Dynamics half-span rig mounted with the center of rotation in the center of the test section viewing window. The pitch range was negative five to positive fifteen degrees with an accuracy of  $\pm 0.01$  degrees. While maintaining the desired Mach number, the wide range of possible angles of attack was varied (Ref 12:1-17).

The model support system allowed the use of a five

component internal type strain gage balance to obtain force and moment data. The balance selected for testing was a General Dynamic half-span balance, number ZM-259. It was capable of measuring normal and axial forces of 250 and 30 pounds respectively. It allowed for roll, yaw, and pitch moments of 500 inch-pounds to be determined (Ref 3). The load sensing elements of the balance were connected to a Wheatstone bridge arranged in such a manner as to give an electrical signal proportional to the deformation. The electrical signal in millivolts was fed to self-balancing potentiometers and by use of shaft-to-analog-to-digital converters were translated to digital outputs. The outputs were reduced to a more usable aerodynamic coefficient form by a CDC 6600 computer. These coefficients were tabulated and plotted. This force measurement system, therefore, provided instantaneous visual monitoring and an automatic digital recording capability (Ref 12:10-17). The pressure sensing instrumentation consisted of differential pressure transducers. Each transducer was capable of reading up to 48 separate pressures as each tap was electrically selected. A series of calibration tests indicated the balance and associated instrumentation capable of measuring forces and moments within  $\pm 1$  percent of the applied load. The pressure data was calibrated to within one tenth of a pound per square foot.

### Models Tested

For this series of tests, two entirely new wings were constructed for use with existing General Dynamics half-span fuselage. The geometry requirements for each wing were dictated by the use of the half-span fuselage due to constraints in available construction techniques and time available. A new fuselage center section was constructed to allow support of each wing at the same fuselage station thus requiring minimum time for the interchange of the wings during testing. As a result, the forward swept configuration tested had less than ideal pitching moment characteristics. Pertinent model dimensions are given in Table 2 and the models are shown in Figs 3 and 4.

Table II  
Model Geometry

Wing Planform Area (sq. in.)	25.725
Root Chord (in.)	6.125
Tip Chord (in.)	2.45
Taper Ratio	0.40
Wing Semi-Span (in.)	7:58
Sweep Angle of Quarter Chord (degrees)	+45, -45
Aspect Ratio	3.34
Mean Aerodynamic Chord (in.)	5.62

The airfoil to be utilized was a newly developed, high

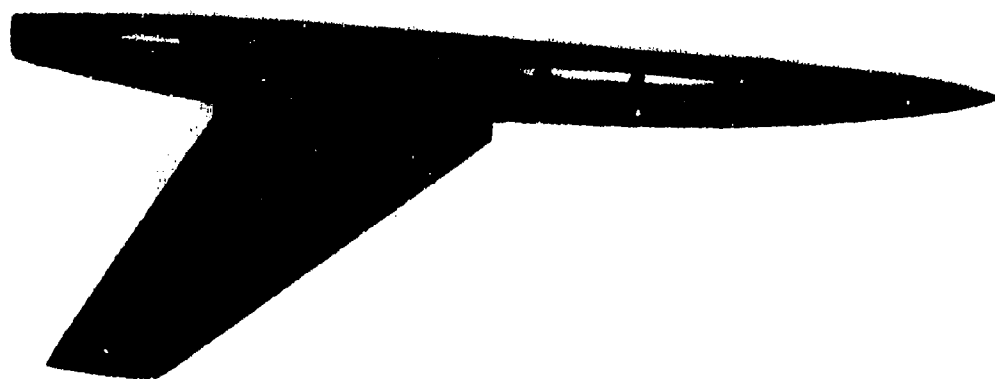


Figure 3. Aft Swept Model used for Wind Tunnel Test



Figure 4. Forward Swept Model used for Wind Tunnel Test



camber, supercritical airfoil section of 5.5 percent local chord thickness ratio. The maximum chord of 6.125 inches occurred at the root thus making the thickness of the section 0.337 inches. For support purposes, an eighth inch thick steel plate was embedded in an epoxy mold of each wing and subsequently mounted to the fuselage center section. The chord on each wing was aligned with the flow direction thus allowing support of the wings on the same fuselage center section. This airfoil was used due to its high lift properties in transonic flow and for the reduction of leading edge separation it exhibited. By utilizing identical sectional and planform geometry, the data comparison and model design and construction of the two wings could be greatly accelerated. Although several significant changes were made to the final design of the models, the basic half-span fuselage with available ZM-259 balance could be used with the newly constructed wings (Ref 5).

Pressures were taken at thirteen separate locations on each wing in one chordwise cut. The pressure taps were aligned at a mid-span location to limit the amount of both fuselage and tip interference on the pressure data. In Table 3, these pressure tap locations are listed in percent chord for the 4.3 inch local chord position on each wing. Only taps 2 and 3 are located on the lower surface of the airfoil.

Table III  
Pressure Tap Locations

Tap Number	% Chord	Inches From Leading Edge
1	0.0	0.0
2,4	5.0	0.215
3,5	10.0	0.430
6	50.0	2.15
7	55.0	2.365
8	60.0	2.58
9	65.0	2.795
10	70.0	3.010
11	75.0	3.225
12	80.0	3.440
13	85.0	3.655

### III. Experimental Procedures

#### Force Measurements

The reduction of data using the half-span balance output voltage was performed on a CDC 6600 digital computer (Ref 12:10). Aerodynamic characteristics are presented in the form of coefficients in the wind axis system. The longitudinal moments were computed about the balance center to enable direct comparison of the different wing configurations. The mean aerodynamic chord of 5.62 inches was computed using:

$$\bar{c} = \frac{2}{3} C_r \frac{1 + \lambda + \lambda^2}{1 + \lambda}$$

where  $C_r$  is the root chord and  $\lambda$  is the taper ratio. It was used as a reference length in the data reduction program.

An important consideration in obtaining true axial force measurements in most wind tunnel tests is the treatment of base drag. This drag arises from the pressure acting on the blunt base of the model. The base pressure is influenced considerably by the presence of the tunnel wall, acting as a boundary to the model base. This influence normally causes the drag values to be smaller than they would be if the model could be tested without a boundary and balance in place (Ref 8:413). Therefore, the measurements taken in testing each model

were corrected to remove this base pressure effect as follows:

$$F_{ac} = F_a - S_b (P - P_b)$$

where  $F_{ac}$  is the axial force adjusted to zero base drag,  $F_a$  is the axial force measured,  $S_b$  is the model base area,  $P$  is the free stream static pressure, and  $P_b$  is the model base pressure (Ref 9:323). The base pressure was measured with a pressure probe located in the base of the model.

#### Test Procedures

The wind tunnel tests were divided into two main procedures. The first test was to obtain the aerodynamic characteristics of each configuration to include lift, drag, and pitching moment coefficients. The method of obtaining these characteristics was to vary angle of attack over a range of negative four to positive fifteen degrees while maintaining a constant Mach number. Each model was placed in position with tunnel off to obtain static pressure and zero tare readings. Once the tunnel was stabilized at the desired Mach number; these readings were again taken and corrected for wind off conditions. Numerous Mach numbers over a range of 0.63 to 0.93 were tested. The total pressure was varied with Mach number to maintain a unit Reynolds number of about two million.

The test settings are given in Table 4.

After force measurements on both configurations were completed, a brief flow visualization study was made. A white tinted oil was brushed on the models for this purpose. Flight conditions representing those tested were then investigated. The oil flow permitted visualization of the interactions of streamlines. Regions of flow separation are normally detectable using this method of flow visualization.

Table IV.  
Test Conditions

---

---

$T_o = 100 \text{ F}$

Data taken at each Mach number for alpha range of  
-5.0 to +15.0 degrees

$P_o$  varied to maintain  $R = 2,000,000$  per ft.

---

---

M	$P_o$ (psf)
0.63	1,210
0.70	1,140
0.80	1,070
0.85	1,050
0.87	1,020
0.90	1,000
0.93	980

---

---

#### IV. Analytical Procedures

In order to obtain initial predictions of the wind tunnel data, a new method of calculating the pressure distribution and aerodynamic characteristics of wing-body-tail combinations was used. The Unified Subsonic-Supersonic Aerodynamics Program (USS Aero) performed the numerical calculations. This program uses subsonic potential flow theory (Ref 13:2).

Both the forward and aft swept configurations were modeled by subdividing the wing as well as the fuselage into a large number of panels. Each of these panels contained an aerodynamic singularity distribution. The modeling for the aft and forward swept configurations is shown in Figs 5 and 6, respectively. A constant source distribution was used on the body panels and a vortex distribution having a linear variation in the streamwise direction was used on the wing panels. The planar option, which uses control points in the plane of the wing, was used and yielded accurate comparisons with experimental data. The non-planar option, which uses control points on the surface of the wing, required double the number of panels and yielded only slightly better results. This mode was not used due to the large increase in computer time with minimal increase in accuracy. The normal components of the velocity induced at specified control points

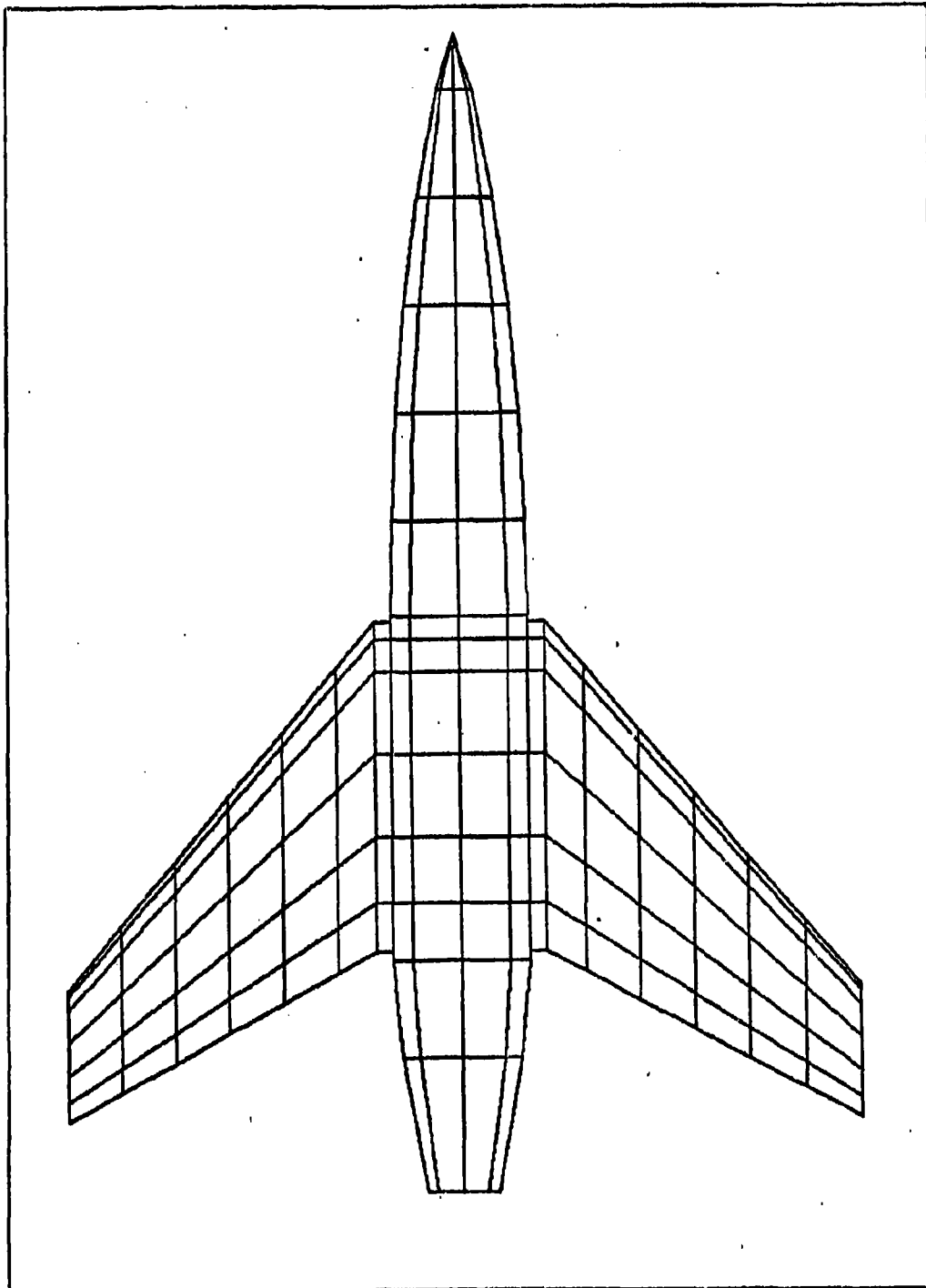


Figure 5. Aft Swept Model Used For USS Aero Prediction Program.

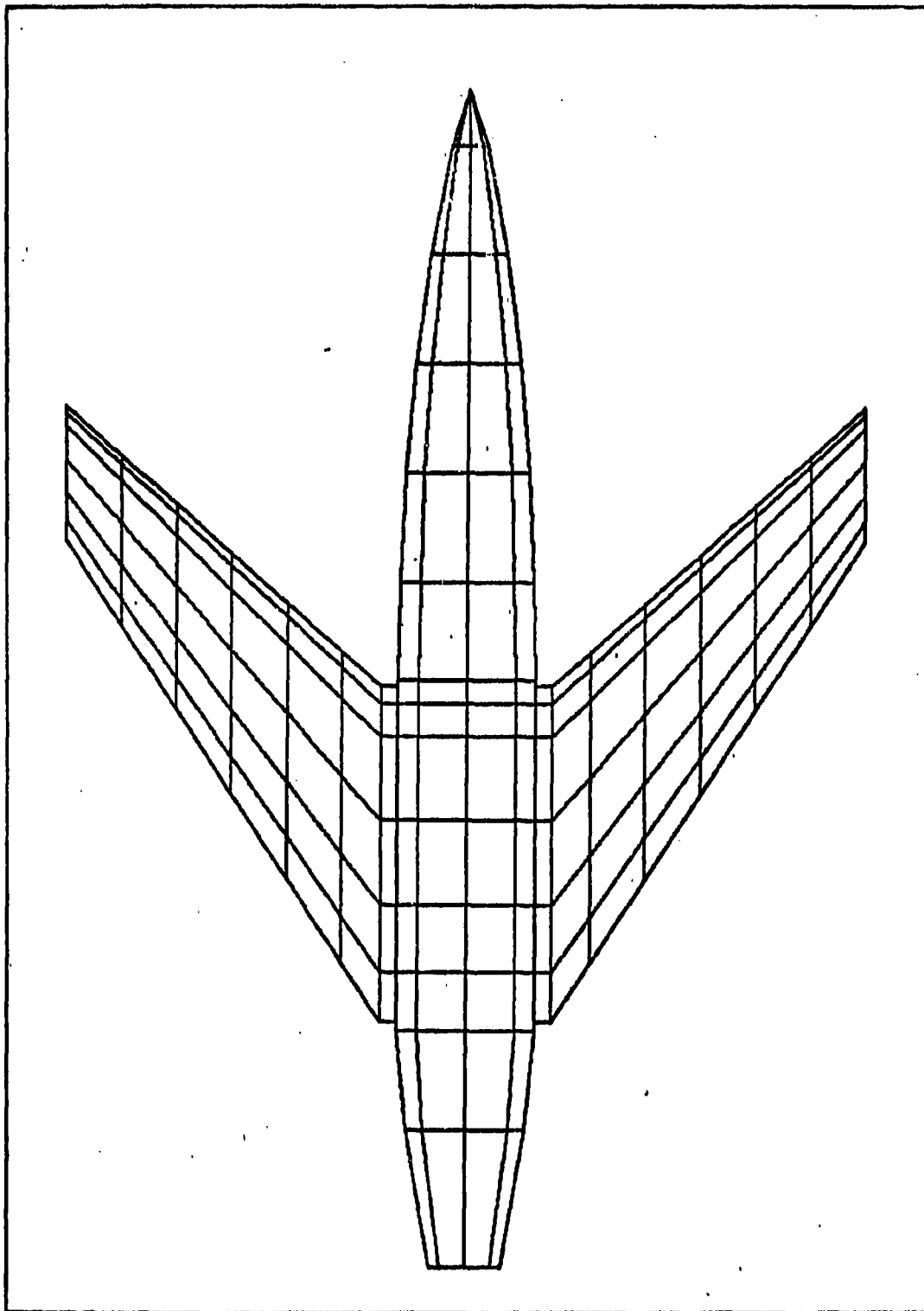


Figure 6. Forward Swept Model Used For USS Aero Prediction Program.



by each singularity distribution were calculated and make up the coefficients of a system of linear equations relating the strengths of the singularities to the magnitude of the normal velocities.

The singularity strengths which satisfy the boundary condition of tangential flow at the control points for a given Mach number and angle of attack were determined by solving the system of equations using an iterative procedure. Once the singularity strengths are known, the pressure coefficients were calculated, and the forces and moments acting on each configuration were determined by numerical integration (Ref. 7:12).

A skin friction coefficient,  $C_f$ , had to be determined and subtracted from the experimental drag coefficient to obtain a valid comparison of the relative accuracy of Woodward's USS Aero program. This allowed comparison of the induced drag coefficient computed by the potential flow analysis to the experimental drag coefficient without skin friction.

The skin friction drag of each configuration was calculated from the T' method (Ref 7:12). The T' method is based on the calculation of a compressible skin friction coefficient from a reference skin friction coefficient, for a selected Mach number, Reynolds number, and adiabatic wall temperature. Smooth flat plate, adiabatic wall, and turbulent boundary layer conditions were assumed. In addition, transition was assumed to occur at the leading

edge of each configuration component. Most of the program is involved with computing wetted areas and reference lengths for each component. Since both configurations had identical wetted areas, Table 5 represents the skin friction coefficient calculated for each Mach number tested. These values of skin friction were subtracted from experimental data before comparison was made to theoretical data.

Table V.  
Skin Friction Coefficients For  
Test Mach Numbers

Mach	Skin Friction Coefficient
0.63	0.01532
0.70	0.01523
0.80	0.01509
0.85	0.01502
0.90	0.01494
0.93	0.01489

Three Mach numbers, representative of the test Mach numbers, were utilized to obtain theoretical data for comparison to the tunnel data for each configuration. Good correlation between theory and experimental data was achieved.

## V. Results

The wind tunnel investigation of the forward and aft swept wing models resulted in a series of aerodynamic coefficients for each configuration tested. The coefficients determined for each model included lift, drag, and pitching moment coefficients. The coefficients are presented in the wind axis system as shown in Fig 7. The results discussed in this section are for Mach numbers of 0.63 and 0.93. The results obtained for Mach numbers between these two values are presented in graphical form in Appendix B. In addition, flow visualization photographs at flight conditions typical of those tested are included.

### Lift

The coefficients for the forward and aft swept models are plotted as a function of angle of attack in Figs 8 and 9 for the low and high Mach number tests, respectively. These values are typical of those obtained at all remaining Mach numbers tested. The slope of the lift curve is approximately 0.060 to 0.065 per degree, depending on the angle of attack and Mach number tested. For all Mach numbers tested, the aft swept wing produced a higher lift coefficient for a given angle of attack as compared to the forward swept wing. As the Mach number was increased to high subsonic values, the aft swept model lift curves tended to shift toward the forward swept model lift curves until the two curves varied by  $\Delta C_L$  equal to 0.035 at

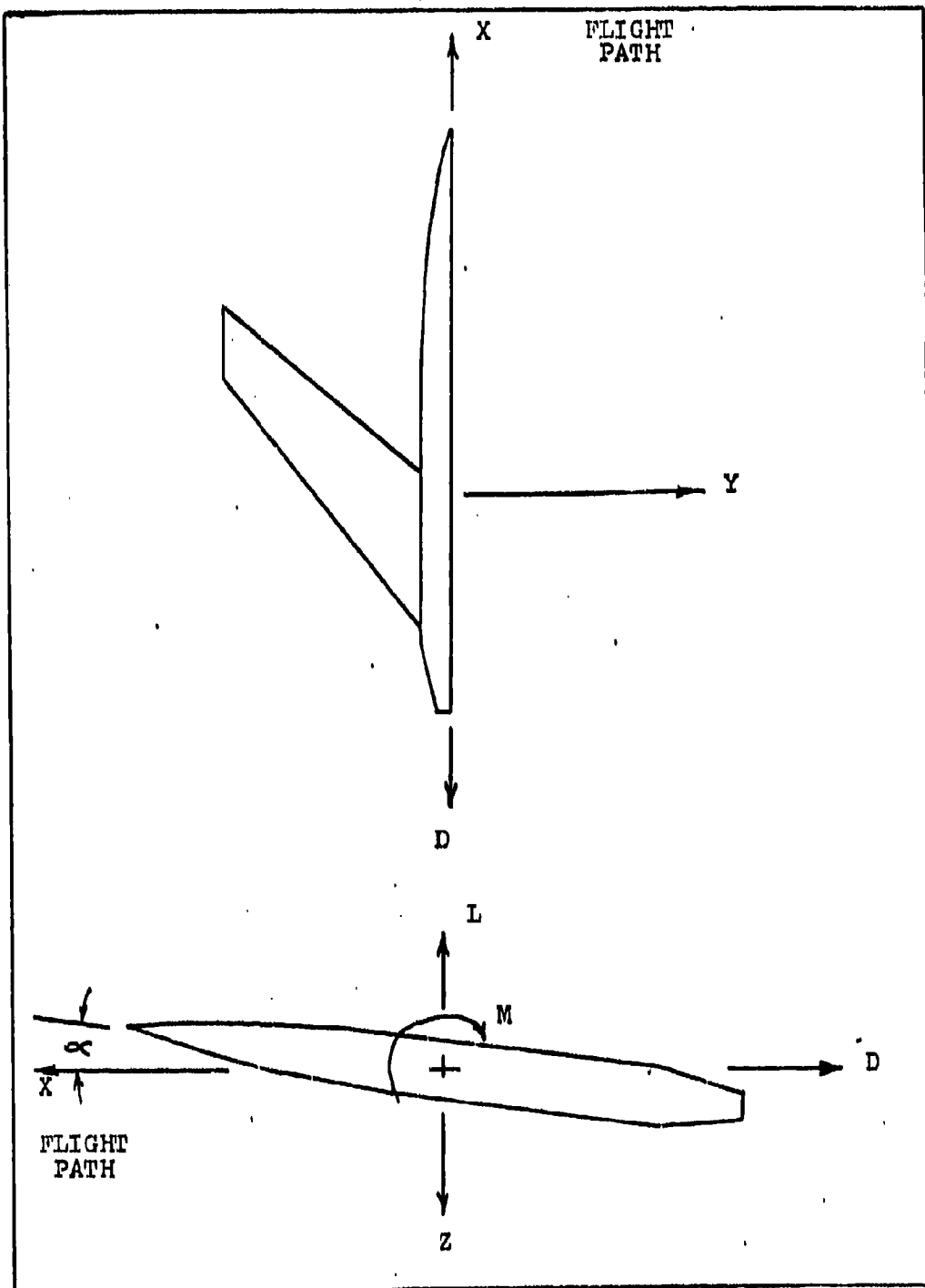


Figure 7. Wind Axis Coordinate used for Aerodynamic Coefficients

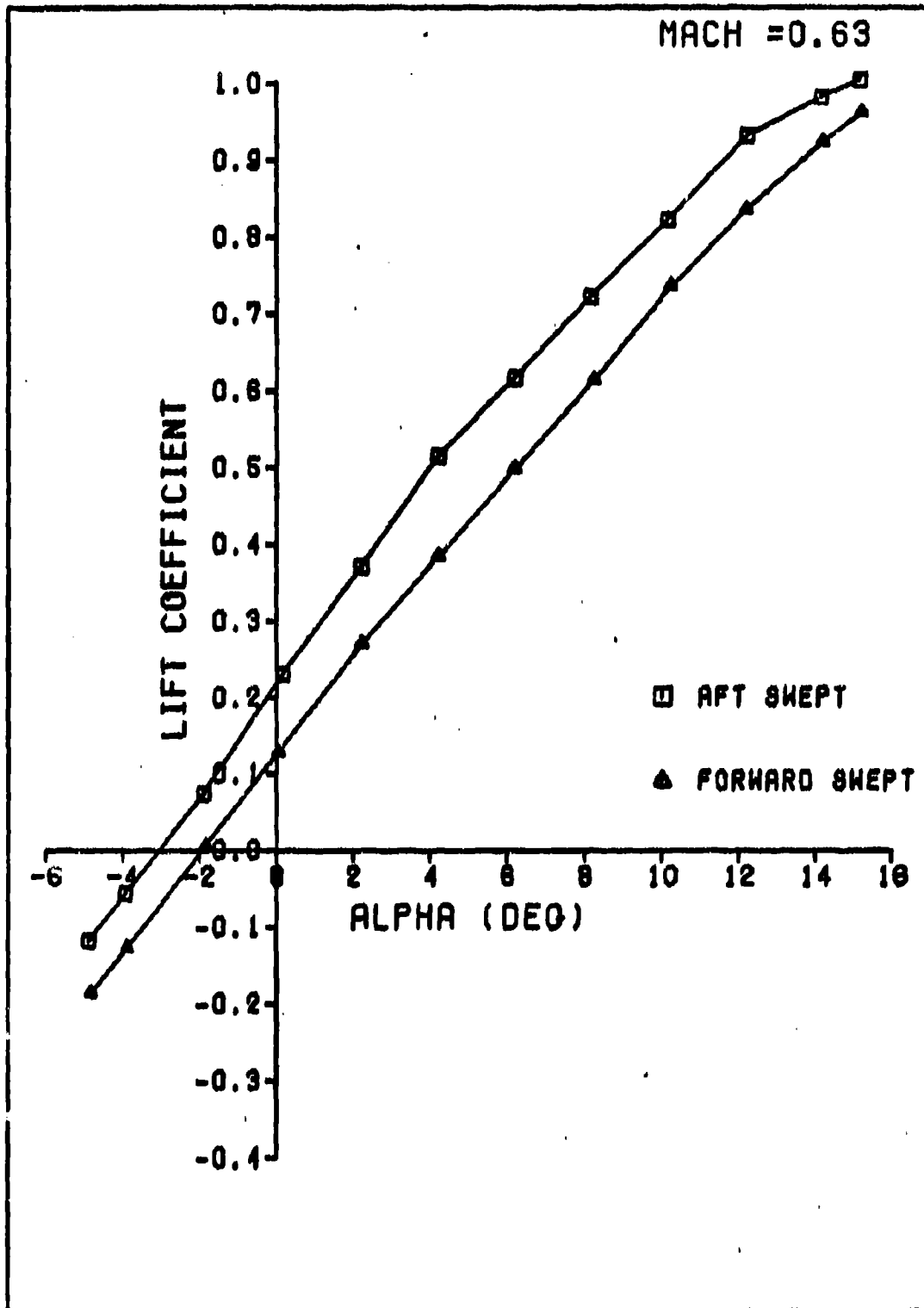


Figure 8.  $C_L$  vs  $\alpha$  for  $M = 0.63$

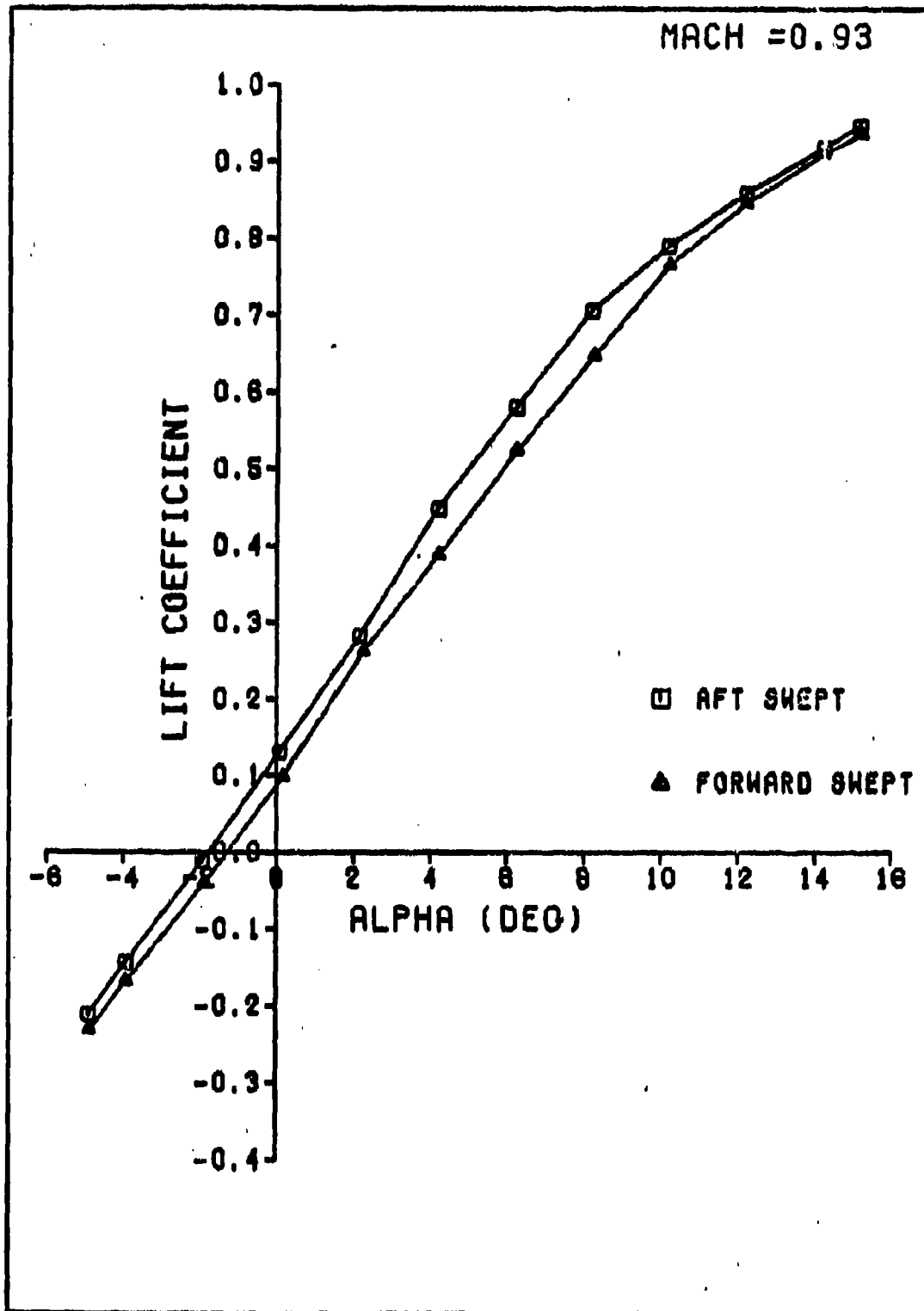


Figure 9.  $C_L$  vs  $\alpha$  for  $M = 0.93$

$M = 0.93$ . The change in angle of zero lift was the major contributor to the shift of the aft swept model lift curve. At  $M = 0.63$  the zero lift angle for the aft swept model was  $-3.2$  degrees whereas at  $M = 0.93$ , it became  $-2.0$  degrees. The forward swept model had an angle of zero lift which varied between  $-2.0$  and  $-1.6$  degrees. The aft swept model showed signs of stalling at a lower angle of attack than the forward swept model for all Mach numbers tested.

### Drag

A typical set of drag coefficients is plotted in Figs 10 and 11 as a function of angle of attack and in Figs 12 and 13 as a function of lift coefficient. For  $M = 0.63$ , the drag coefficient at zero angle of attack,  $C_{D_0}$ , was  $0.038$  for the forward swept model and  $0.042$  for the aft swept model. As Mach number was increased to  $M = 0.93$ , the values of  $C_{D_0}$  changed to  $0.042$  and  $0.051$  for the forward and aft models, respectively. For all Mach numbers tested the forward swept model displayed less drag up to approximately ten degrees alpha. Above this angle the two drag curves crossed and the forward swept model produced more drag for a given alpha.

The maximum lift to drag ratio may be determined by drawing the tangent to the  $C_D$  versus  $C_L$  curve from the origin (Ref 9:330). For  $M = 0.63$ , this yields an  $L/D|_{\max}$  for the aft swept model of  $8.3$  at a  $C_L$  of  $0.51$ . For the forward swept model, this ratio was  $8.4$  at a  $C_L$  of  $0.48$ .

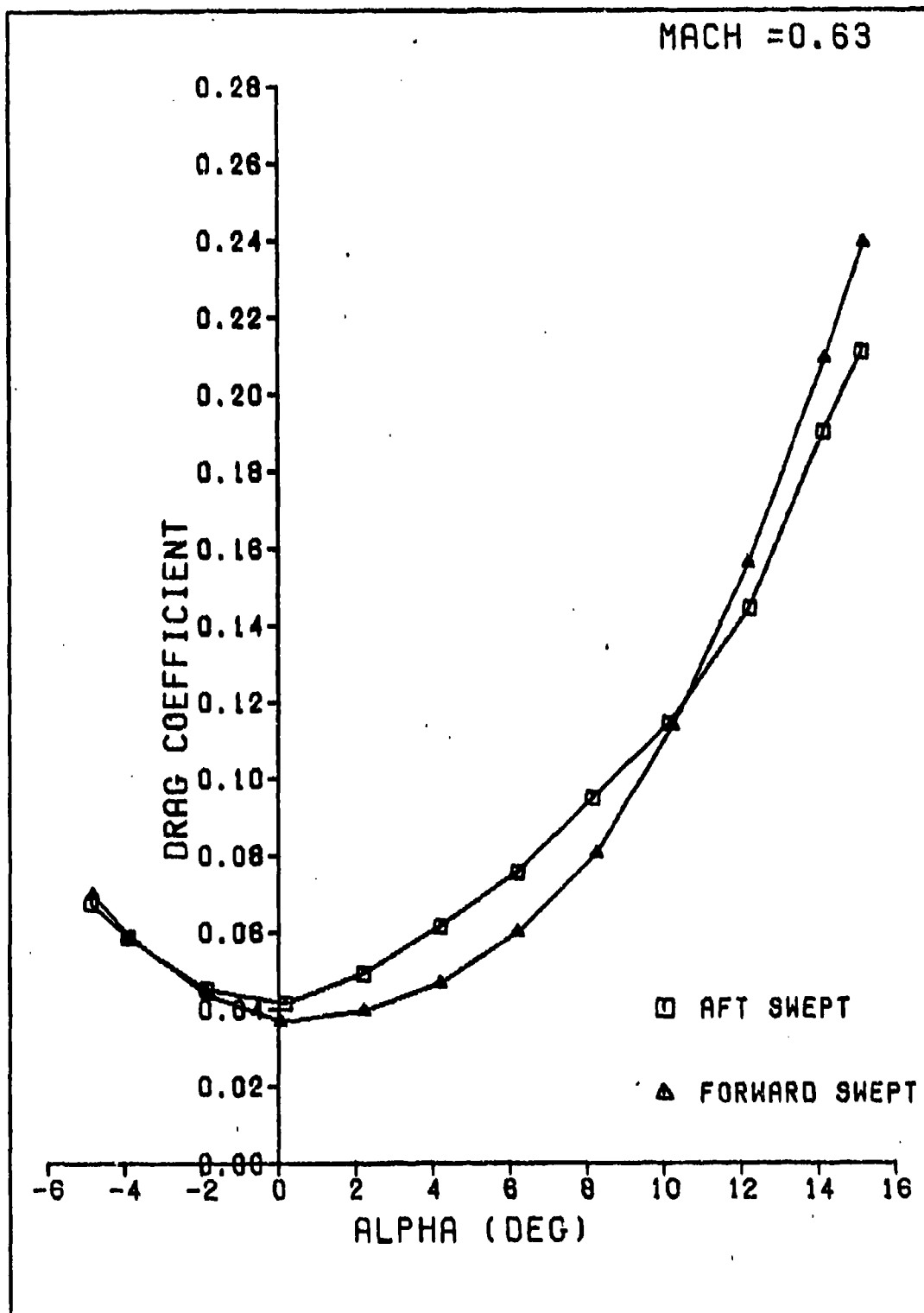


Figure 10.  $C_D$  vs  $\alpha$  for  $M = 0.63$



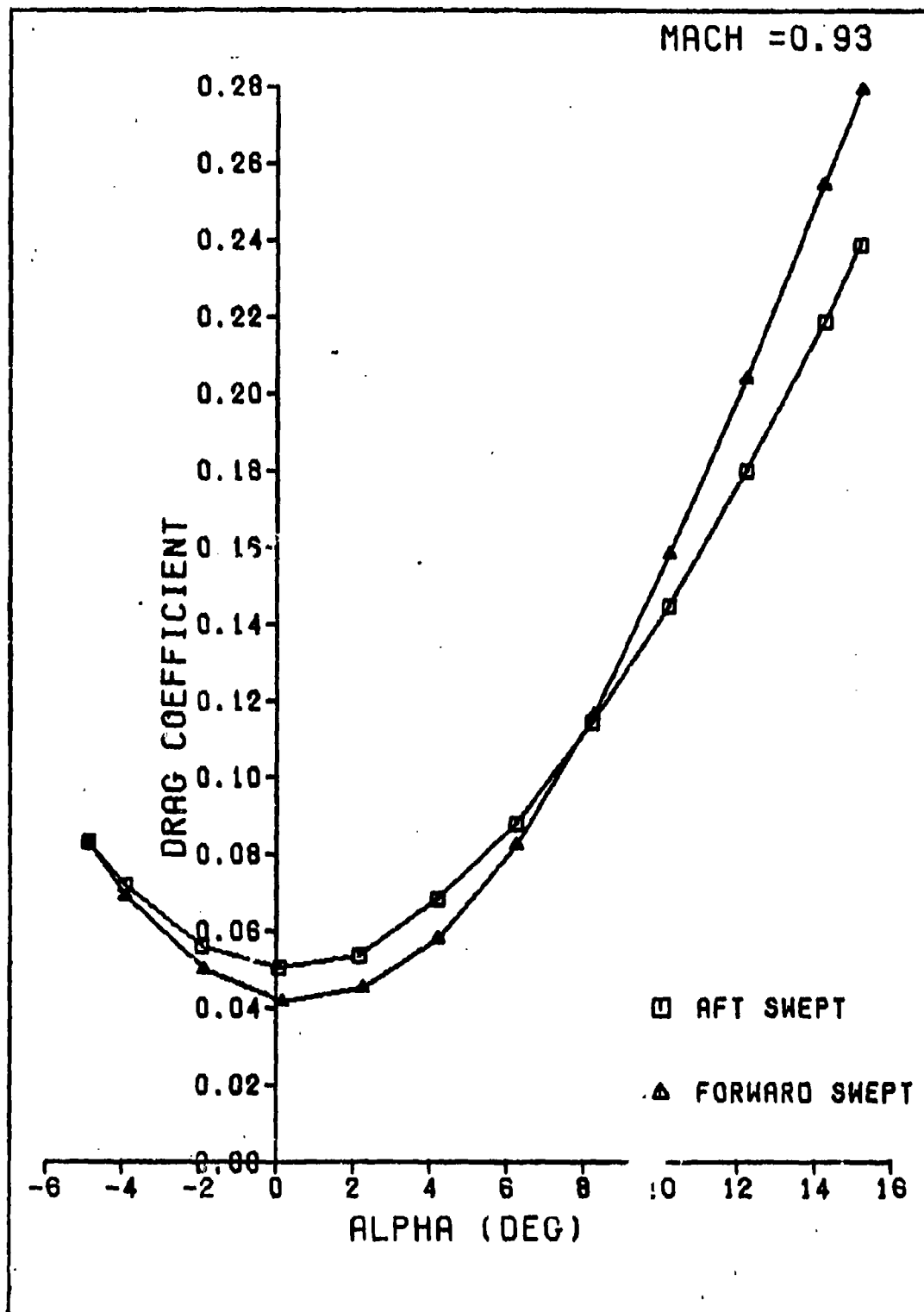


Figure 11.  $C_D$  vs  $\alpha$  for  $M = 0.93$

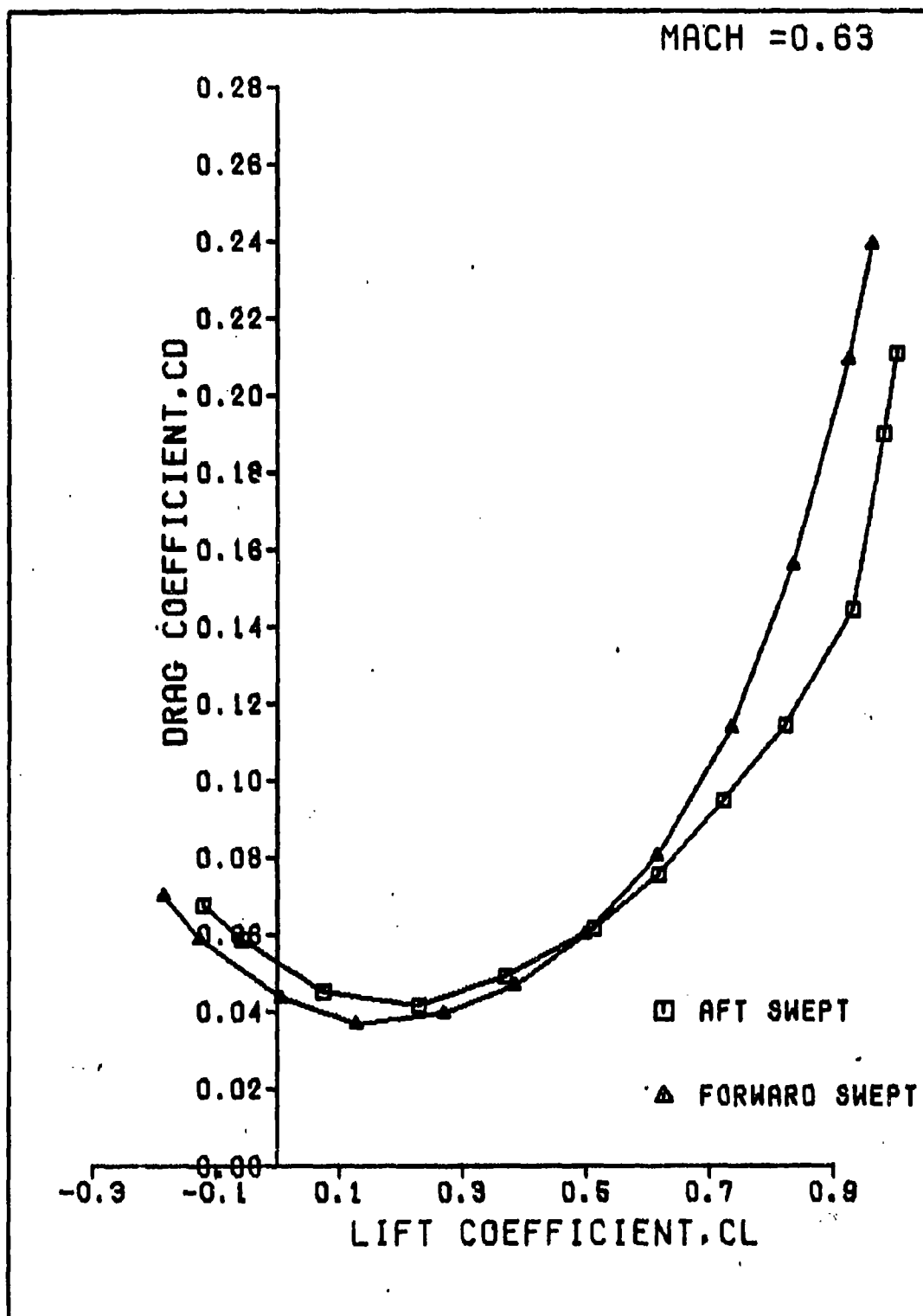


Figure 12.  $C_D$  vs  $C_L$  for  $M = 0.63$

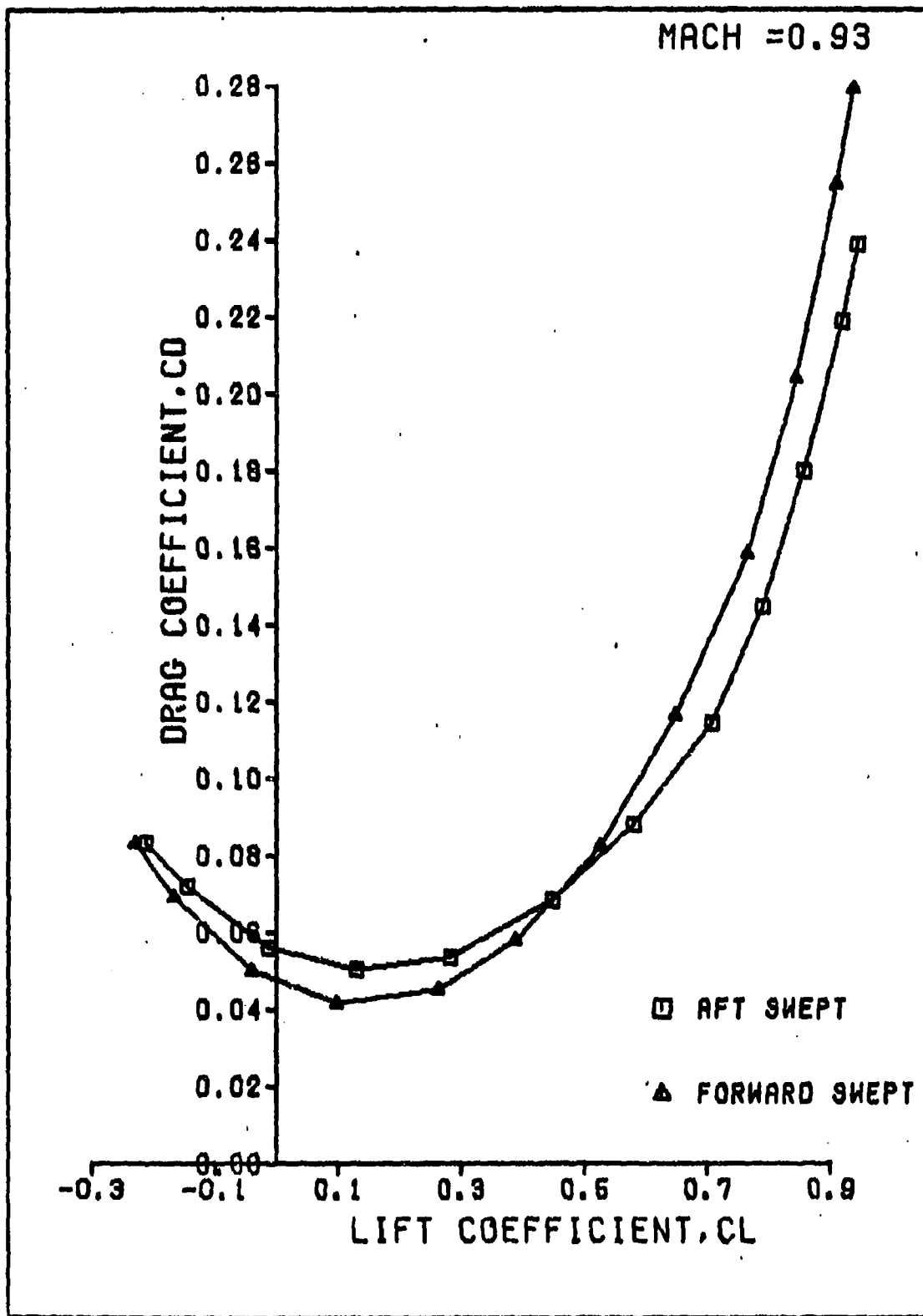


Figure 13.  $C_D$  vs  $C_L$  for  $M = 0.93$

This corresponds to an angle of attack of 4.1 degrees and 6.2 degrees for the aft and forward swept models, respectively. This shows that the forward swept model was capable of higher angles of attack for the same lift to drag ratio. The lift to drag ratio is plotted in Figs 14 and 15 as a function of angle of attack for direct comparison.

Figure 16 shows the effect of Mach number on the drag coefficient at a constant lift coefficient. A point on the curve that is sometimes used for reference is the drag divergence Mach number,  $M_{DD}$ . The  $M_{DD}$  is the Mach number at which  $dC_D/dM$  is equal to 0.10 (Ref 2:2). The  $M_{DD}$  decreases with an increase in alpha or an increase in lift coefficient. For the aft swept model,  $M_{DD}$  is above 0.93 for alpha less than or equal to five degrees. It is approximately 0.84 at an alpha equal to eight degrees. For the forward swept model a drag divergence Mach was not indicated since the drag continued to increase in an approximately linear manner with increase in Mach number.

#### Pitching Moment

The pitching moment about the balance center is represented in Figs 17 and 18. The slope of this curve varies little with Mach number for each model. Due to constraints in model fabrication, the forward swept configuration resulted in a positive slope to the pitching moment curve. This indicates the need of shifting the location of the root chord to a more rearward position to

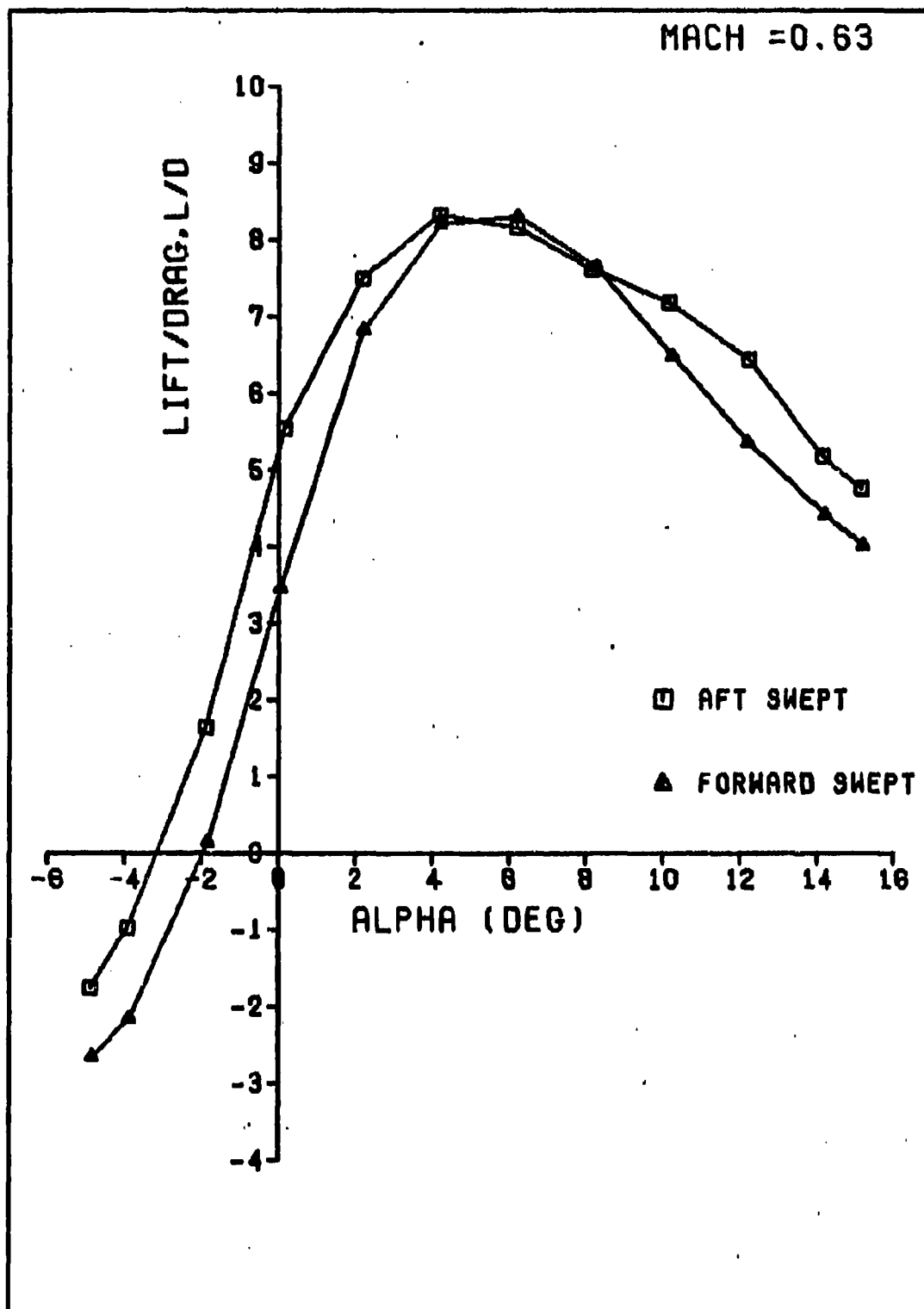


Figure 14. L/D vs  $\alpha$  for M = 0.63

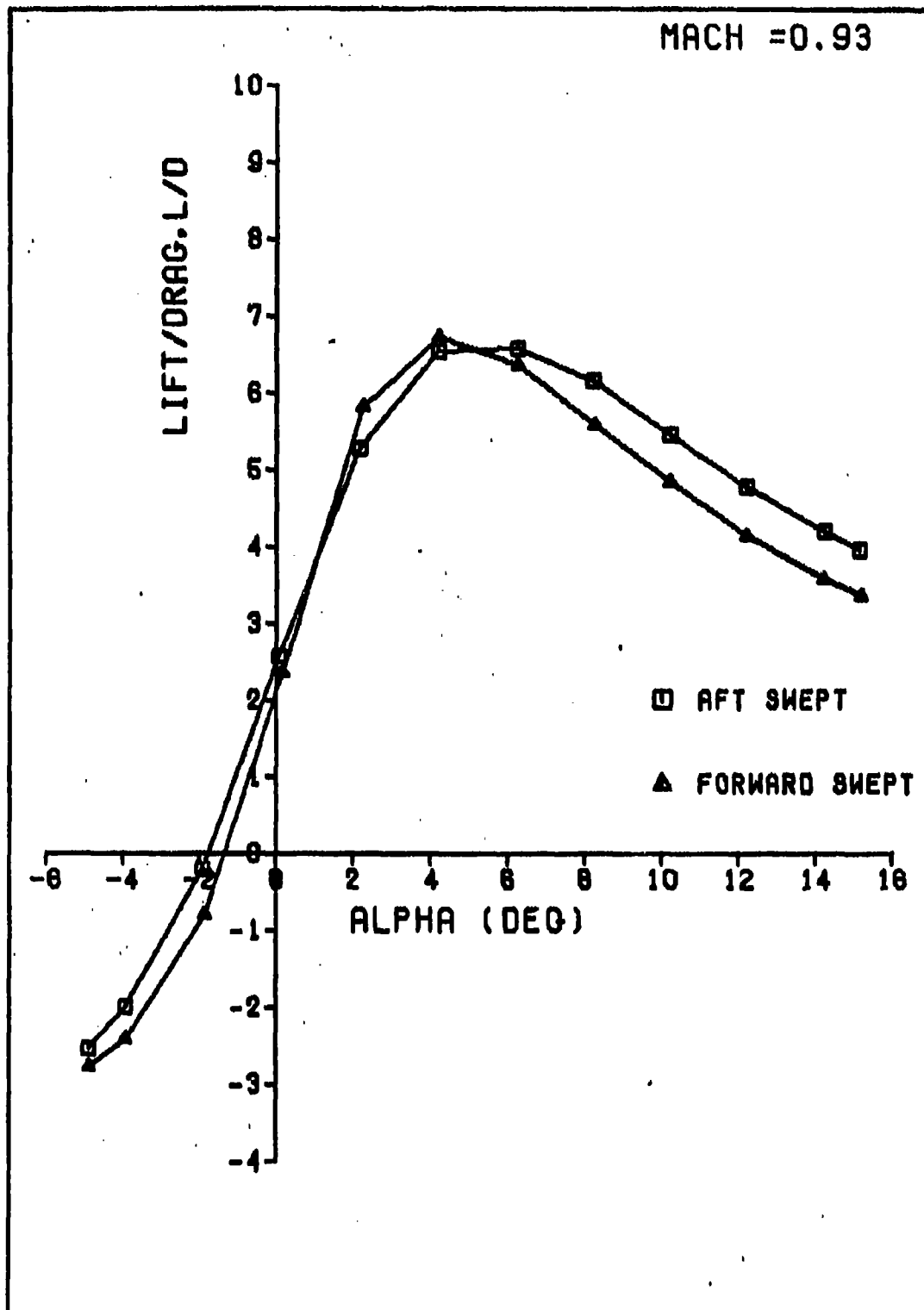


Figure 15. L/D vs  $\alpha$  for M = 0.93

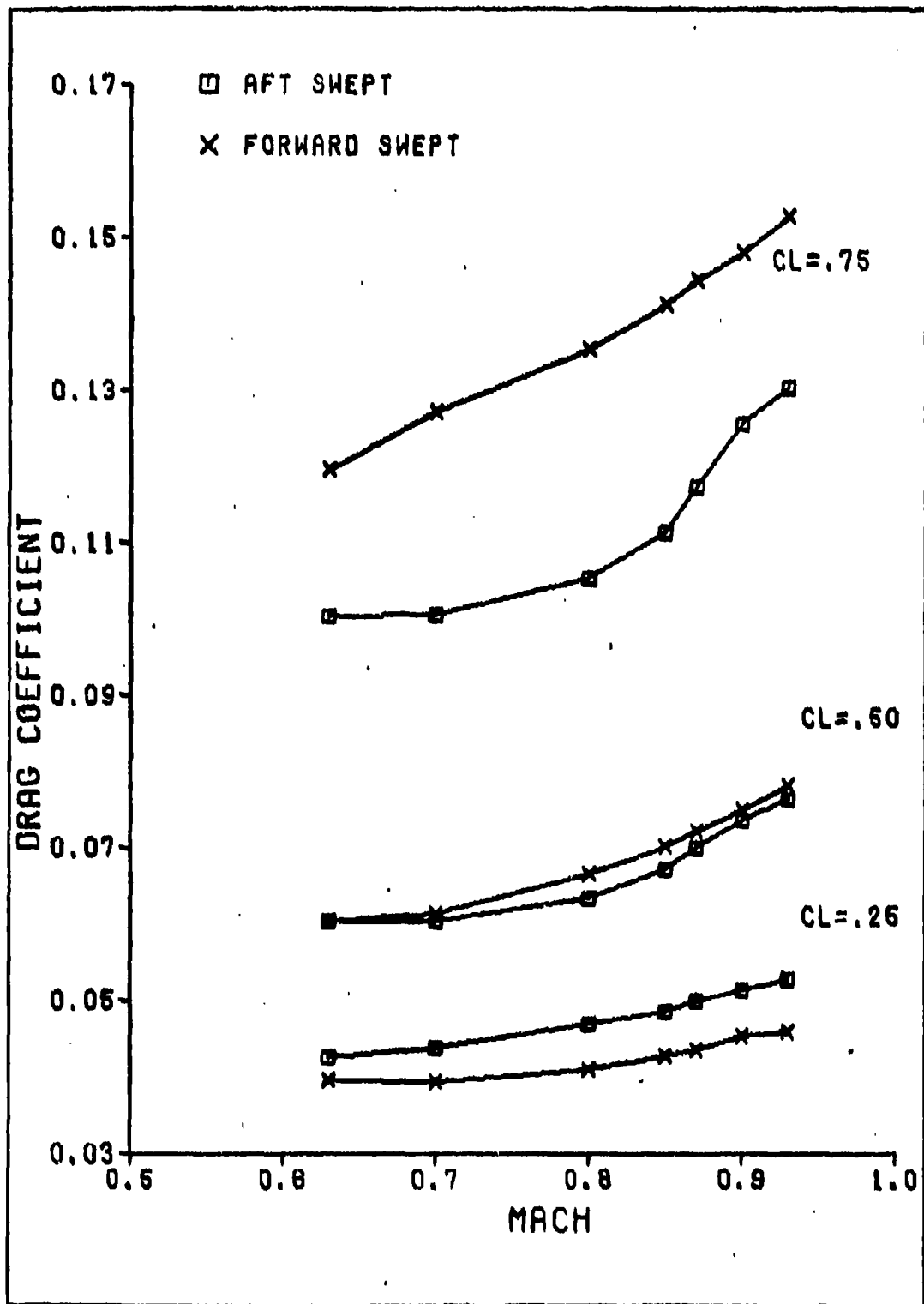


Figure 16.  $C_D$  vs Mach at Constant  $C_L = 0.25, 0.50, 0.75$

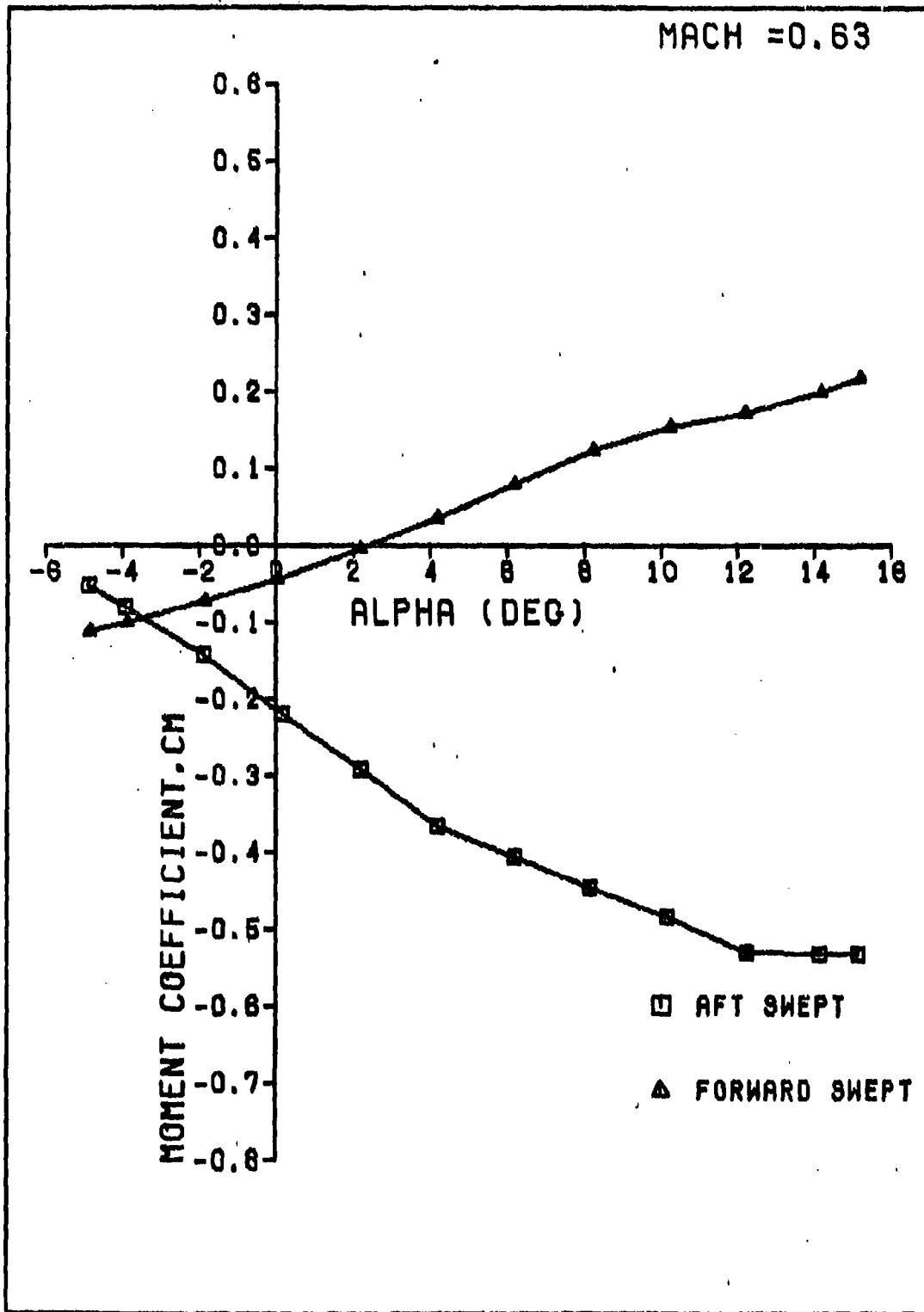


Figure 17.  $C_M$  vs  $\alpha$  for  $M = 0.63$



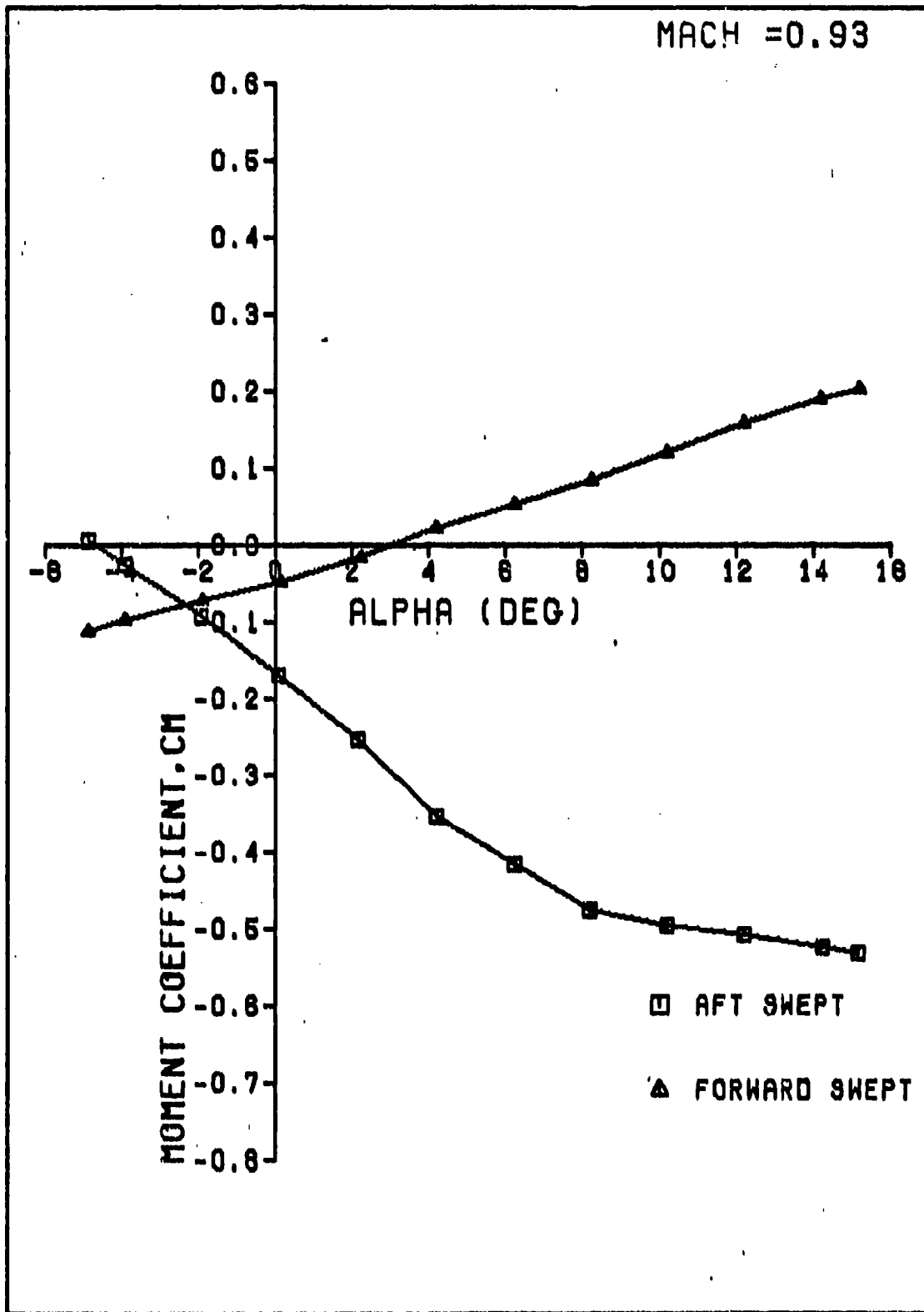


Figure 18.  $C_M$  vs  $\alpha$  for  $M = 0.93$

obtain a stable pitching moment for this configuration. Although the slopes of the two curves are opposite, a comparison of the relative magnitude of each slope indicated the forward swept model was less sensitive to changes in angle of attack. For  $M = 0.63$ , at an angle of attack of four degrees, the slope of the pitching moment curve is approximately  $+0.020$  per degree for the forward swept model and  $-0.038$  per degree for the aft swept model. The slope changes are, of course, dependent on the angle of attack.

#### Predictions

The lift and drag coefficient curves for both the USS Aero predictions and experimental data are shown for comparison in Figs 19 to 21 for the forward swept model and in Figs 25 to 27 for the aft swept model. The lift coefficient curves compare extremely well with the USS Aero program predicting approximately the same slope and zero lift angle of attack as obtained from experimental data. Drag comparisons are shown in Figs 22 to 24 for the forward swept model and in Figs 28 to 30 for the aft swept model. Note that the USS Aero program only predicts induced drag and does not include any skin friction drag. The experimental data was corrected by subtracting out the computed skin friction drag as discussed previously. The predicted drag curves displayed the same shape of the drag polar obtained from experimental values with small differences in values of  $C_{D_0}$ . For the panel distribution used

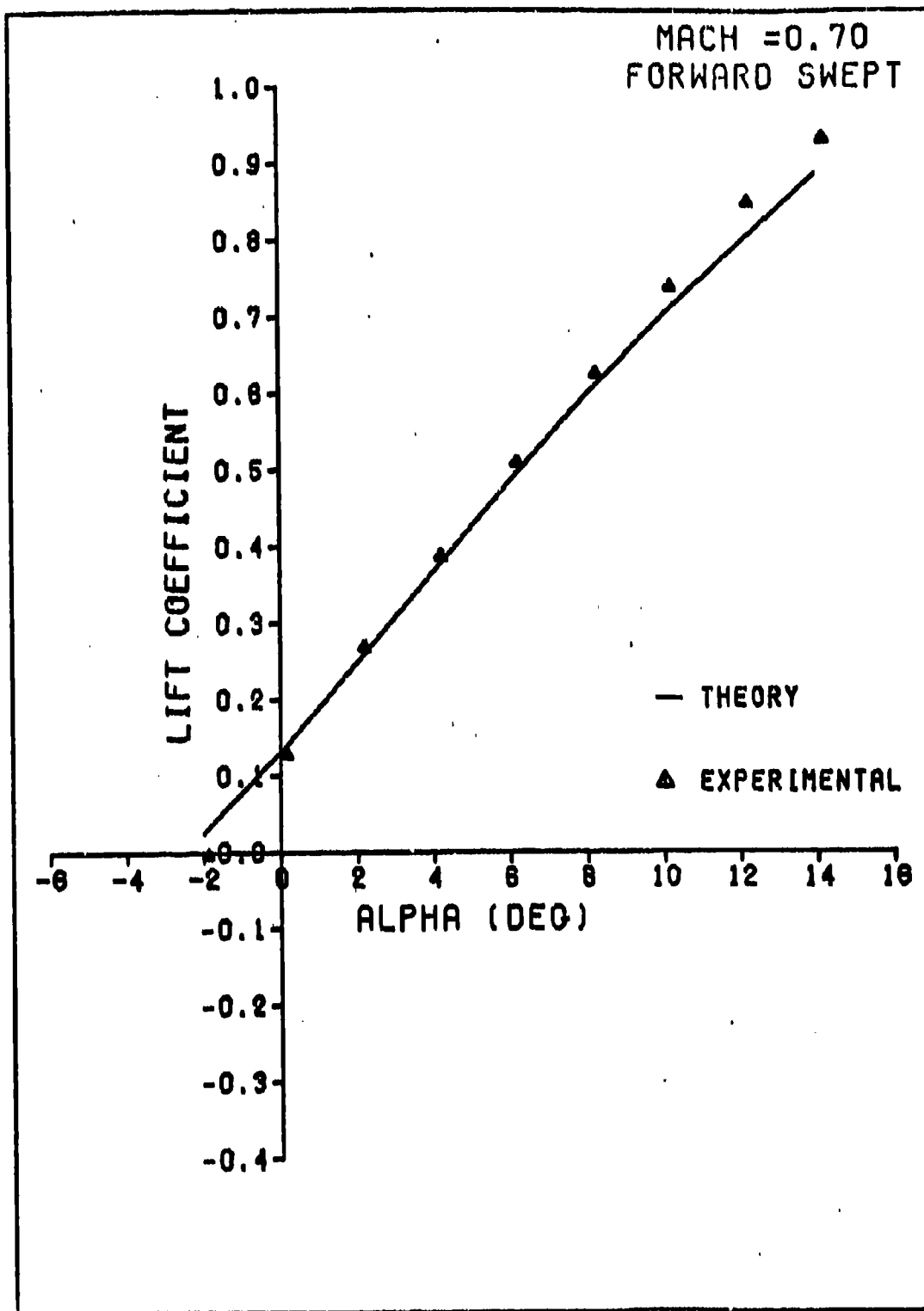


Figure 19. Theoretical  $C_L$  vs  $\alpha$ , for the Forward Swept Model at  $M = 0.7$

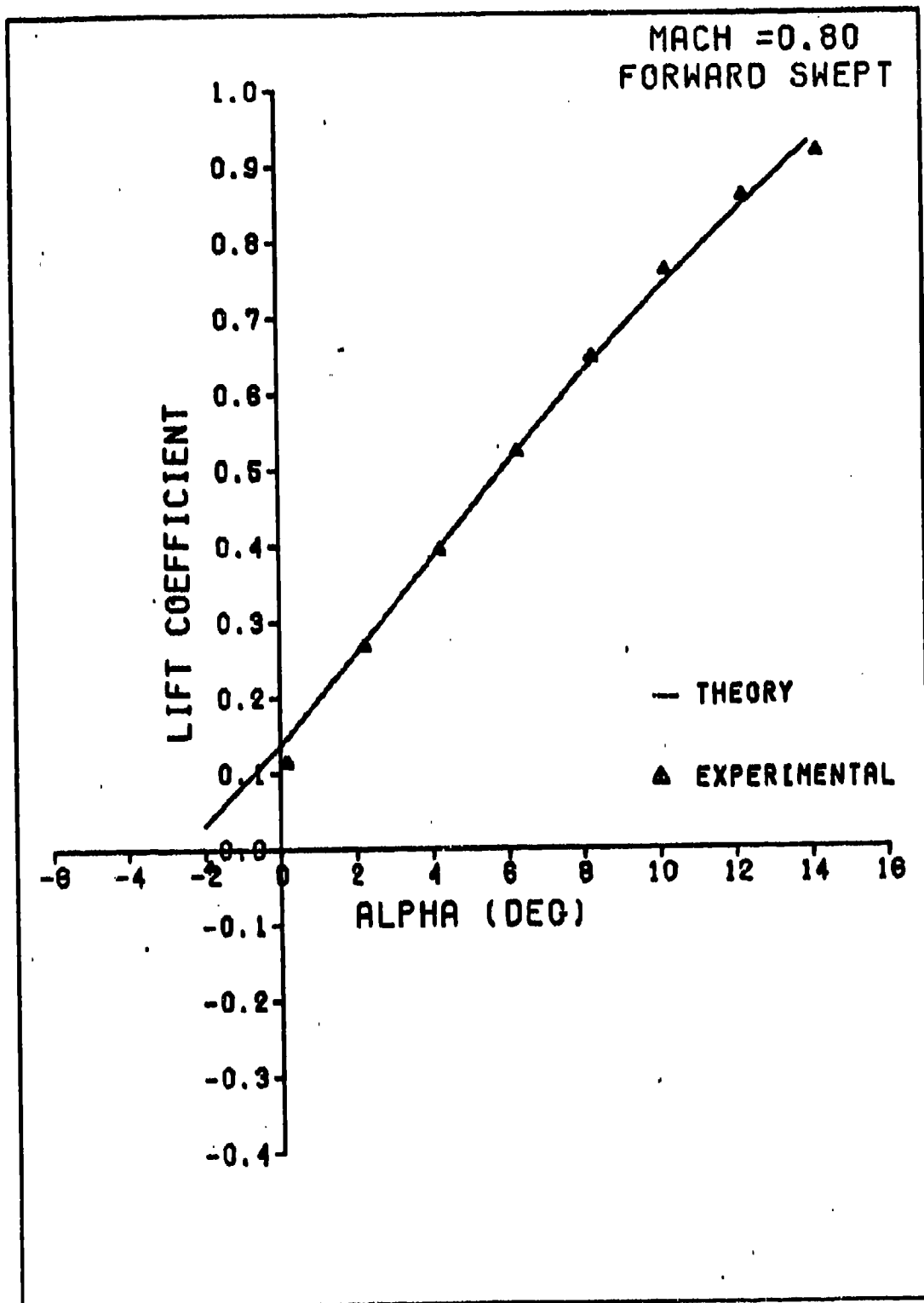


Figure 20. Theoretical  $C_L$  vs  $\alpha$  for the Forward Swept Model at  $M = 0.8$

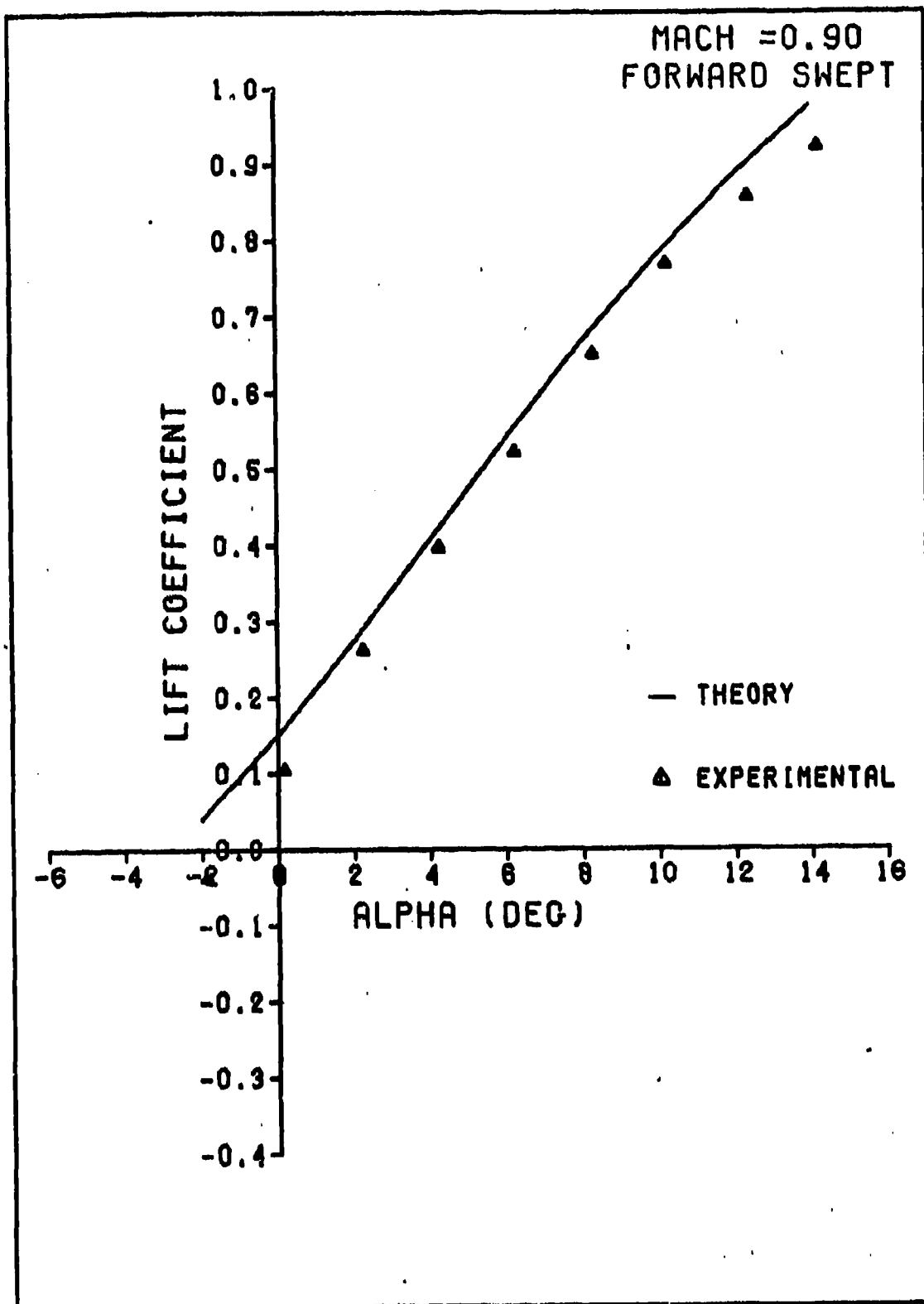


Figure 21. Theoretical  $C_L$  vs  $\alpha$  for the Forward Swept Model at  $M = 0.9$

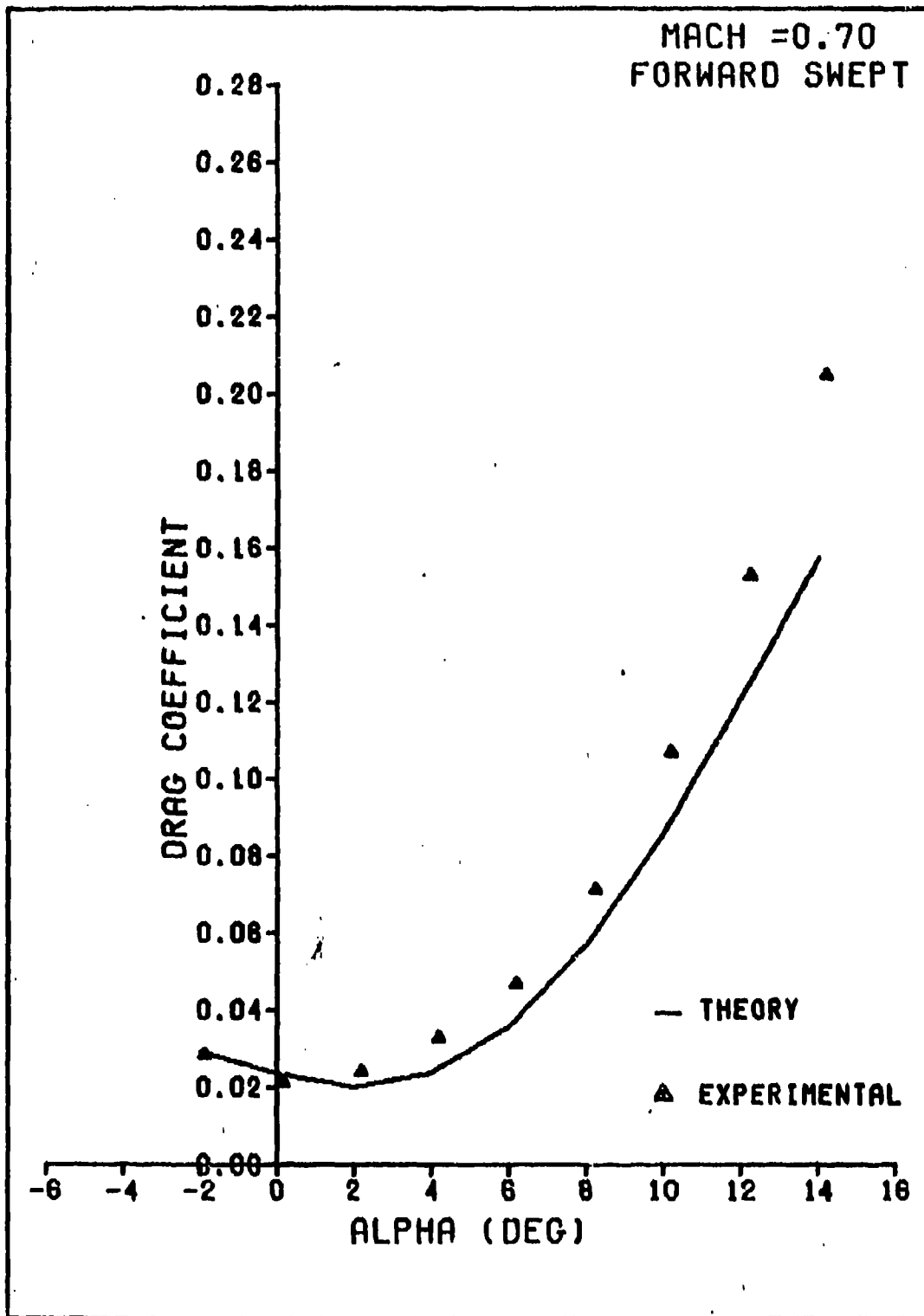


Figure 22. Theoretical  $C_D$  vs  $\alpha$  for the Forward Swept Model at  $M = 0.7$

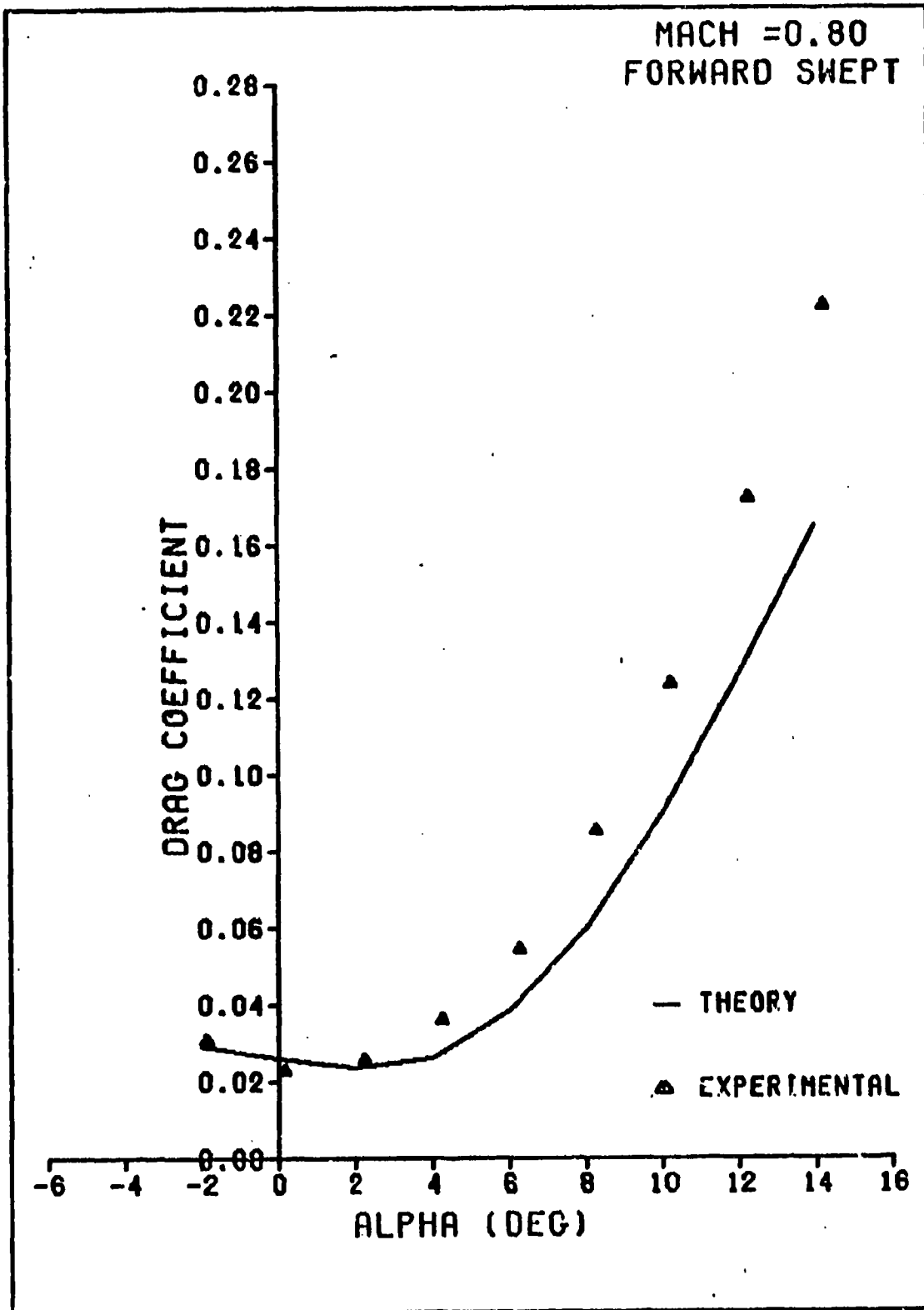


Figure 23. Theoretical  $C_D$  vs  $\alpha$  for the Forward Swept Model at  $M = 0.8$

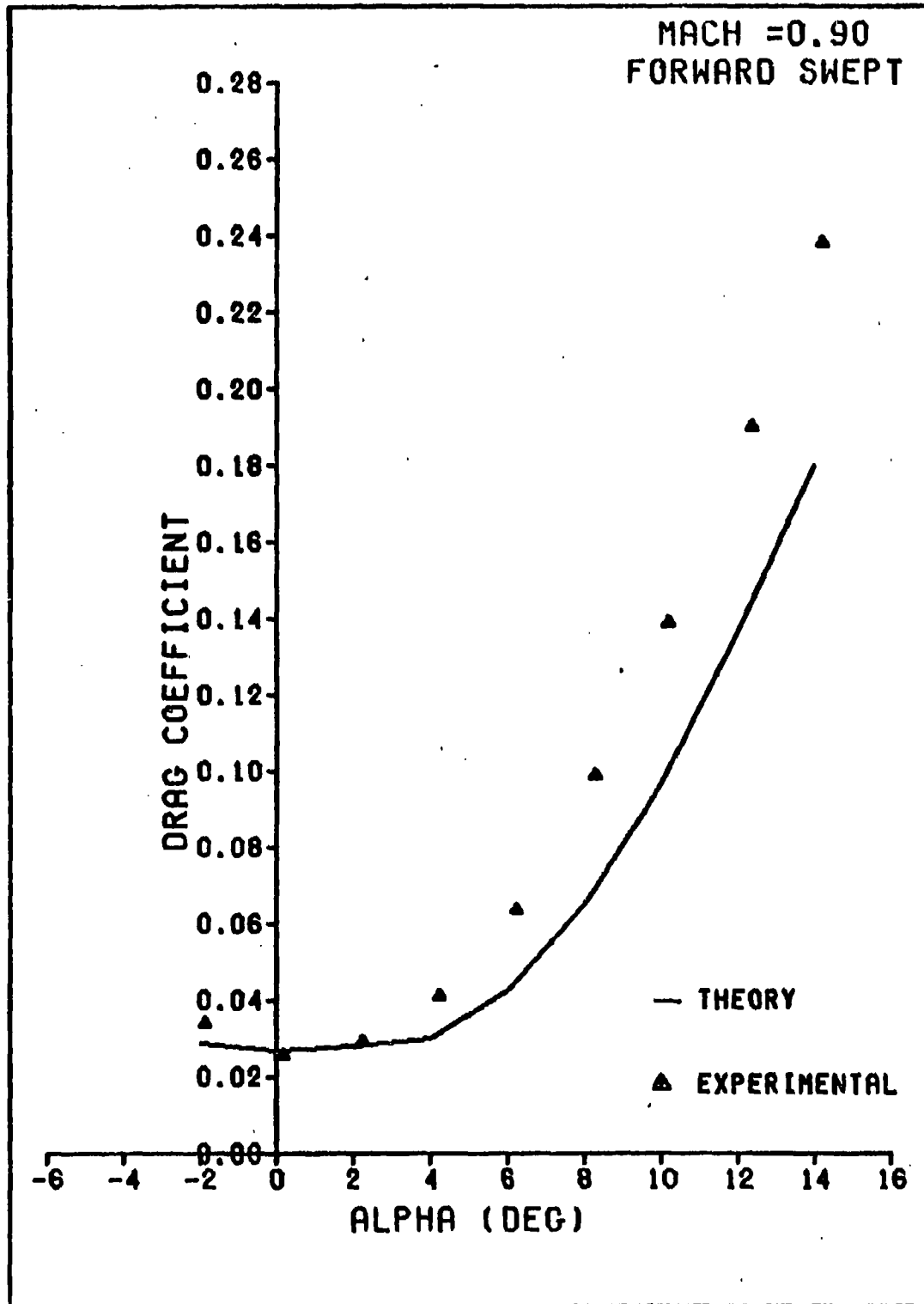


Figure 24. Theoretical  $C_D$  vs  $\alpha$  for the Forward Swept Model at  $M = 0.9$



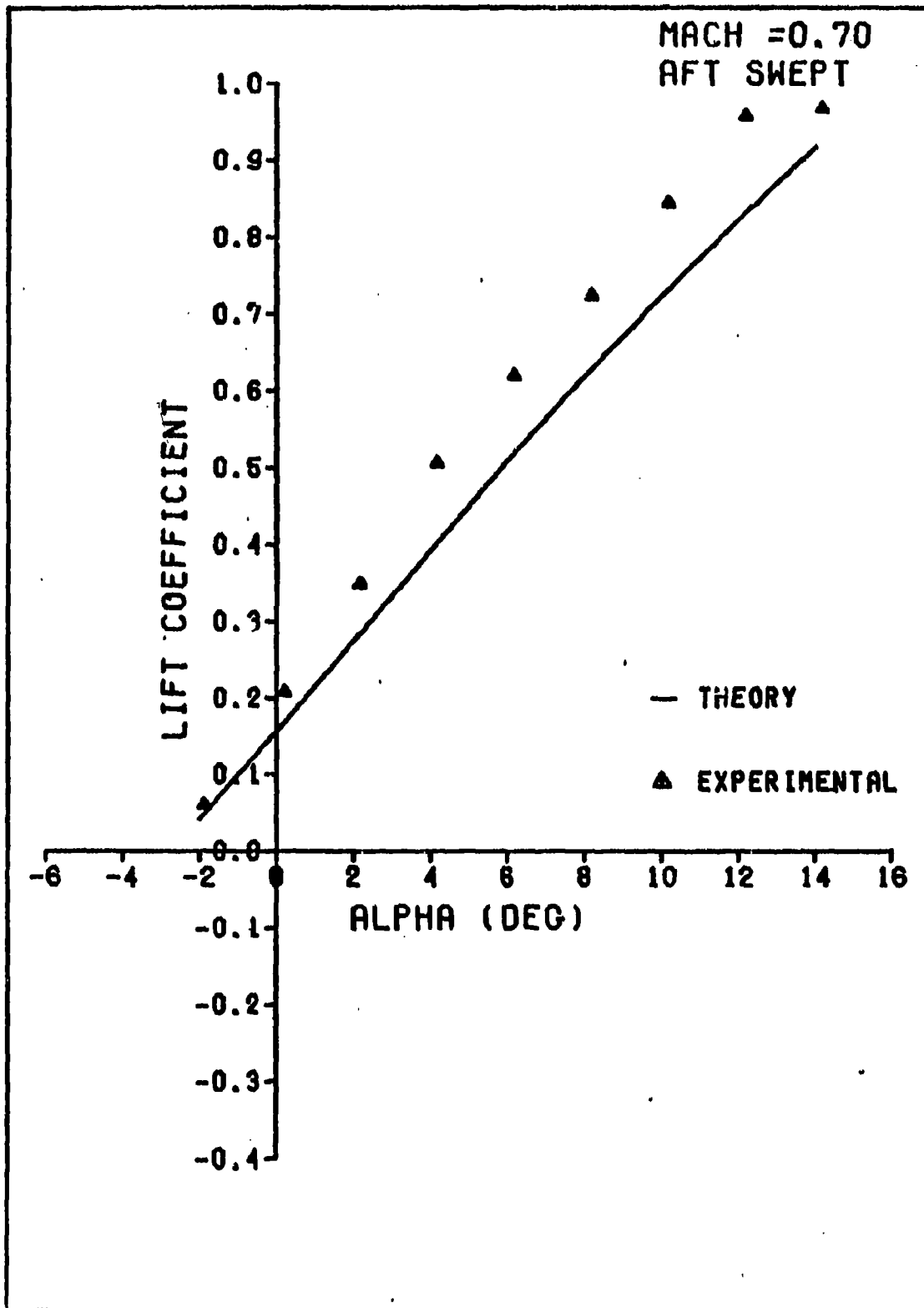


Figure 25. Theoretical  $C_L$  vs  $\alpha$  for the Aft Swept Model at  $M = 0.7$

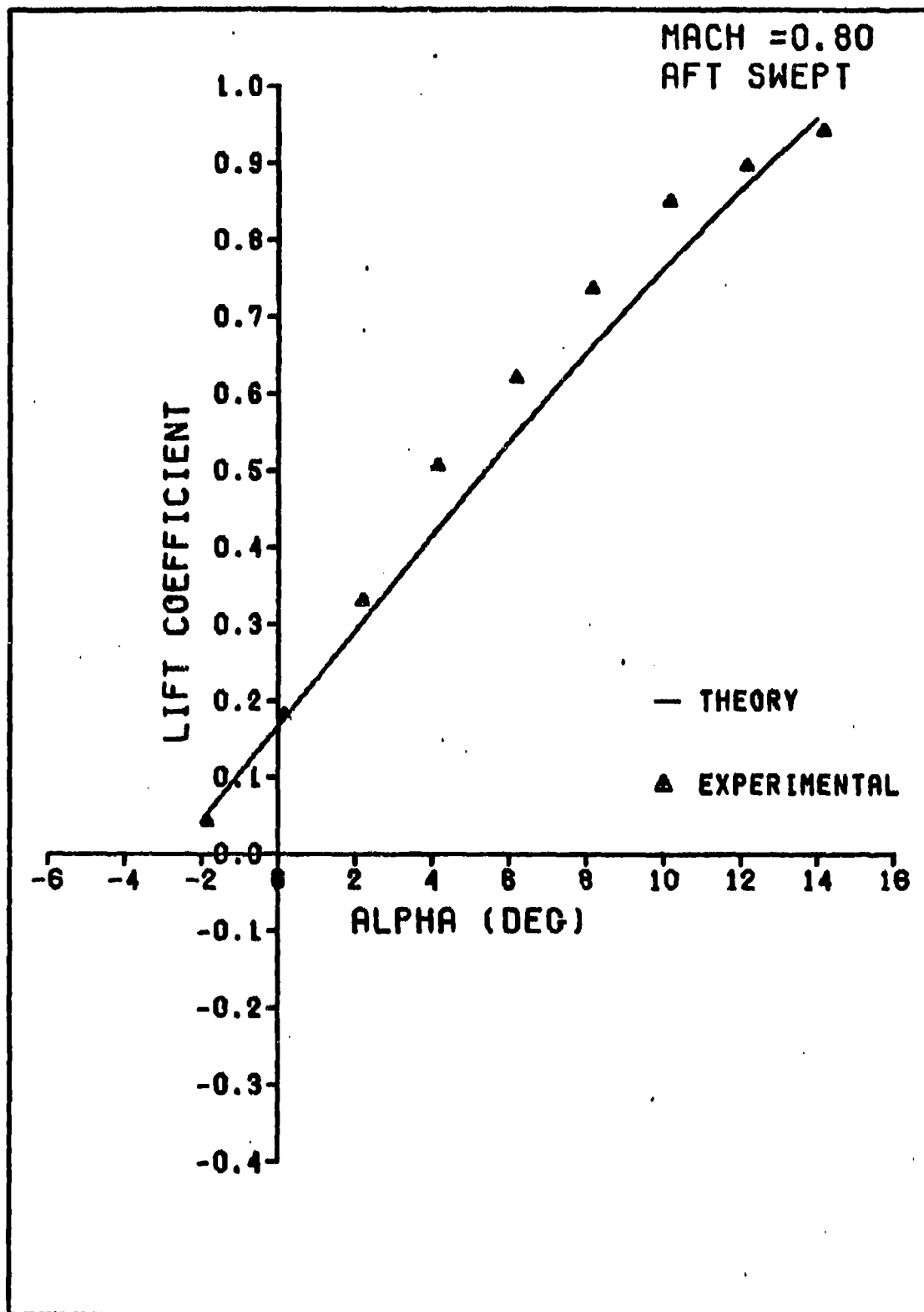


Figure 26. Theoretical  $C_L$  vs  $\alpha$  for the Aft Swept Model at  $M = 0.8$

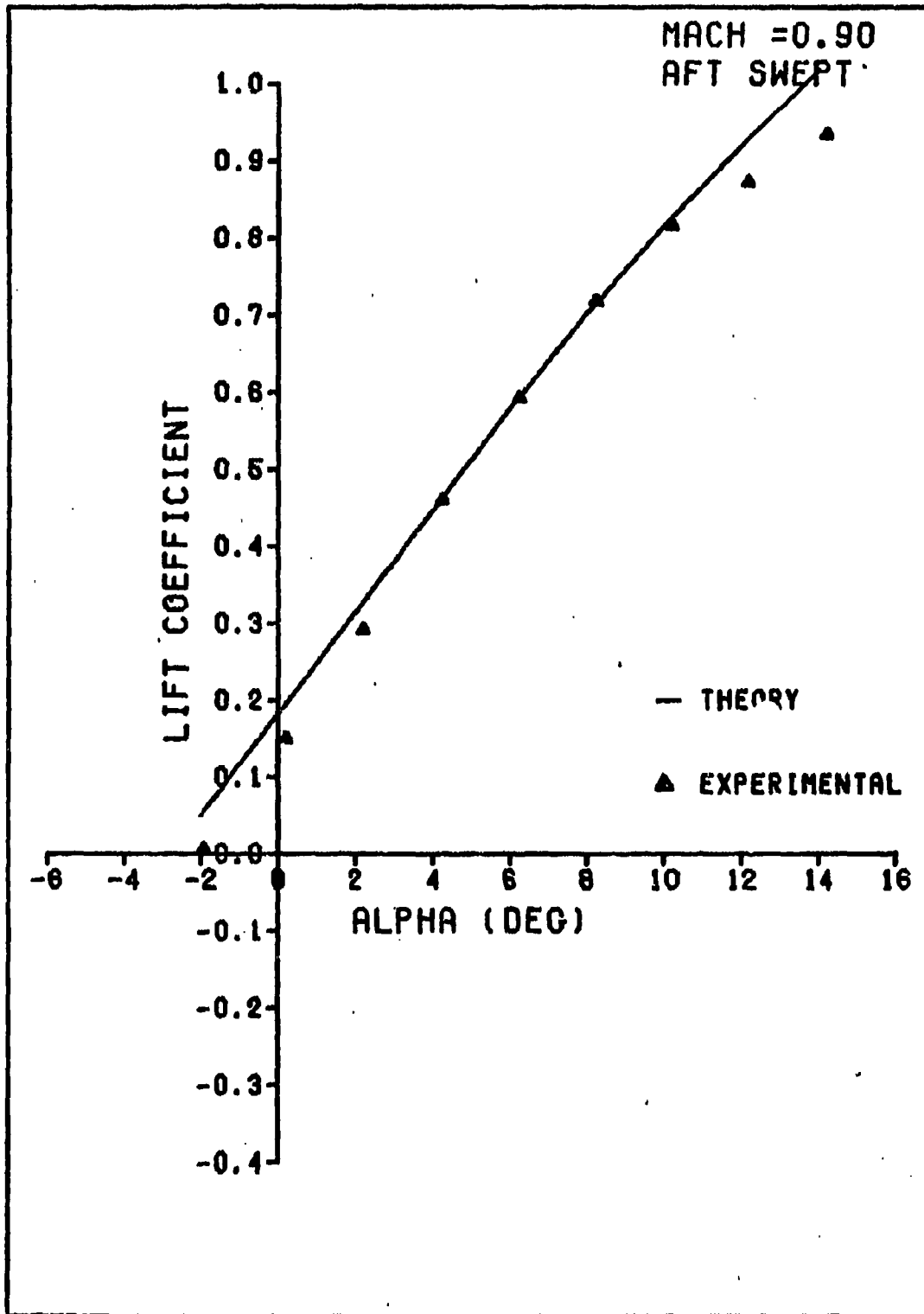


Figure 27. Theoretical  $C_L$  vs  $\alpha$  for the Aft Swept Model at  $M = 0.9$

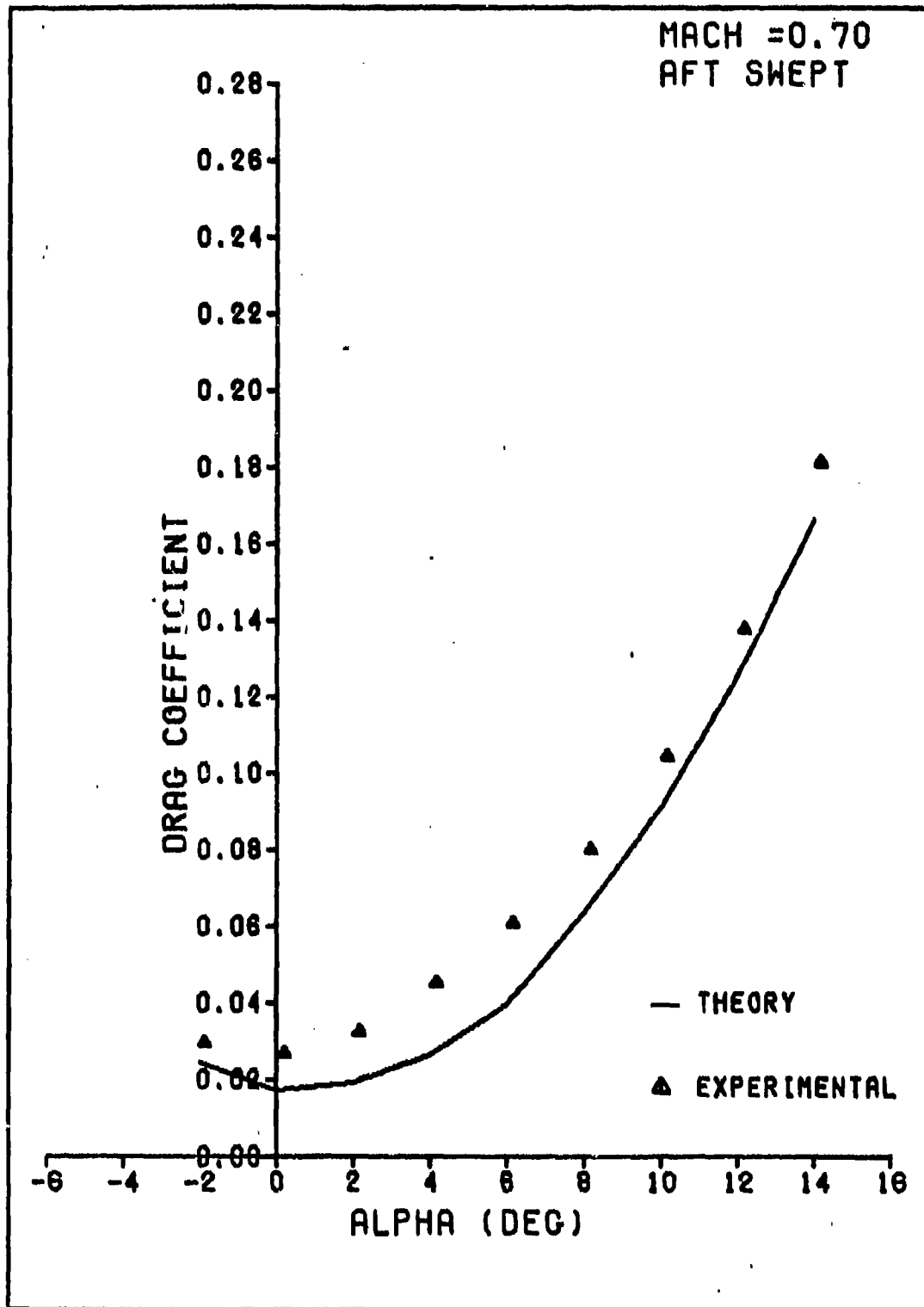


Figure 28. Theoretical  $C_D$  vs  $\alpha$  for the Aft Swept Model at  $M = 0.7$

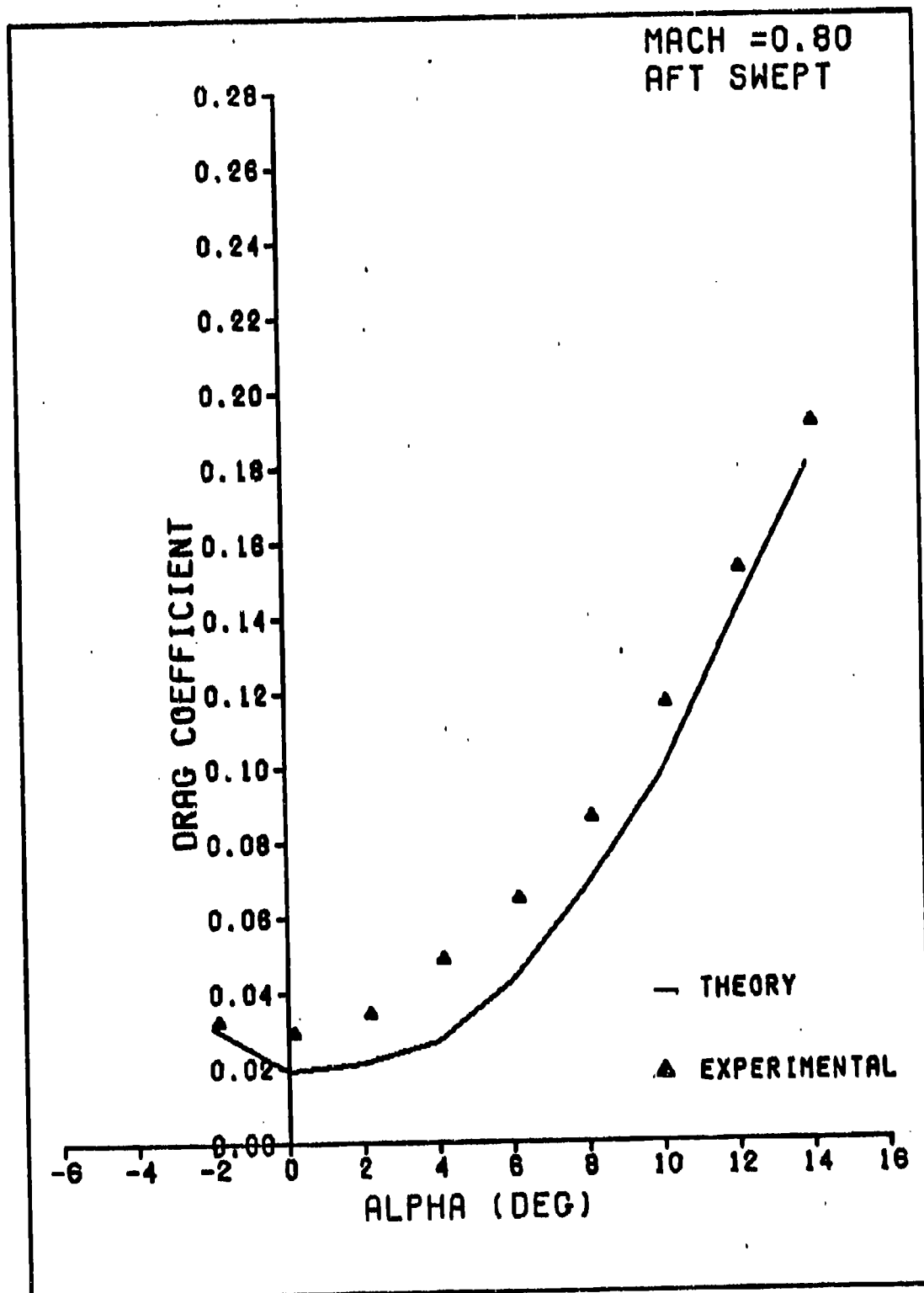


Figure 29. Theoretical  $C_D$  vs  $\alpha$  for the Aft Swept Model at  $M = 0.8$

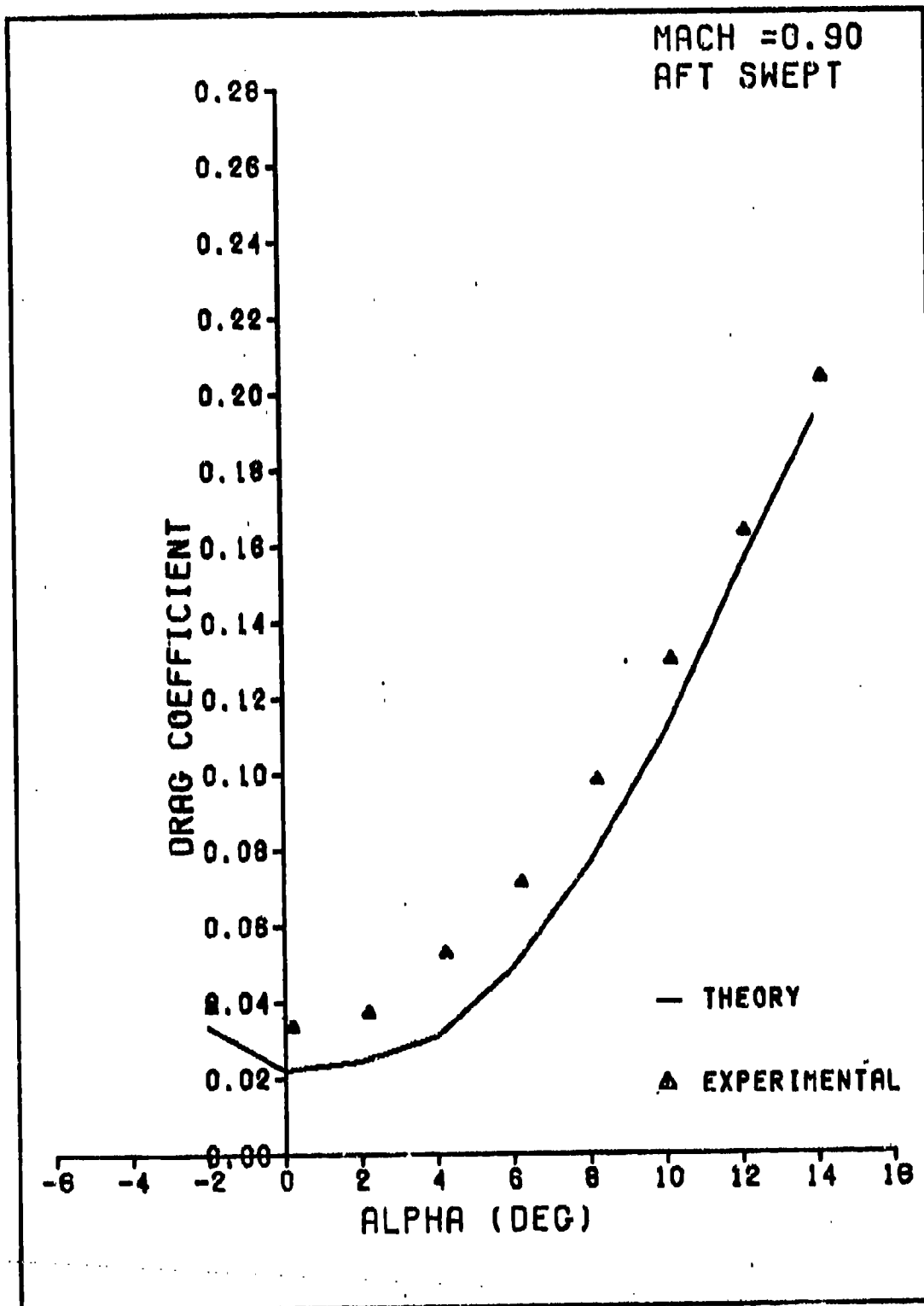


Figure 30. Theoretical  $C_D$  vs  $\alpha$  for the Aft Swept Model at  $M = 0.9$

on these models, the USS Aero program provided well-behaved and consistent data for comparison to experimental results.

### Pressure Distribution

The pressure data obtained from this test are presented as a pressure coefficient,  $C_p$ , plotted as a function of percent chord as shown in Figs 31 to 34. At  $M = 0.63$ , the data produced a smooth curve with no shock present. For  $M = 0.93$ , for the aft swept model, a definite shock can be observed between 70 and 75 percent chord location. For the forward swept model a compression begins at the 70 percent chord location but is gradual and therefore should not be referred to as a shock.

Although not plotted, the five pressure taps located around the leading edge provided data which indicated that even at the highest angle of attack tested, leading edge separation did not occur. Only at negative alphas did separation develop on the lower surface due to the large amount of camber in the airfoil tested. Due to the thinness of the airfoil section, more pressure taps on each wing was not possible. Therefore, a complete pressure distribution including data between the 10 and 50 percent chord locations were not obtained.

### Oil Visualization

The results of the oil flow study can be seen in Figs 35 through 40. Figure 35 shows the aft swept wing at

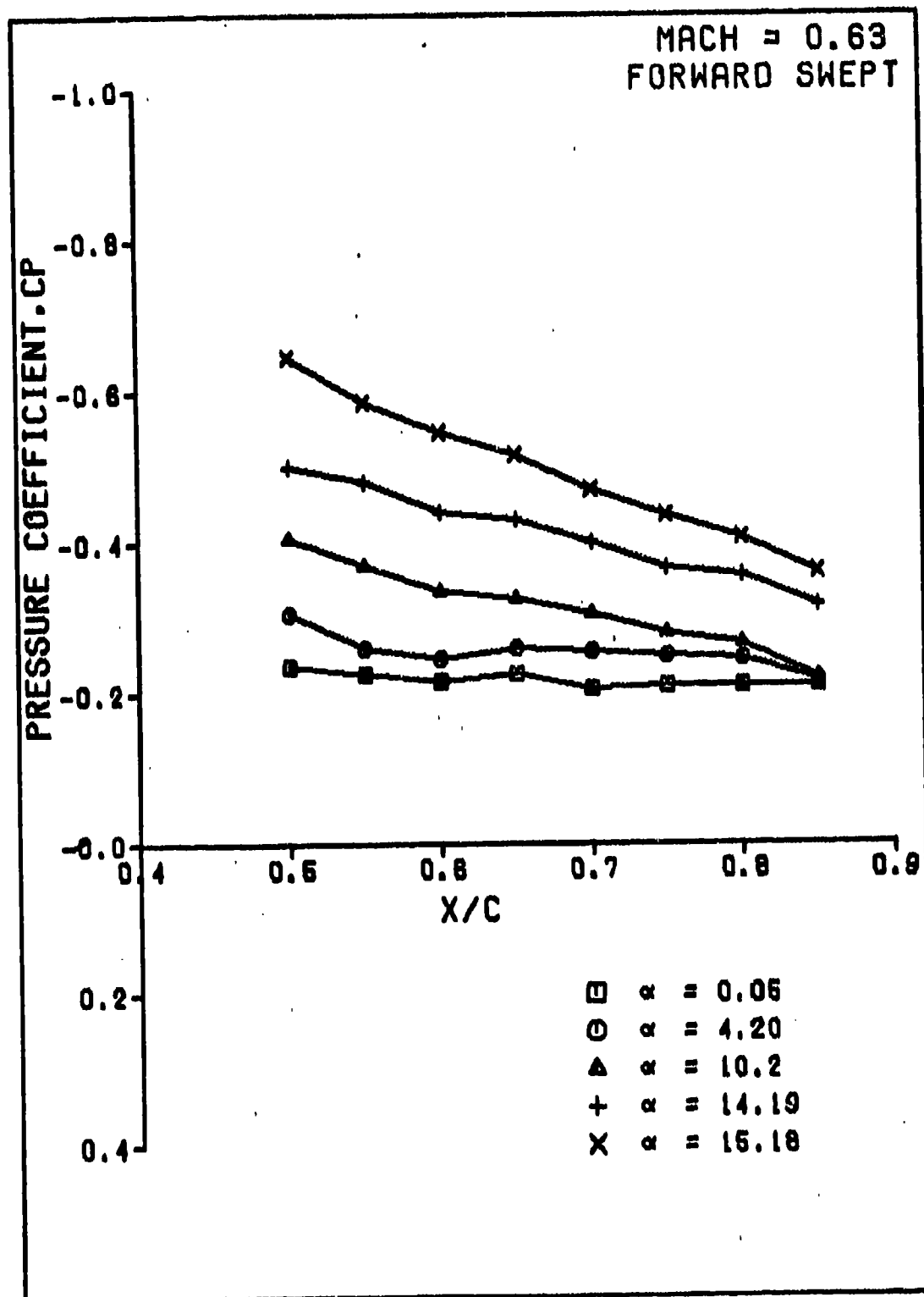


Figure 31.  $C_p$  vs  $X/C$  for the Forward Swept Model at  $M = 0.63$



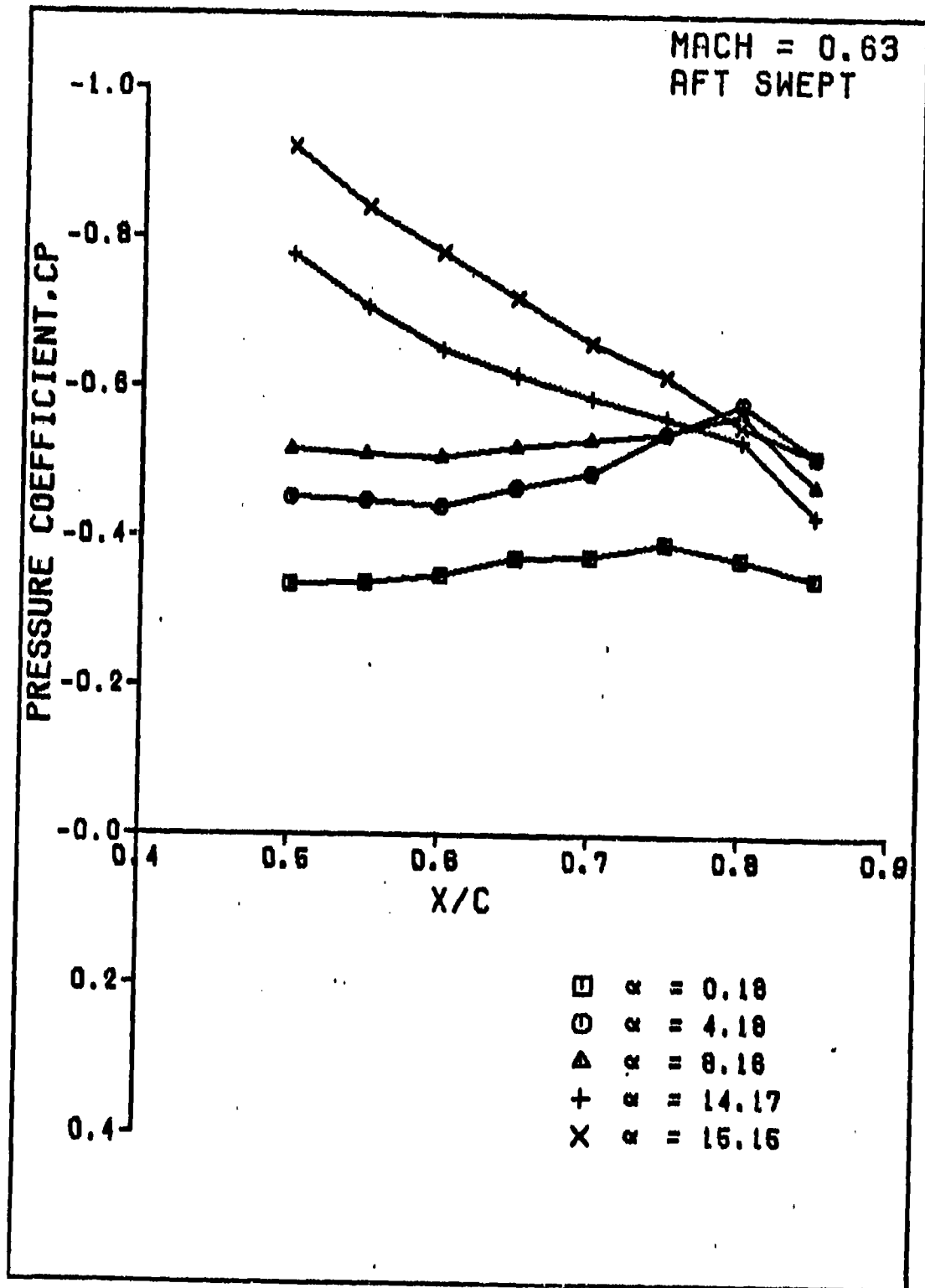


Figure 32.  $C_D$  vs  $X/C$  for the Aft Swept Model at  $M = 0.63$

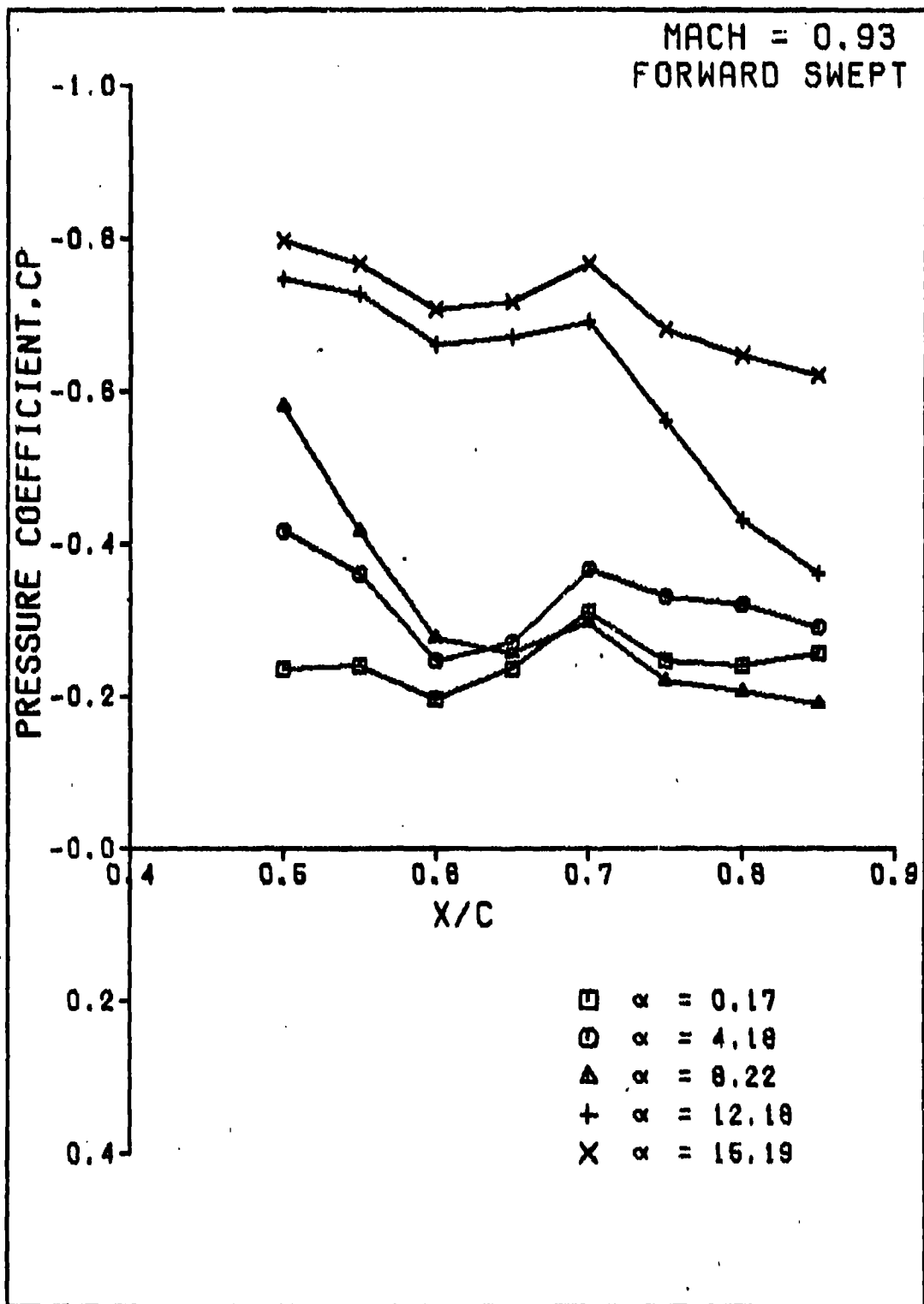


Figure 33.  $C_p$  vs  $X/C$  for the Forward Swept Model at  $M = 0.93$

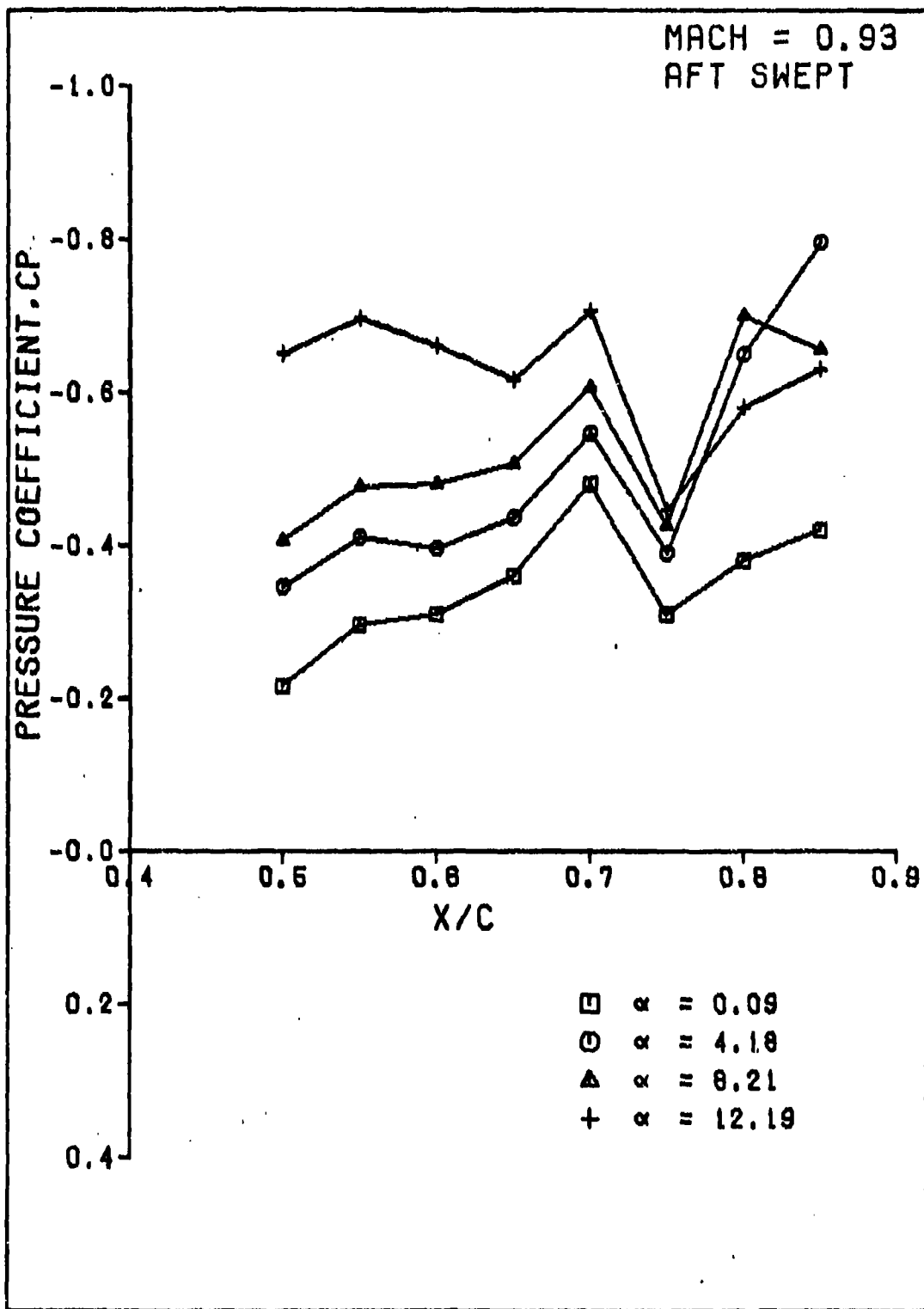


Figure 34.  $C_p$  vs X/C for the Aft Swept Model at  $M = 0.93$

$\alpha = 4$ ,  $M = 0.63$ . Compare this to Fig 36, the forward swept wing at  $\alpha = 4$ ,  $M = 0.63$ , and it is apparent that neither wing displays any flow separation. Some spanwise flow can be seen on the forward swept oil photograph but it is not known whether the aft swept model produced spanwise flow also. Note that a thin section on each wing appearing about mid-span is due to tape used to protect the pressure taps and is not an aerodynamic phenomena. Figure 37 and Fig 38 present the aft swept model at  $\alpha = 10$ ,  $M = 0.63$  and the forward swept model at the same conditions. The wing tip of the aft swept wing and the root of the forward swept wing show indications of flow separation. Note that the flow inward along the trailing edge of the forward swept wing is more pronounced than before.

Figures 39 and 40 show the same wings at  $\alpha = 10$ ,  $M = 0.93$ . The flow separation has developed into a full stall on the tip of the aft swept wing and on the root of the forward swept wing with flow reversal apparent. The flow on the outboard section of the forward swept wing remains attached even at an angle of ten degrees.

The interference of the body on each wing could not be determined since photographs of each model had to be taken at an angle from the tip. Flow patterns near the root chord were not clearly visible on either model.

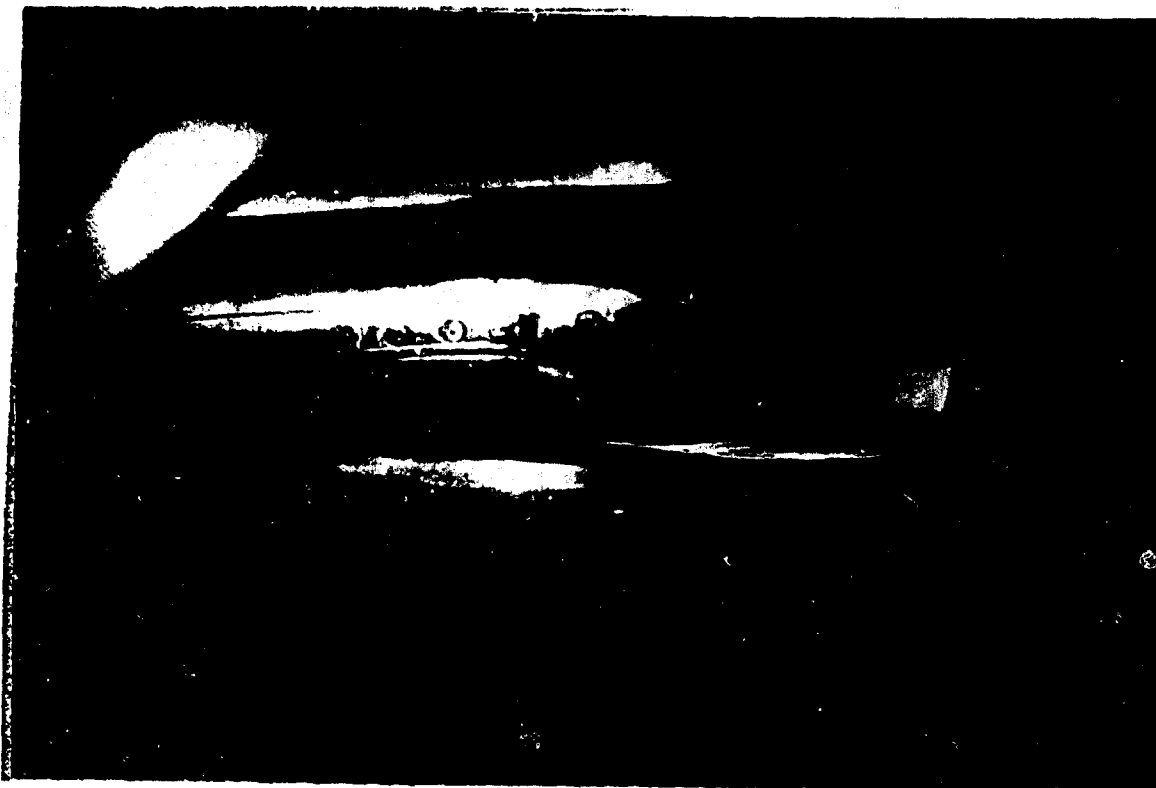


Figure 35. Oil Flow of Forward Swept Wing at  
 $M = 0.63$  ,  $\alpha = 4$  , Flow Right to Left

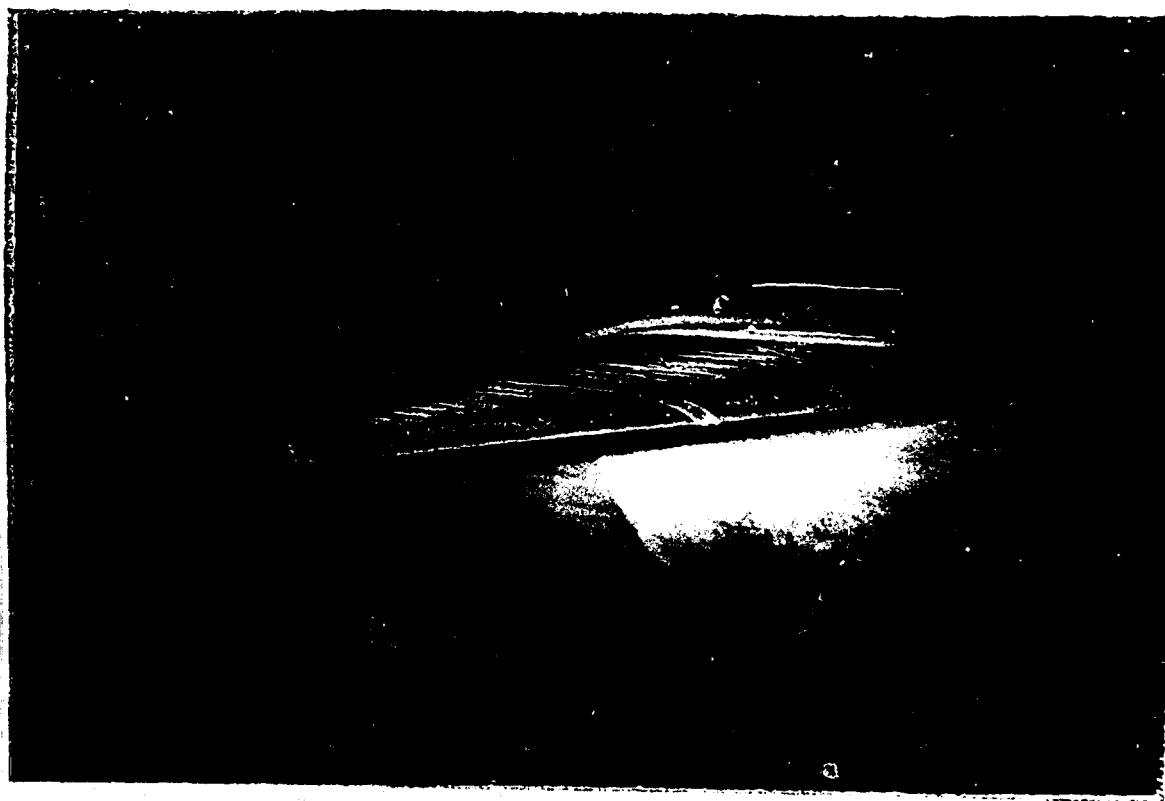


Figure 36. Oil Flow of Aft Swept Wing at  
 $M = 0.63$  ,  $\alpha = 4$  , Flow Right to Left

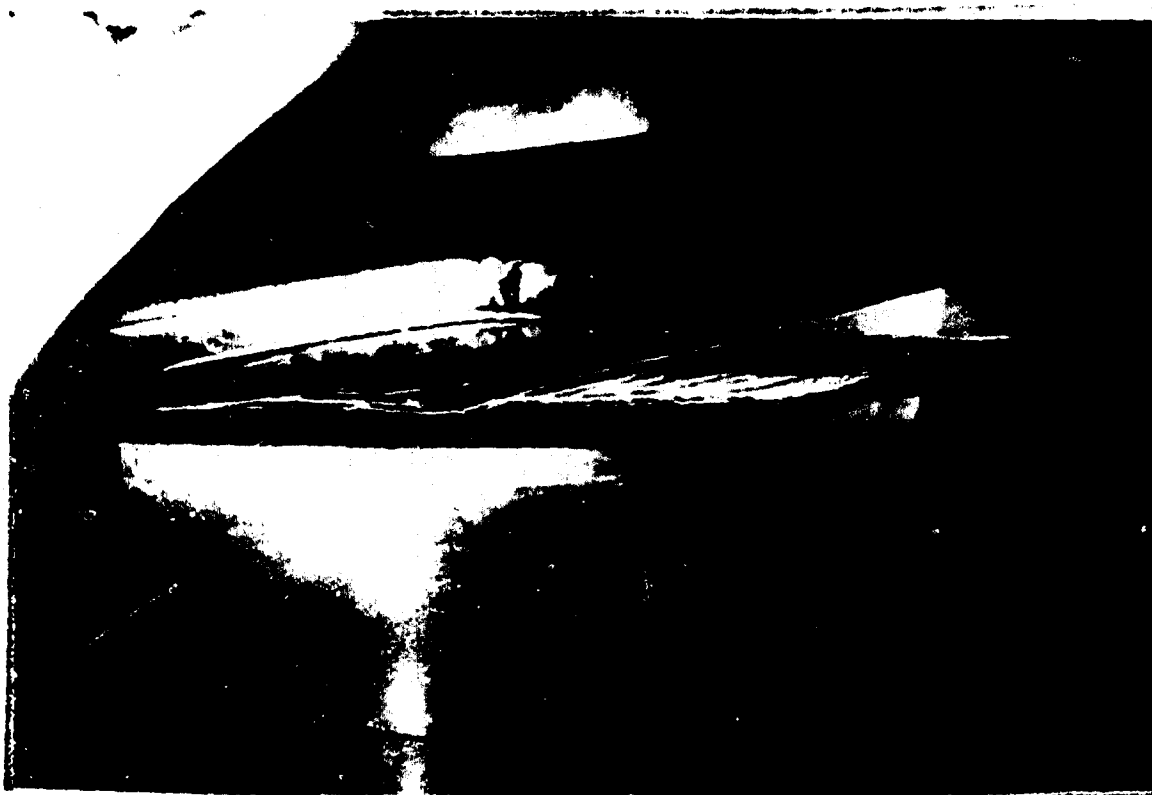


Figure 37. Oil Flow of Forward Swept Wing at  
 $M = 0.63$  ,  $\alpha = 10$  , Flow Right to Left

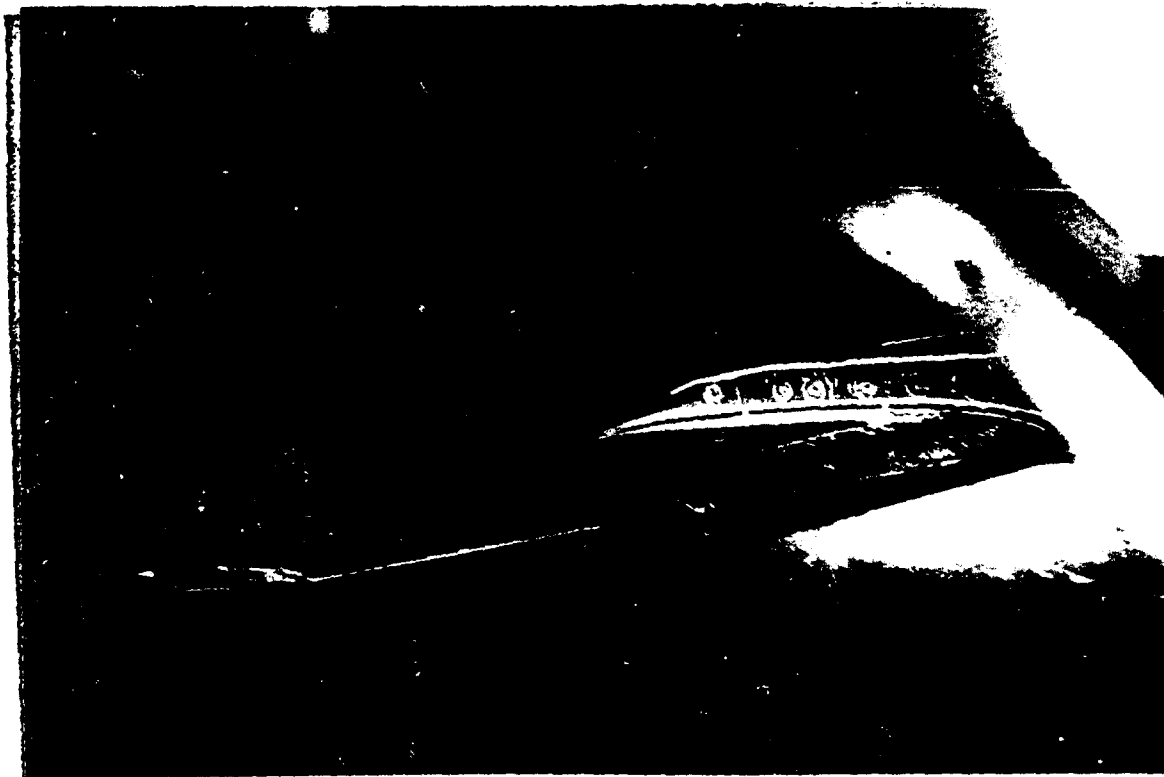


Figure 38. Oil Flow of Aft Swept Wing at  
 $M = 0.63$  ,  $\alpha = 10$  , Flow Right to Left

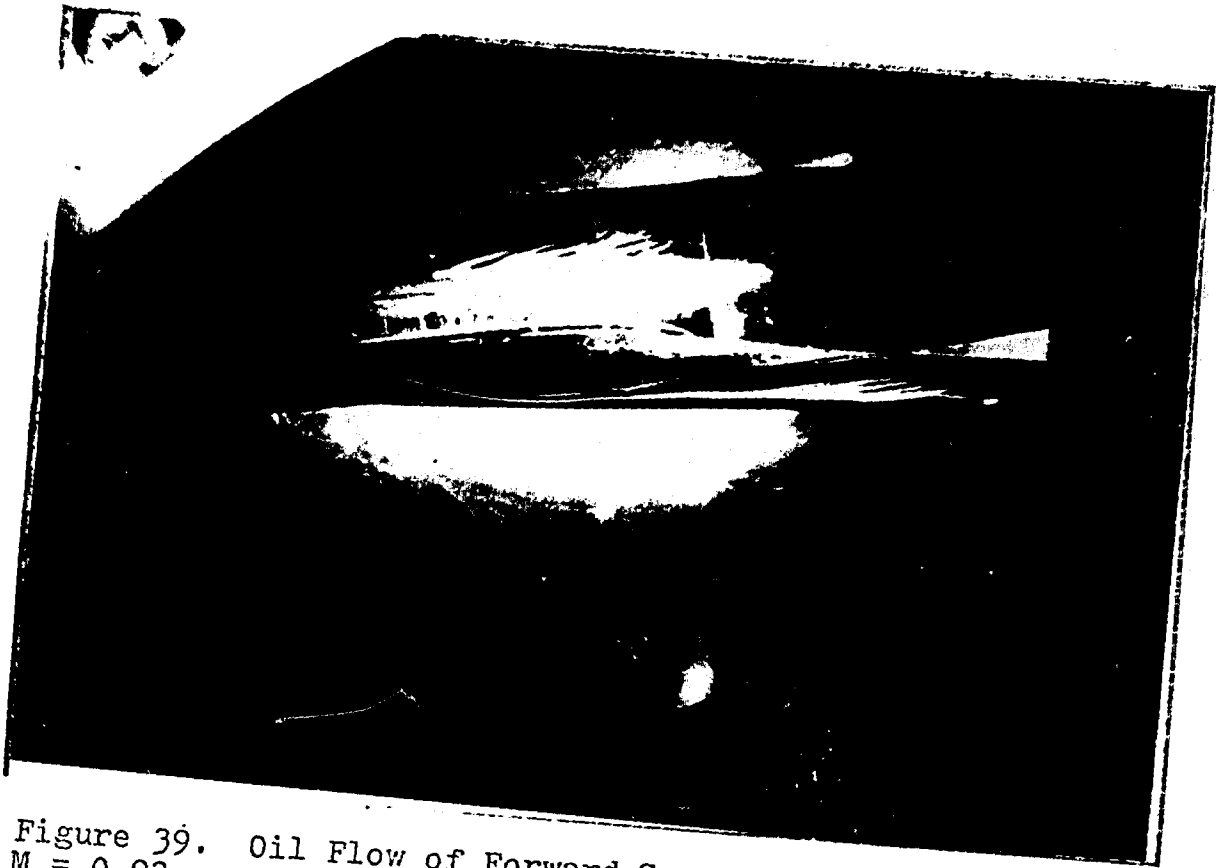


Figure 39. Oil Flow of Forward Swept Wing at  
 $M = 0.93$  ,  $\alpha = 10$  , Flow Right to Left

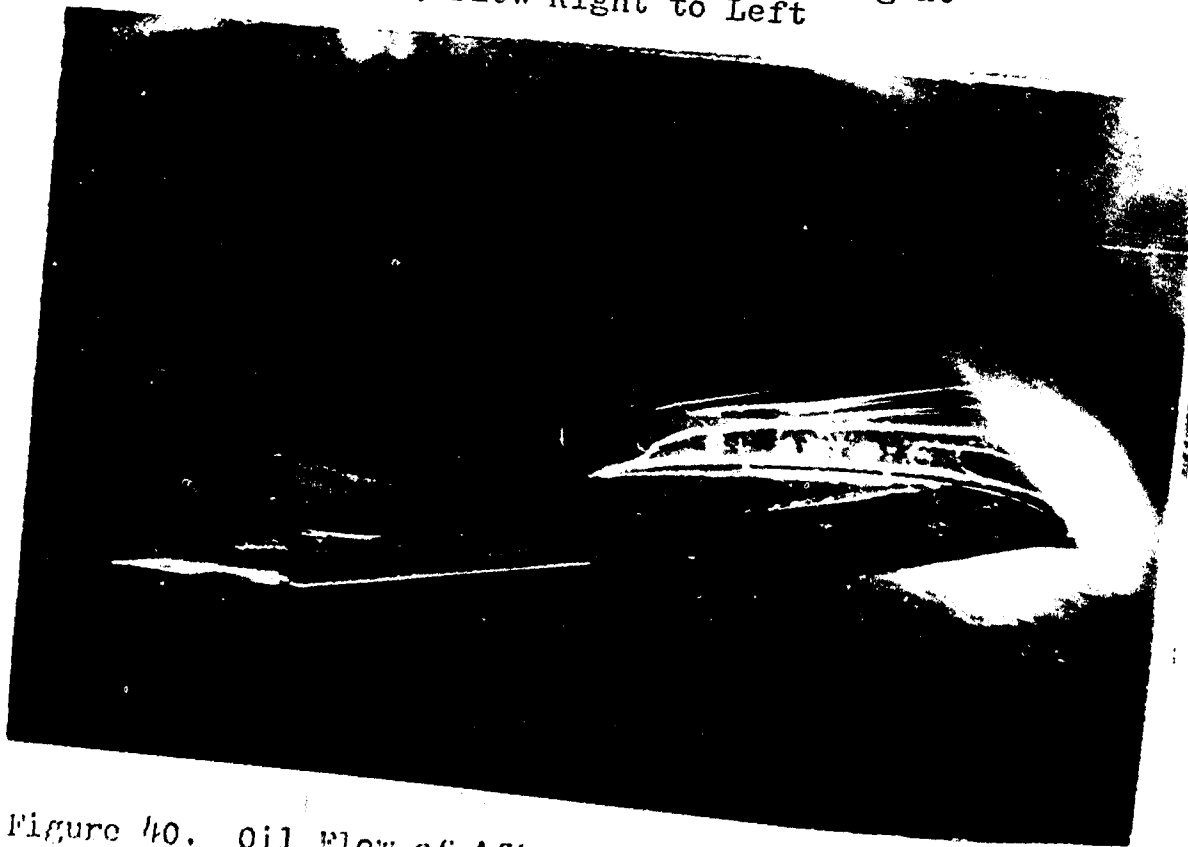


Figure 40. Oil Flow of Aft Swept Wing at  
 $M = 0.93$  ,  $\alpha = 10$  , Flow Right to Left

## VI. Conclusions and Recommendations

### Conclusions

The following conclusions were drawn based upon the results of the wind tunnel tests as discussed in Section V.

1. It was concluded that the data obtained in this study was reliable and accurate as indicated by the numerous tests for repeatability and data comparisons with the USS Aero Program.

2. It was concluded that the highly cambered, super-critical airfoil alleviated any problem of leading edge separation for this configuration. Since both models did not experience any leading edge separation effects, the stall indications were delayed to the point of neither wing stalling even at an angle of attack of fifteen degrees.

3. It was concluded that the forward swept wing was capable of a higher useable angle of attack than the aft swept wing. For each Mach number tested, the lift coefficient obtained for the aft swept wing was matched by the forward swept wing but required a higher angle of attack. When the aft swept wing began to stall, the forward swept wing lift curve continued to increase up to the highest angle of attack tested. The actual stall of each wing was above fifteen degrees so the extent of increase in useable angle of attack could not be determined.

4. It was concluded that the drag coefficient for the forward swept wing was consistently lower than the similar



aft swept wing for lift coefficients below approximately 0.50 which corresponds to an angle of attack less than eight degrees alpha. This indicates that the forward swept wing could be used more efficiently than the aft swept wing for normal cruise flight operations, thus requiring less fuel.

### Recommendations

The following recommendations follow from the results of the wind tunnel tests:

1. The USS Aero Program correctly predicts the trends in the aerodynamic characteristics of the configurations tested. It is recommended that the USS Aero Program be used to predict the effects of small design changes and these predictions be used to adjust the wind tunnel data.

2. It is recommended that the location of the forward swept wing be moved aft of the present location to obtain a stable pitching moment configuration. The longitudinal stability coefficients could then be studied to determine the size, shape, and location of a canard surface.

3. The oil flow study indicated that a large portion of the root section of the forward swept wing had lost its effectiveness due to flow separation. It is recommended that the use of a forward swept canard in conjunction with the forward swept wing be tested to determine its effect upon maintaining attached flow at higher angles of attack.

The use of winglets should also be considered to determine their effect on the aerodynamic characteristics.

4. It is recommended that the data obtained from this study be used as a basis for a performance study of a forward swept wing aircraft. Advantages and/or disadvantages of the forward swept wing could be identified to support the development of a forward swept wing aircraft.

## Bibliography

1. Armed Forces Supply Support Center. Strength of Metal Aircraft Elements, Military Handbook 5A, March 1965.
2. Corning G. Supersonic and Subsonic Airplane Design. Ann Arbor, Michigan: Braun-Brumfield, Inc., 1970.
3. Klein, G.J. Development of a Half-Span Model Test System for the AFFDL-TGF, Contract F-33615-74-C-3085, Vol 1, Ft. Worth, Texas: General Dynamics Corporation Sept. 1975.
4. Krone, N.J. Divergence Elimination With Advanced Composites. AIAA Paper 75-1009, August, 1975.
5. Lawrence, J.R. Development of a Half-Span Model Test System For The AFFDL-TGF, Contract F-33615-74-C-3085, Vol. 2, Ft. Worth, Texas: General Dynamics Corporation, September 1975.
6. McCormack, G.M. and W.L. Cook, A Study of Stall Phenomena on a 45 Degrees Swept Forward Wing, NACA Technical Note 1797, Washington: National Advisory Committee for Aeronautics, January 1949.
7. Middleton, M.D. and J.L. Lundry, A Computational System For Aerodynamic Design and Analysis, NASA Contractor Report 2715, Washington: National Aeronautics and Space Administration, July 1976.
8. Pope, A. Wind Tunnel Testing. New York: John Wiley and Sons, Inc., 1961.
9. -----, and K.L. Goin, High Speed Wind Tunnel Testing, New York: John Wiley and Sons, Inc., 1965.
10. Roskam, J. Flight Dynamics of Rigid and Elastic Airplanes. Kansas: Roskam Aviation and Engineering Corporation, 1975.
11. Roark, R.J. and W.C. Young. Formulas for Stress and Strain (5th Edition). New York: McGraw-Hill Book Company, 1975.

12. White, H.L., Trisonic Gasdynamic Facility User Manual. Task Number 14760401. Wright-Patterson Air Force Base, Ohio: Air Force Flight Dynamics Laboratory, June 1973.
13. Woodward, F.A. An Improved Method For the Aerodynamic Analysis of Wing-Body-Tail Configurations in Subsonic and Supersonic Flow. NASA Contractor Report-2228, Part I, Washington: National Aeronautics and Space Administration, May 1973.

APPENDIX A  
MODEL STRESS ANALYSIS

## Appendix A

### Model Stress Analysis

A stress analysis of the two newly constructed wings was required to insure they could withstand the loads expected during the wind tunnel tests. A rather stringent ultimate factor of safety of 4.0 was required to insure against model failure. Each model was analyzed and evaluated against this criterion. Two basic assumptions, which tend to yield conservative estimates, were used throughout this analysis. First, the pressure distribution across the wing was assumed uniform. Secondly, the entire load of the wing was assumed concentrated at the centroid of the wing instead of the theoretical center of pressure. Both assumptions produce higher bending moments and tip loads than would be expected.

#### Design Loads

The maximum aerodynamic loads expected for each wing was determined using a value of  $C_{L_{max}} = 1.0$ , which was obtained from previous two-dimensional tests of the supercritical airfoil. The maximum aerodynamic lift is:

$$L = C_{L_{max}} q S \quad (1)$$

where  $q$  is the dynamic pressure and the reference area,  $S = 0.2393 \text{ ft}^2$ . The maximum dynamic pressure in this test,

which occurred at  $M = 0.93$ , is given by:

$$q = \frac{K}{2} P M^2 \quad (2)$$

where  $K$  is the ratio of specific heat,  $M$  is the Mach number, and  $P$  is the static pressure. The relationship for static pressure is given by:

$$P = P_0 \left( 1 + \frac{M^2}{5} \right)^{-\frac{K}{K-1}} \quad (3)$$

where  $P_0$  is the total pressure. Using Fig 14 of Ref 12, the total pressure of the tunnel can be found as a function of Mach number and Reynolds number. The maximum load for this test occurred at  $M = 0.93$  and  $R = 2,000,000$  per foot at which  $P_0 = 1000$ psf. Using Eq (2) and Eq (3), the maximum dynamic pressure was computed as 346.4 psf.

Referring to Fig 41, the maximum aerodynamic load is shown to be a function of angle of attack given by:

$$N = \frac{L}{\cos \alpha} \quad (4)$$

where  $N$  is the maximum normal aerodynamic force,  $L$  is 82.9 lbf from Eq (1), and  $\alpha$ , the angle of attack, is fifteen degrees. This yields a maximum aerodynamic load of 85.8 lbf.

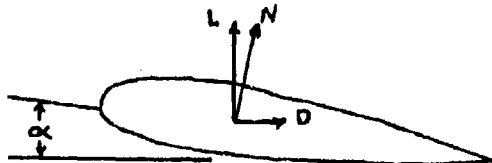


Figure 41. Load Diagram of Wing Section.

The average pressure acting over the entire wing from assumption one, is:

$$P_{AVG} = \frac{N}{S} \quad (5)$$

where S, the reference area, is 0.2393 ft<sup>2</sup>. In this analysis, loads were considered at section A-A, where the bending moment is maximum, and at section B-B, where the steel insert ended and only epoxy carried the loads as shown in Fig 42 and Fig 43.

### Section A-A

#### Bending Stress.

For both the forward and aft swept wings, since the planform area was identical, the force acting outboard of section A-A is given by:

$$N_{A-A} = P_{AVG} S_A \quad (6)$$

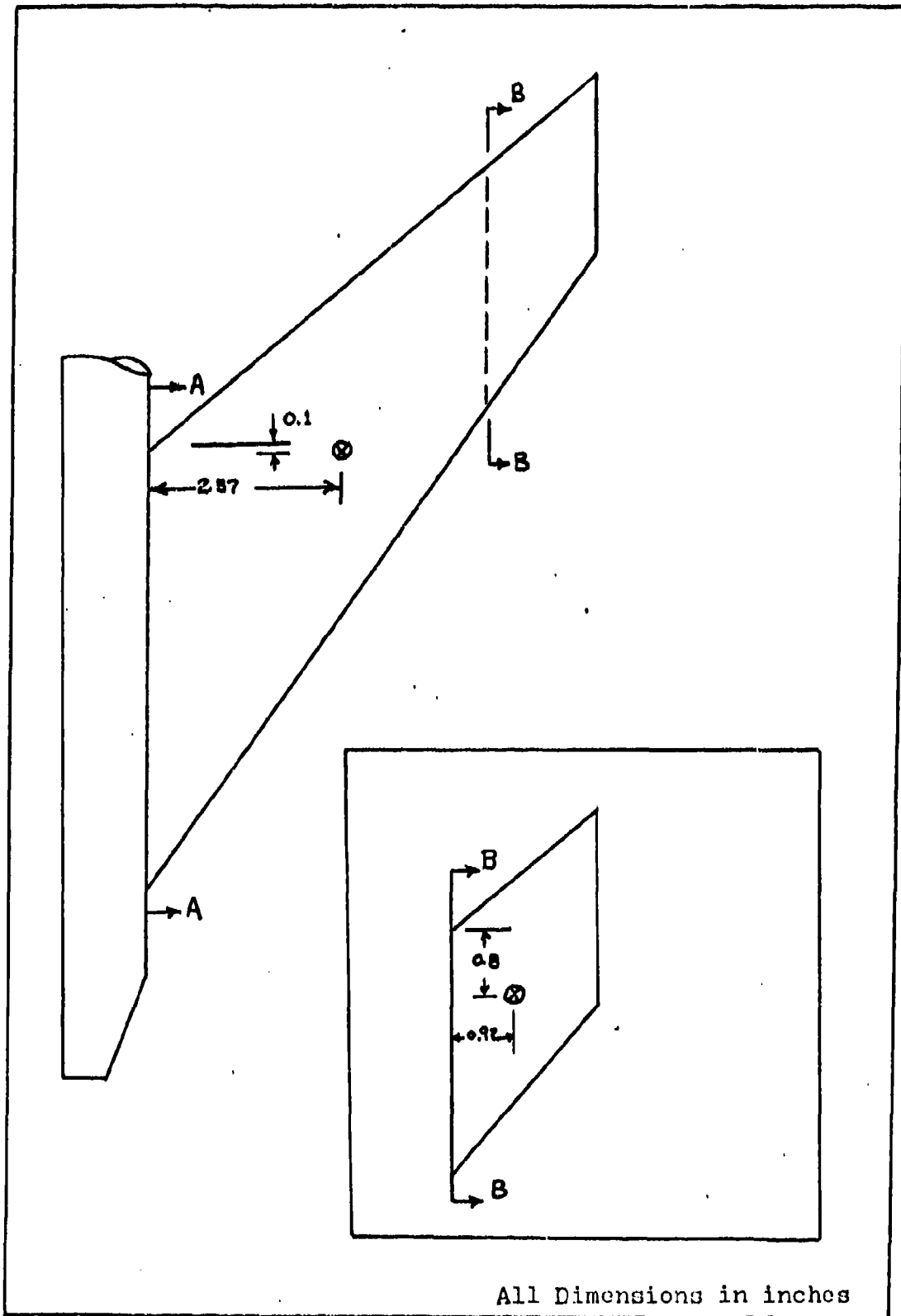
where S<sub>A</sub>, the area outboard of A-A, is 0.1786 ft<sup>2</sup>. A normal force equal to 64.2 lbf is obtained using Eq (6).

For the bending moment at section A-A, the following equation was used:

$$M_{A-A} = N_{A-A} \bar{Y}$$

where  $\bar{Y}$  from Fig 42 and Fig 43 is 2.57 inches for both wings. This results in a bending moment of 165 inch-lbf at this section.





All Dimensions in inches

Figure 42. Schematic of Forward Swept Wing used for Stress Analysis

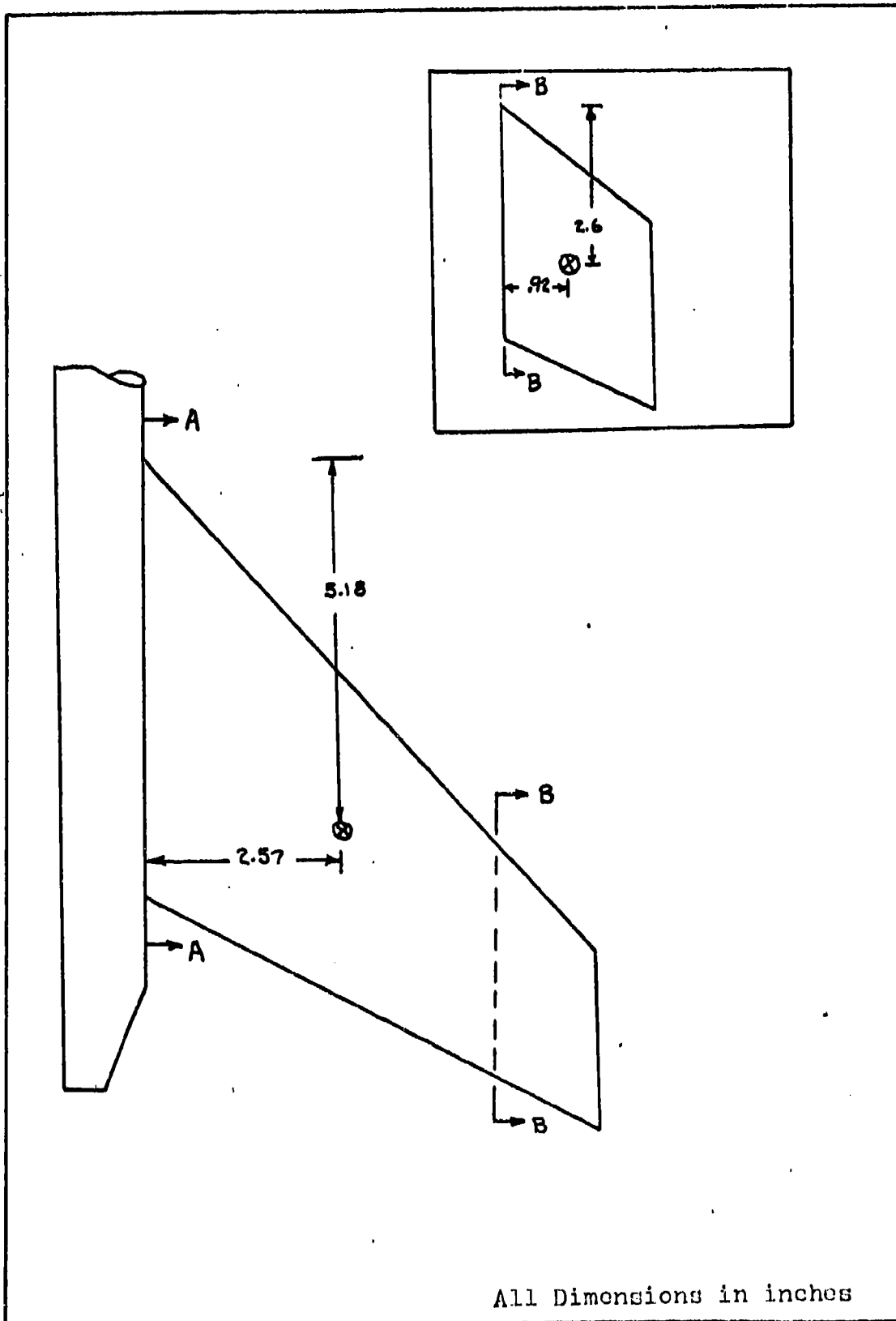


Figure 43. Schematic of Aft Swept Wing used for Stress Analysis

To evaluate the stresses at section A-A, the steel insert was modeled as a thin beam shown in Fig 44:

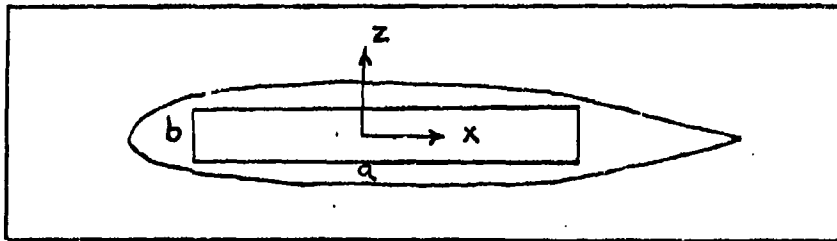


Figure 44. Wing Modeled as a Thin Beam.

An expression for the moment of inertia about the x-axis is given by:

$$I_x = \frac{a b^3}{12} \quad (7)$$

where a and b are the dimensions of the beam. At any point on the cross-section, the bending stress  $\sigma$  is given by:

$$\sigma = \frac{M}{I_x} Z \quad (8)$$

where  $Z = b/2$ , for the maximum stress at the surface. Substituting Eq (7) into Eq (8) yields the expression:

$$\sigma_{max} = \frac{6 M}{a b^2} \quad (9)$$

which gives the maximum stress on the beam. The insert dimensions at section A-A are 3.125 by 0.125 inches. This yields a maximum bending stress of 21,120 lbf/in<sup>2</sup> for both forward and aft swept wings.

### Shearing Stress.

The maximum shearing stress, using the same thin beam model in Fig 44, is given by:

$$\tau_{MAX} = T \left( \frac{3a + 1.8b}{a^2 b^2} \right) \quad (10)$$

where T, the twisting moment is:

$$T = N_{A-A} (\bar{X} - 3.06) \quad (11)$$

for each wing (Ref 11:194): From Fig 42,  $\bar{X} = 5.18$  inches for the aft swept and results in a twisting moment of 136 in-lbf using Eq (11). For the forward swept wing from Fig 43,  $\bar{X} = 0.1$  inch and results in  $T = 190$  in-lbf. Using Eq (10), a maximum shearing stress of 8921 lbf/in<sup>2</sup> is obtained for the aft swept wing and 12,464 lbf/in<sup>2</sup> for the forward swept wing.

### Safety Factors.

For the insert material, SAE 4140 steel, the following properties exist:

$F_{Ty}$	(yield tensile stress)	=	132,000 psi
$F_{Su}$	(ultimate shearing stress)	=	90,000 psi
$F_{Tu}$	(ultimate tensile stress)	=	150,000 psi
$F_{Sy}$	(yield shearing stress)	=	79,200 psi

(Ref 1 :162)

The Factor of Safety (FS), for ultimate and yield, is computed

using the following interaction formula (Ref 5:20):

$$FS = \frac{1}{\sqrt{\left(\frac{\sigma_{MAX}}{F_T}\right)^2 + \left(\frac{\tau_{MAX}}{F_S}\right)^2}} \quad (12)$$

The ultimate FS for the aft swept wing was 5.81 and 5.06 for the forward swept wing. The yield FS was 5.43 for the aft wing and 4.67 for the forward swept wing.

### Section B-B

#### Bending Stress.

For both the aft and forward swept wings, the force acting outboard of section B-B is given as:

$$N_{B-B} = P_{AVG} S_B$$

where the area outboard of B-B,  $S_B = 0.0427 \text{ ft}^2$ . This yields a normal force of 15.4 lbf for each wing.

For the bending moment at section B-B, the equation

$$M_{B-B} = N_{B-B} \bar{Y}$$

was utilized where  $\bar{Y} = 0.92$  inches for both wings. This yields a bending moment of 14.17 in-lbf for each wing.

The wing section at B-B is also modeled as a thin beam with dimensions,  $a = 3.2$  in. and  $b = 0.1655$  in. The maximum bending stress using Eq (9) is  $970 \text{ lbf/in}^2$ .

#### Shearing Stress.

For both wings, the twisting moment at section

B-B is given as:

$$T = N_{s-e} (\bar{x} - 1.85)$$

where  $X = 2.6$  in. for the aft wing and  $X = 0.80$  in. for the forward swept wing. The twisting moment for the aft and forward swept wings is 11.55 in-lbf and 15.6 in-lbf, respectively. The maximum shearing stress, using the Eq (10) and the dimensions of section B-B, was 407.6 lbf/in<sup>2</sup> for the aft wing and 550.3 lbf/in<sup>2</sup> for the forward swept wing.

#### Safety Factors.

The aluminum base epoxy used to mold the wings has a bond strength of 4650 lbf/in<sup>2</sup>. Using this property and Eq (12), the ultimate FS at section B-B for the aft swept wing was computed as 4.42. For the forward swept wing the FS was 4.24.

An analysis of the loads on the fuselage was not considered necessary since it was designed for loads much greater than those expected in this test. The analysis of this component can be found in Ref 5.

APPENDIX B  
AERODYNAMIC CHARACTERISTICS PRESENTED  
IN GRAPHICAL FORM

The results of the wind tunnel tests for Mach Numbers from 0.70 to 0.90 are presented graphically in this appendix.

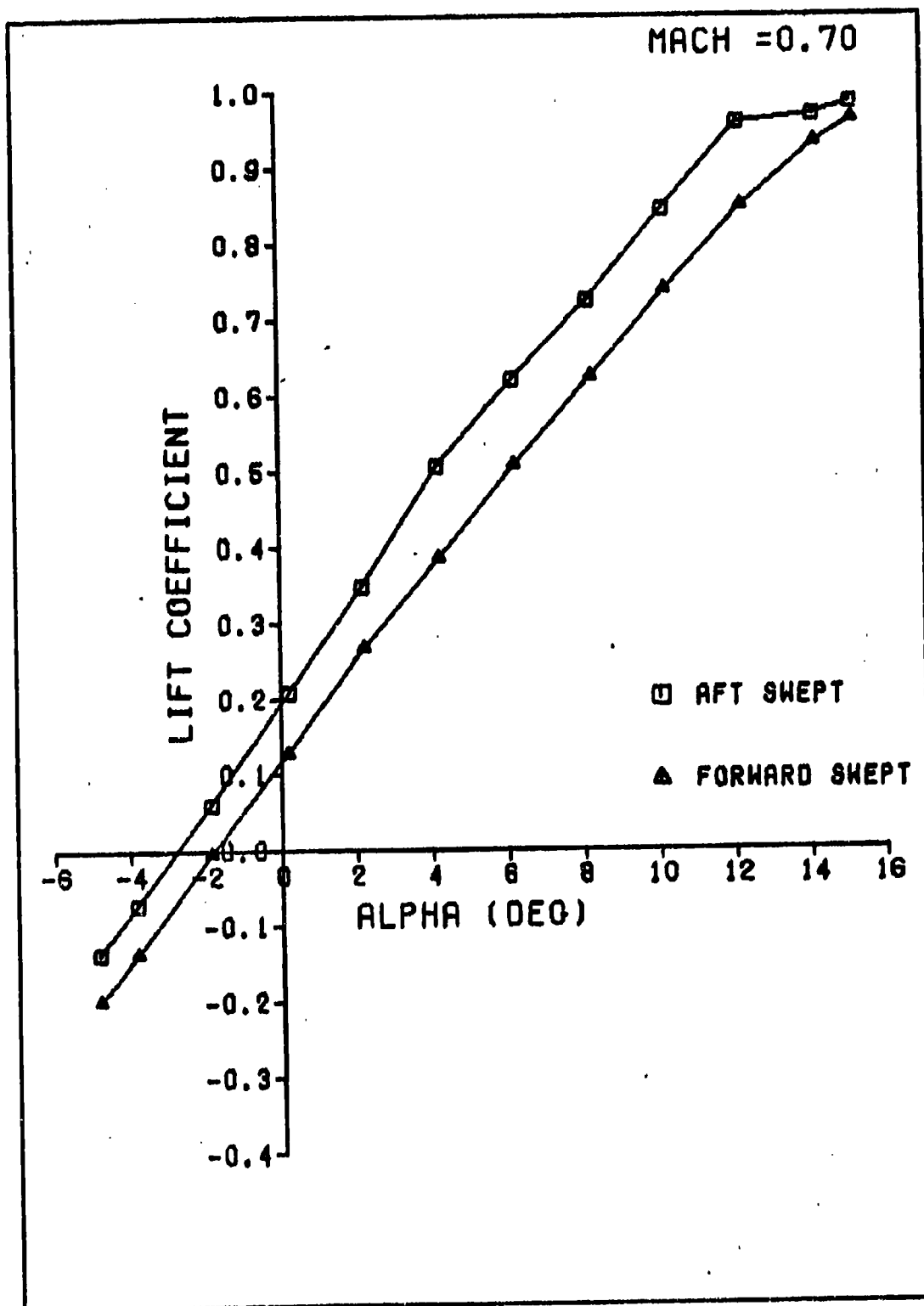


Figure 45.  $C_L$  vs  $\alpha$  for  $M = 0.7$



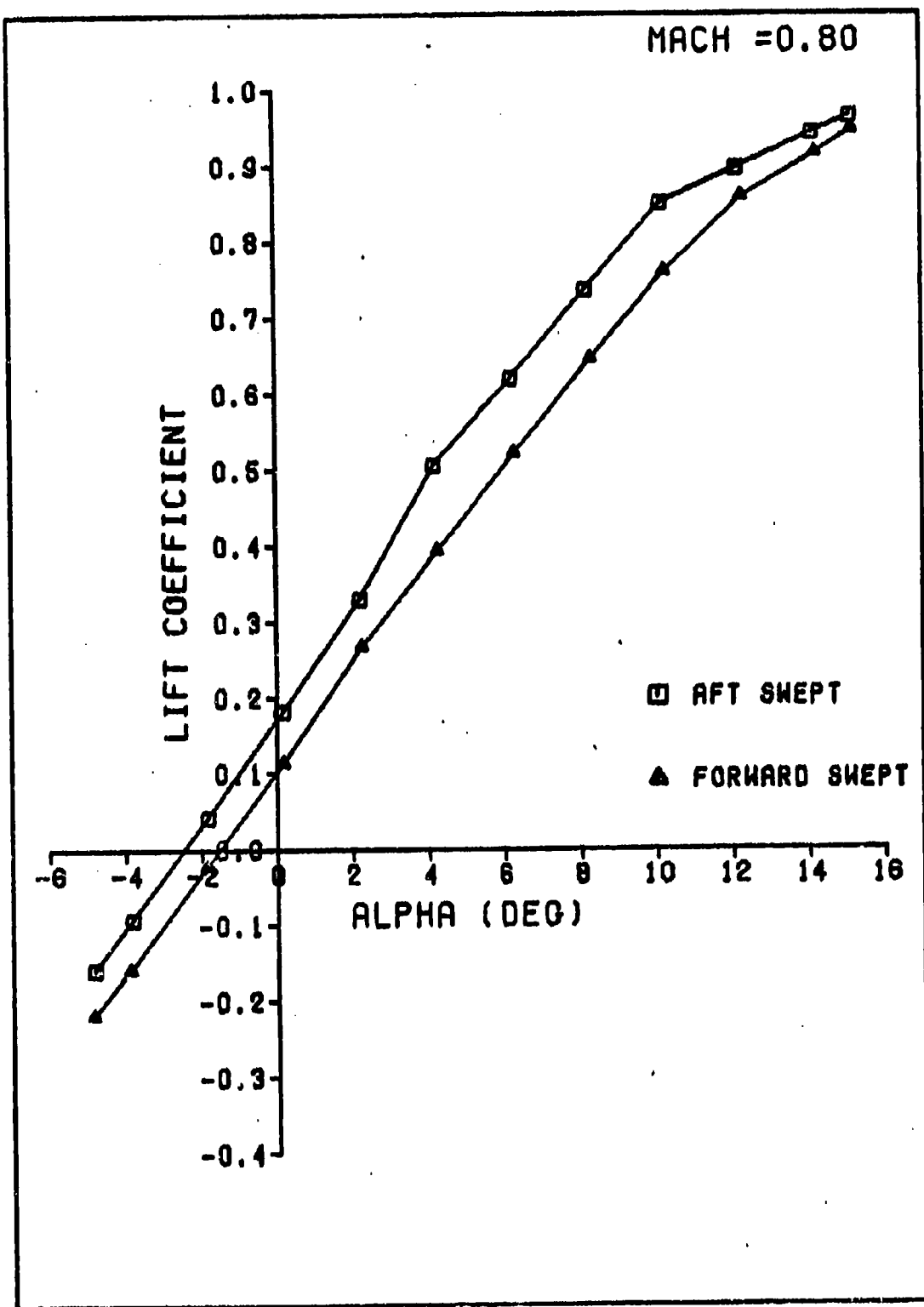


Figure 46.  $C_L$  vs  $\alpha$  for  $M = 0.8$

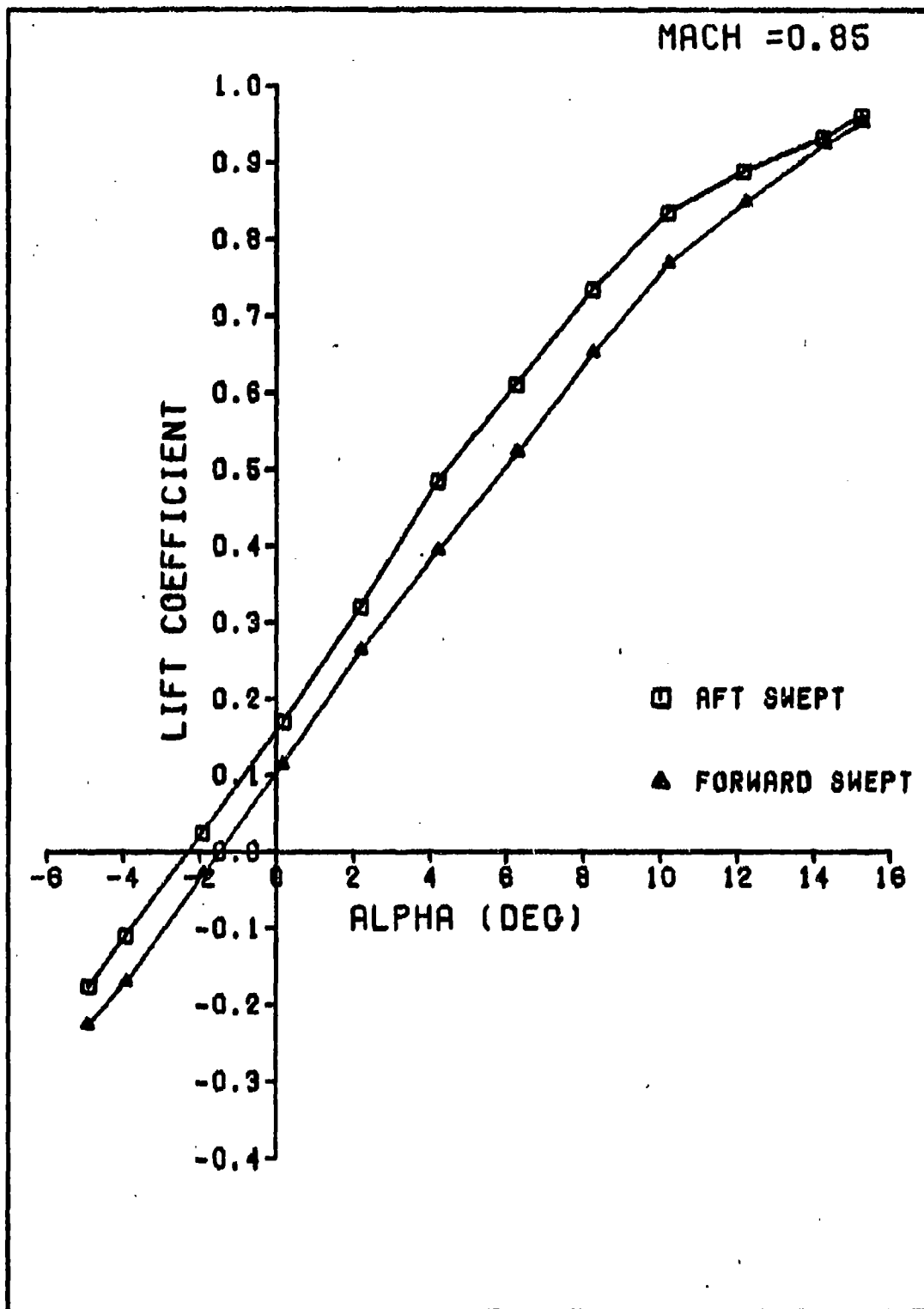


Figure 47.  $C_L$  vs  $\alpha$  for  $M = 0.85$

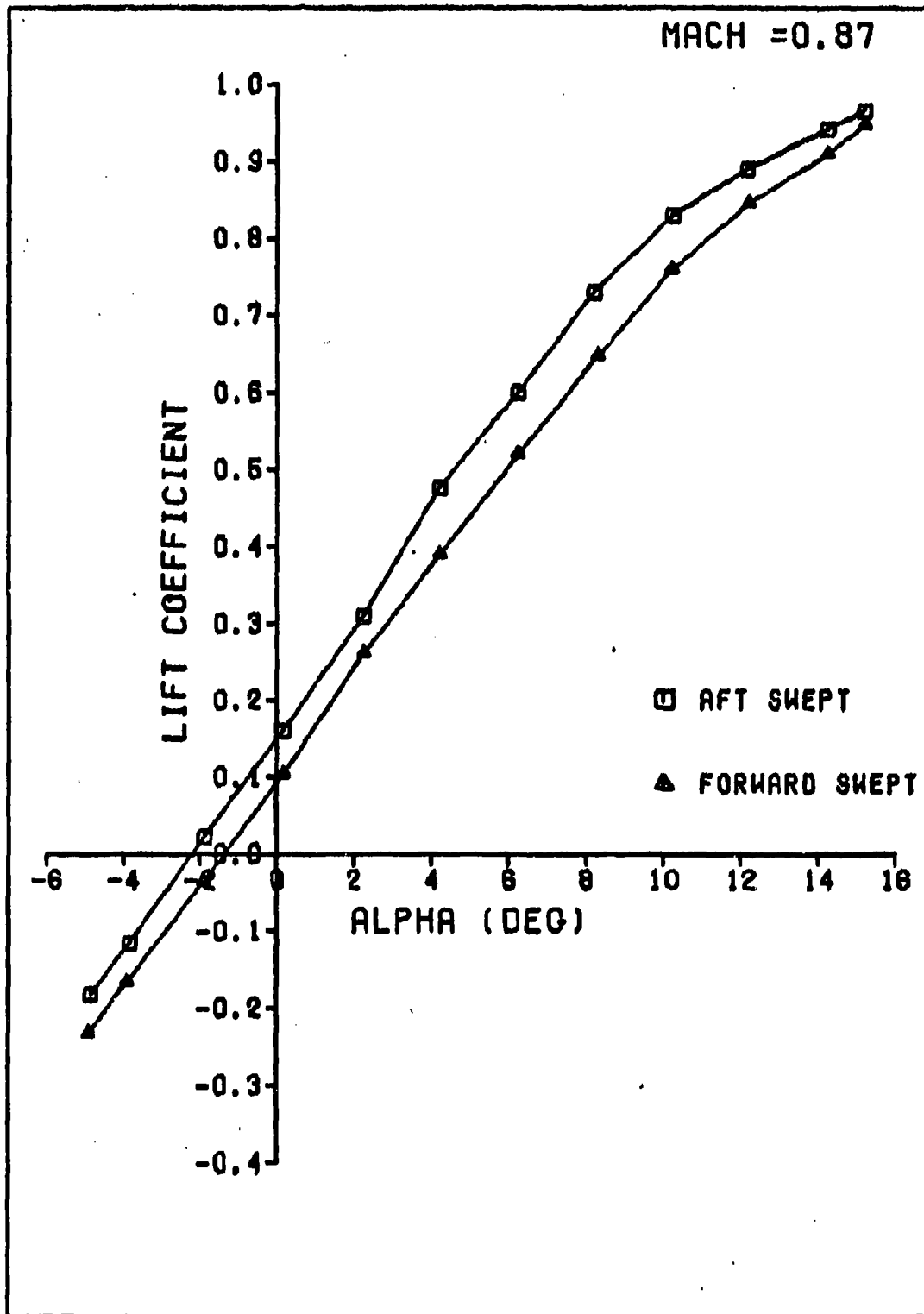


Figure 48.  $C_L$  vs  $\alpha$  for  $M = 0.87$

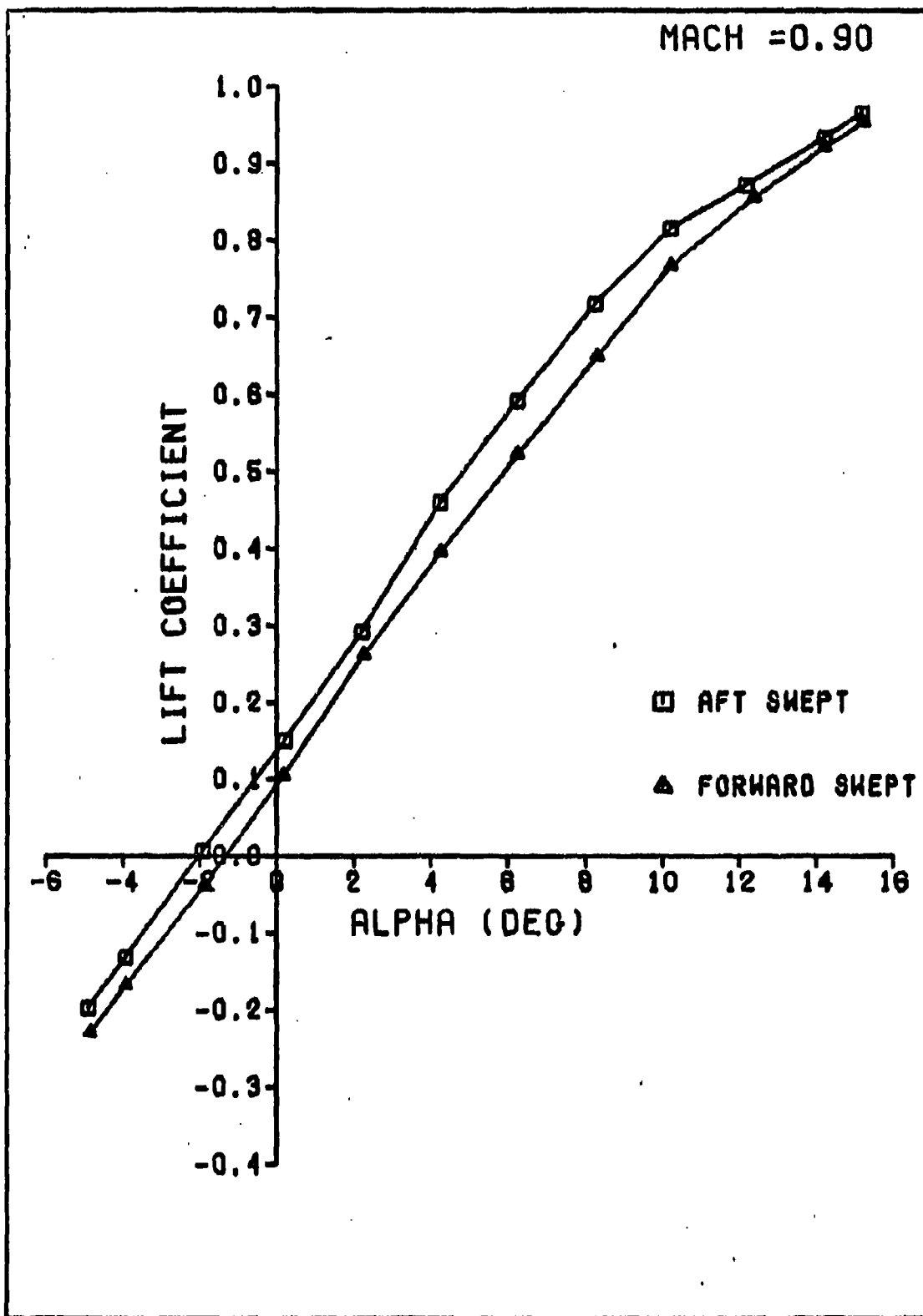


Figure 49.  $C_L$  vs  $\alpha$  for  $M = 0.9$

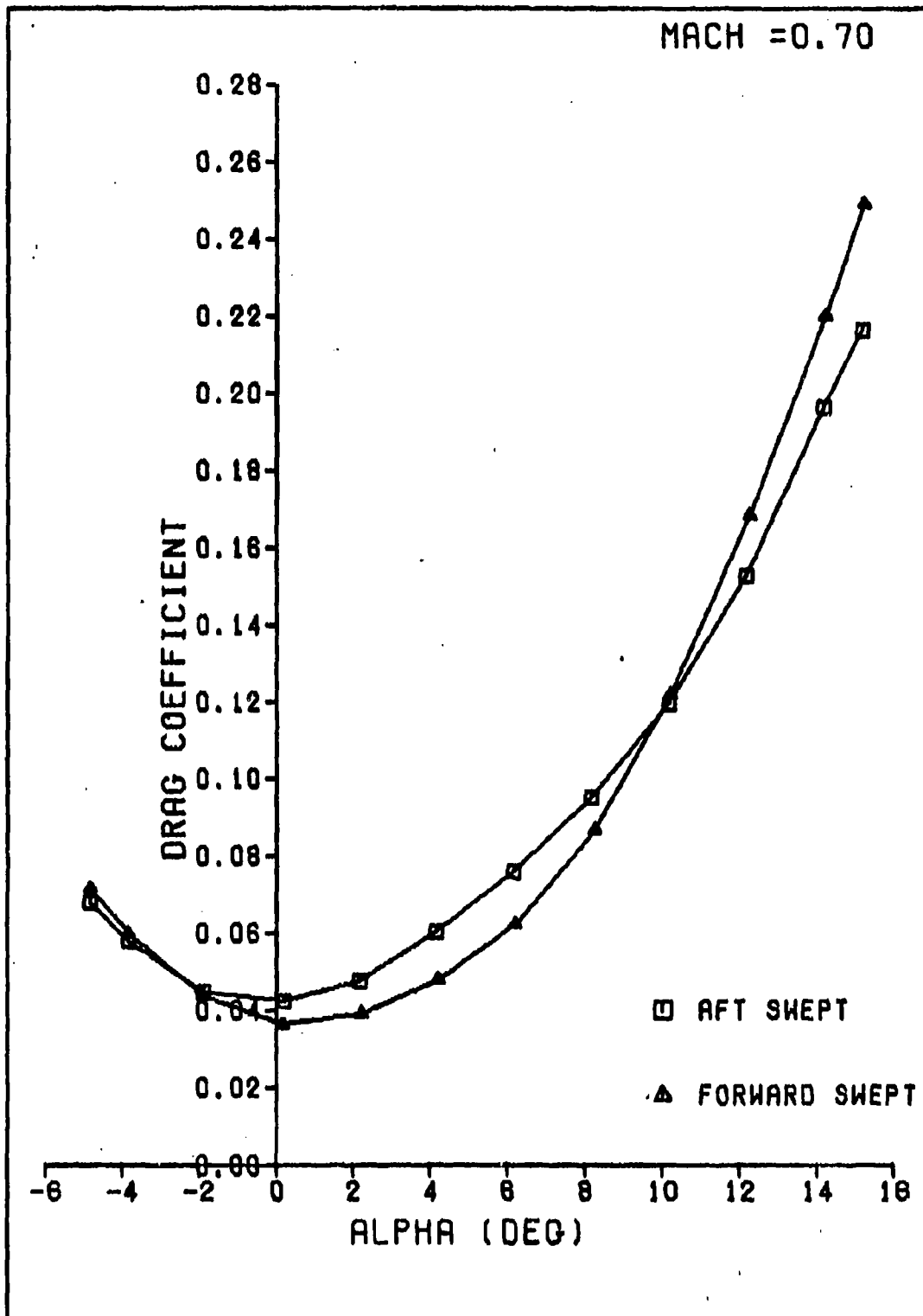


Figure 50.  $C_D$  vs  $\alpha$  for  $M = 0.7$

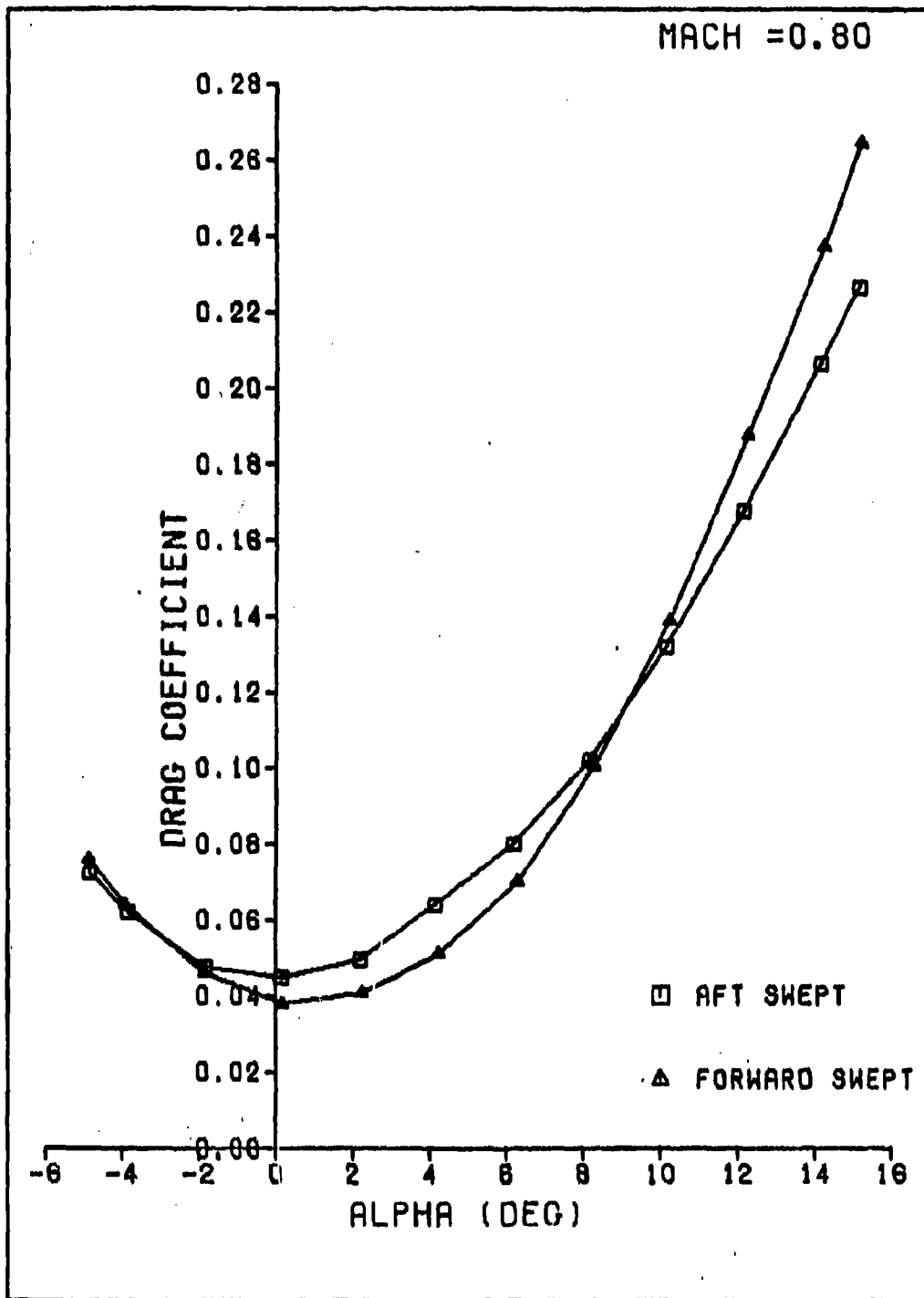


Figure 51.  $C_D$  vs  $\alpha$  for  $M = 0.8$

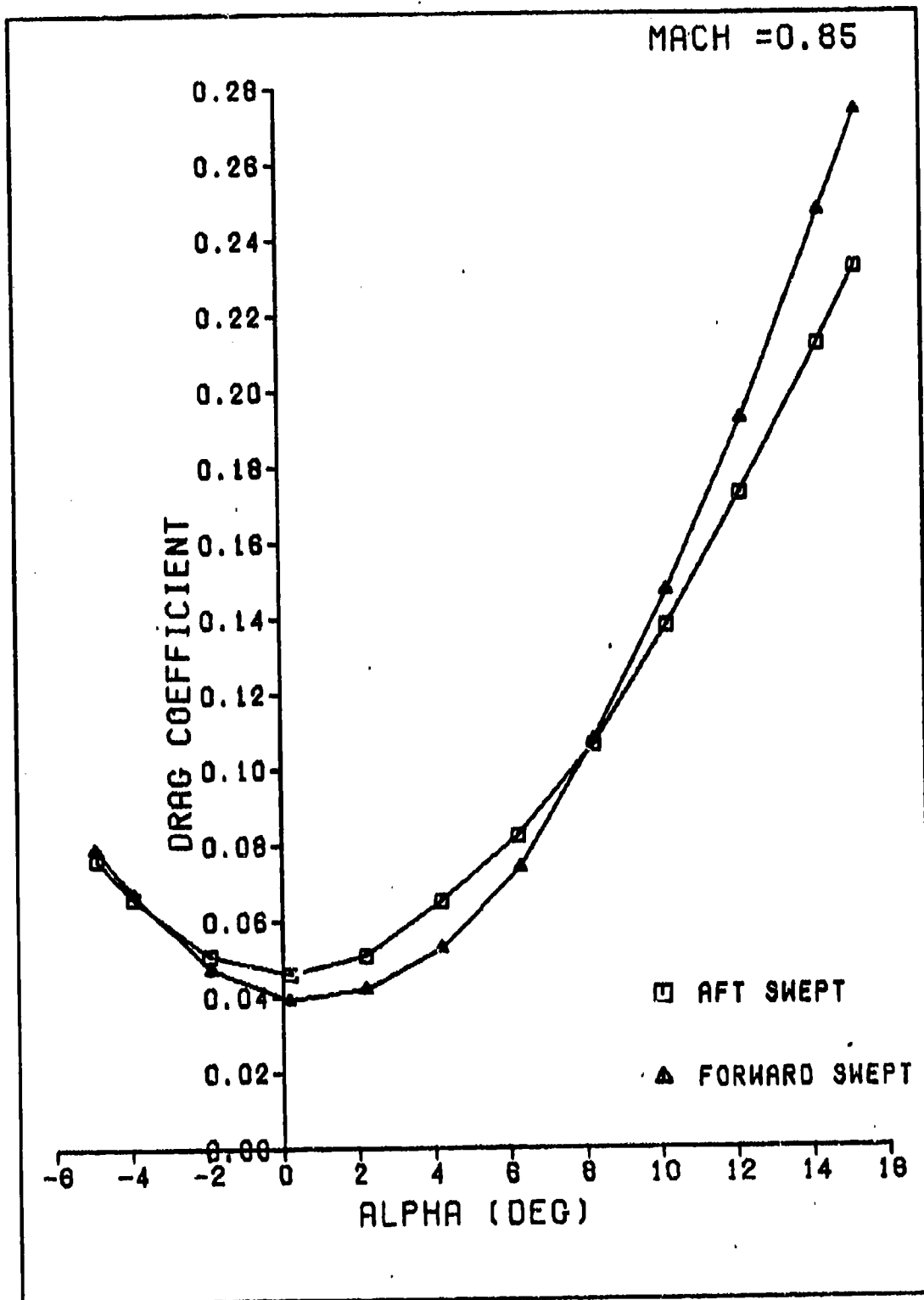


Figure 52.  $C_D$  vs  $\alpha$  for  $M = 0.85$

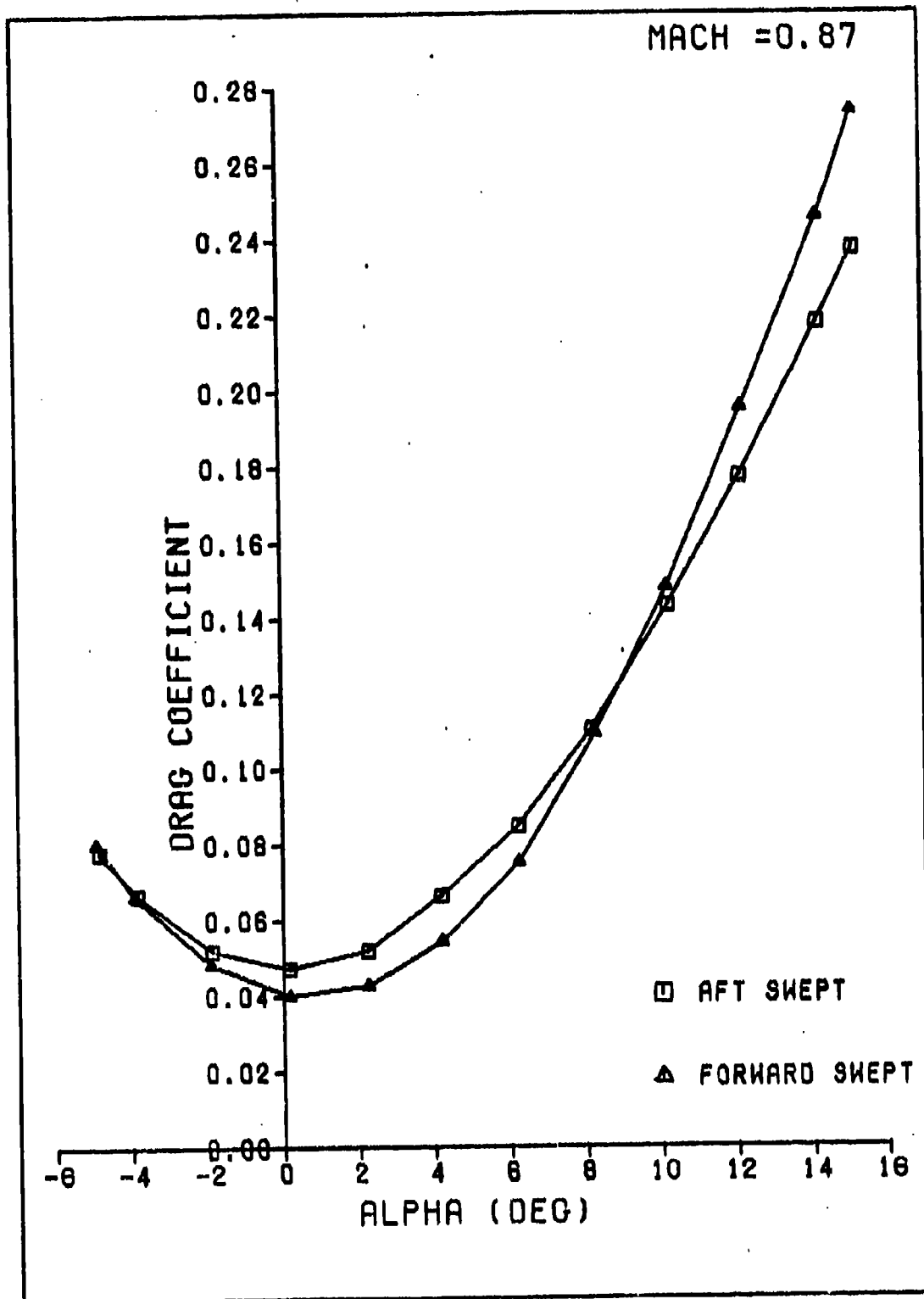


Figure 53.  $C_D$  vs  $\alpha$  for  $M = 0.87$



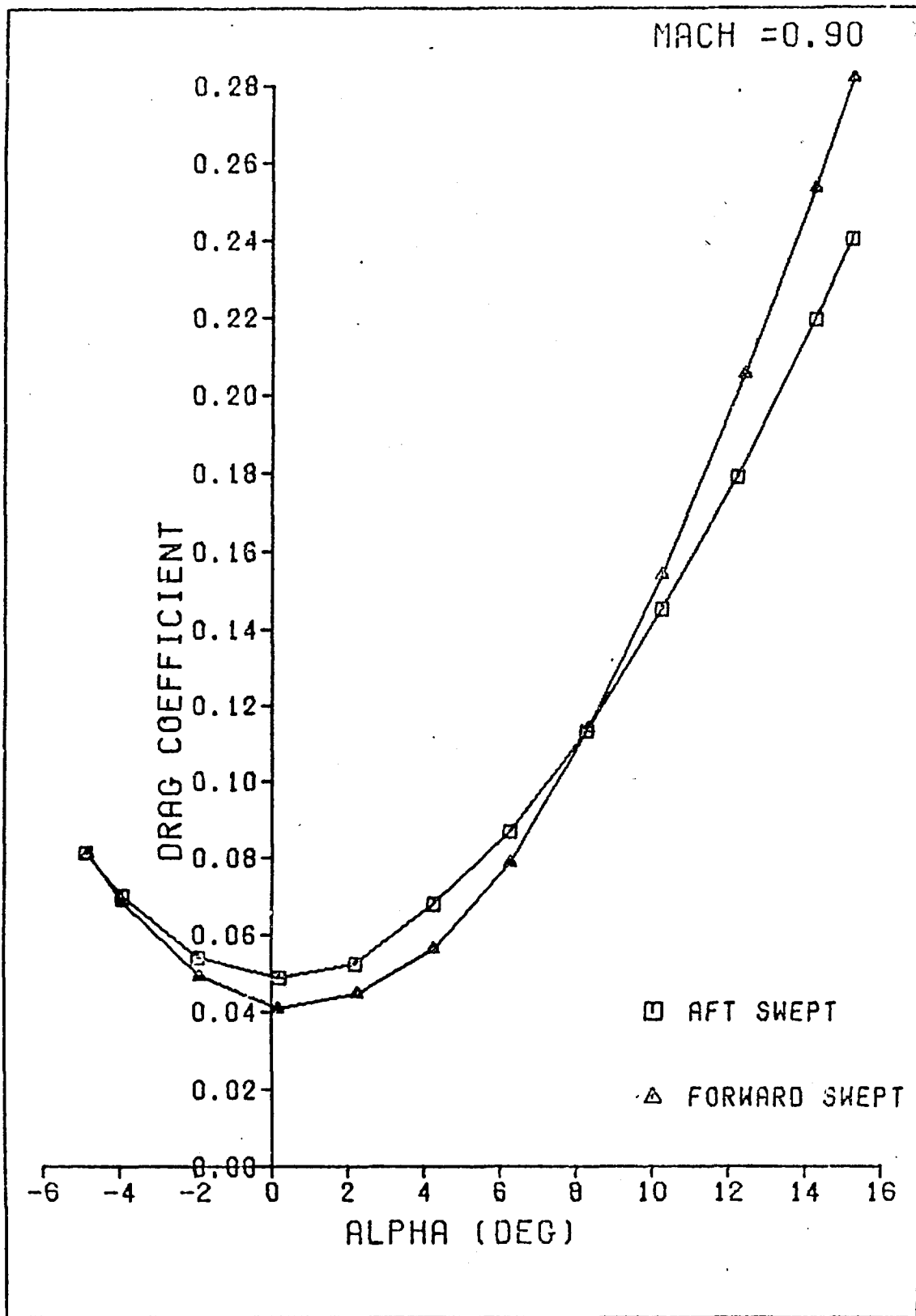


Figure 54.  $C_D$  vs  $\alpha$  for  $M = 0.9$

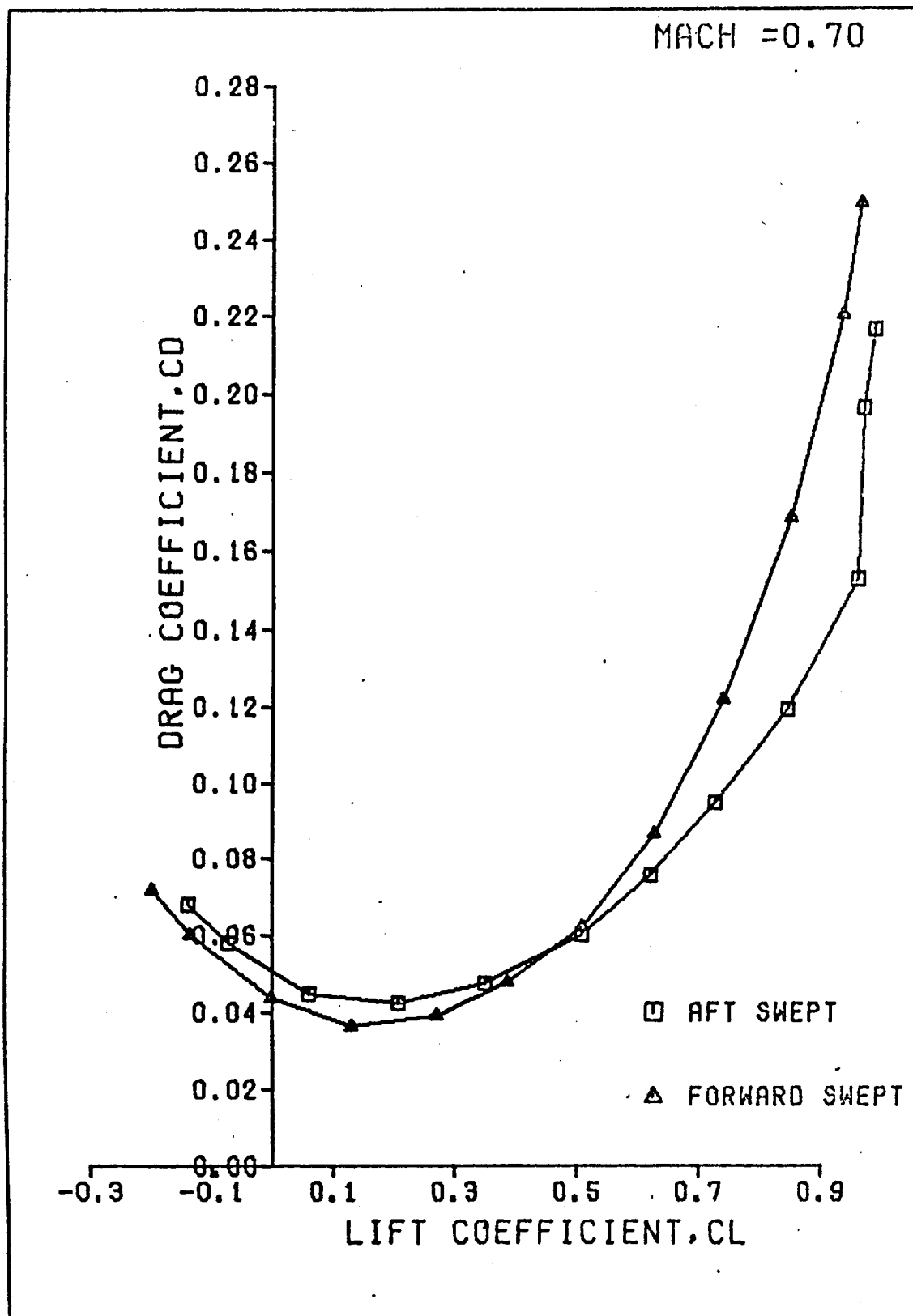


Figure 55.  $C_D$  vs  $C_L$  for  $M = 0.7$

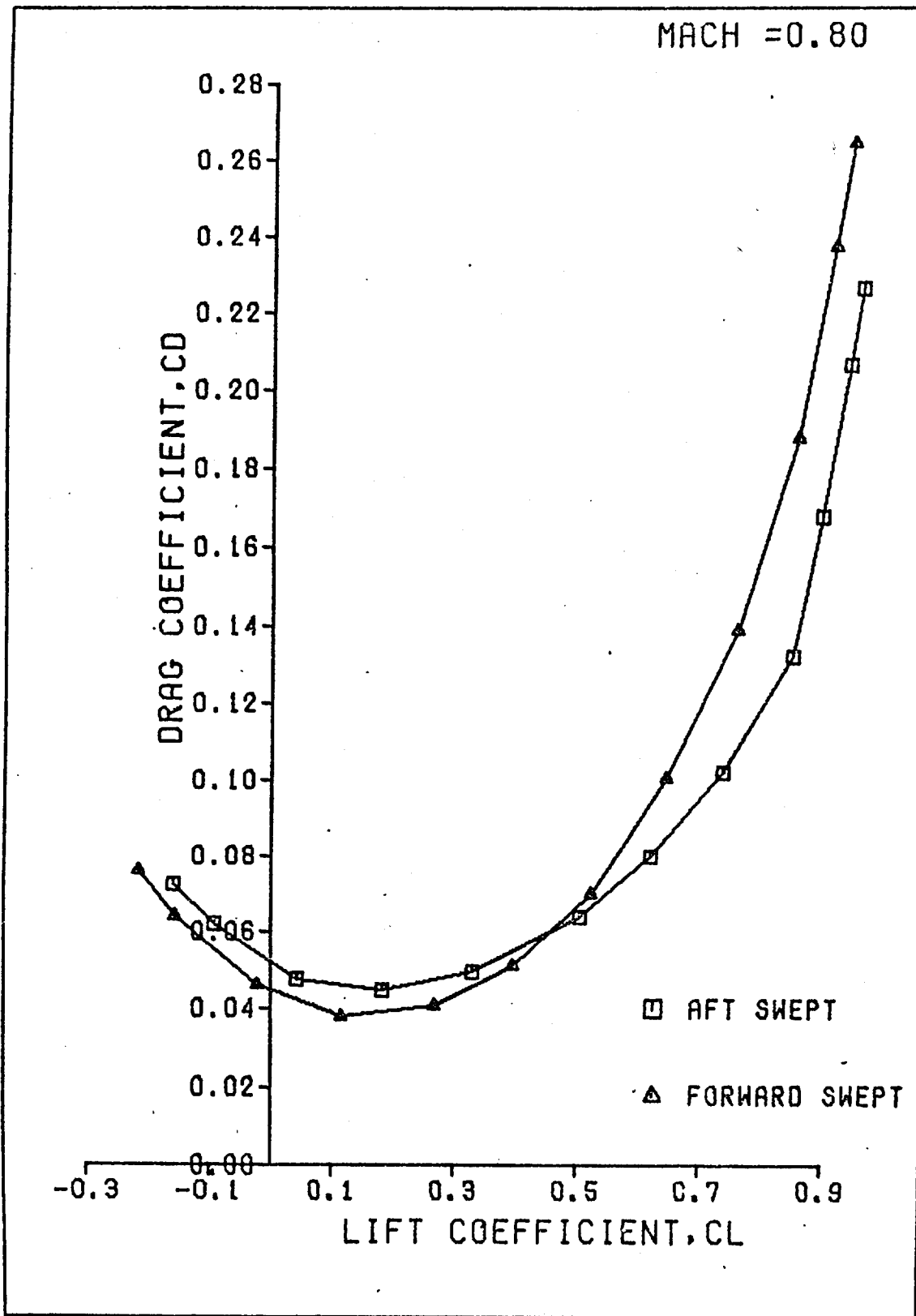


Figure 56.  $C_D$  vs  $C_L$  for  $M = 0.8$

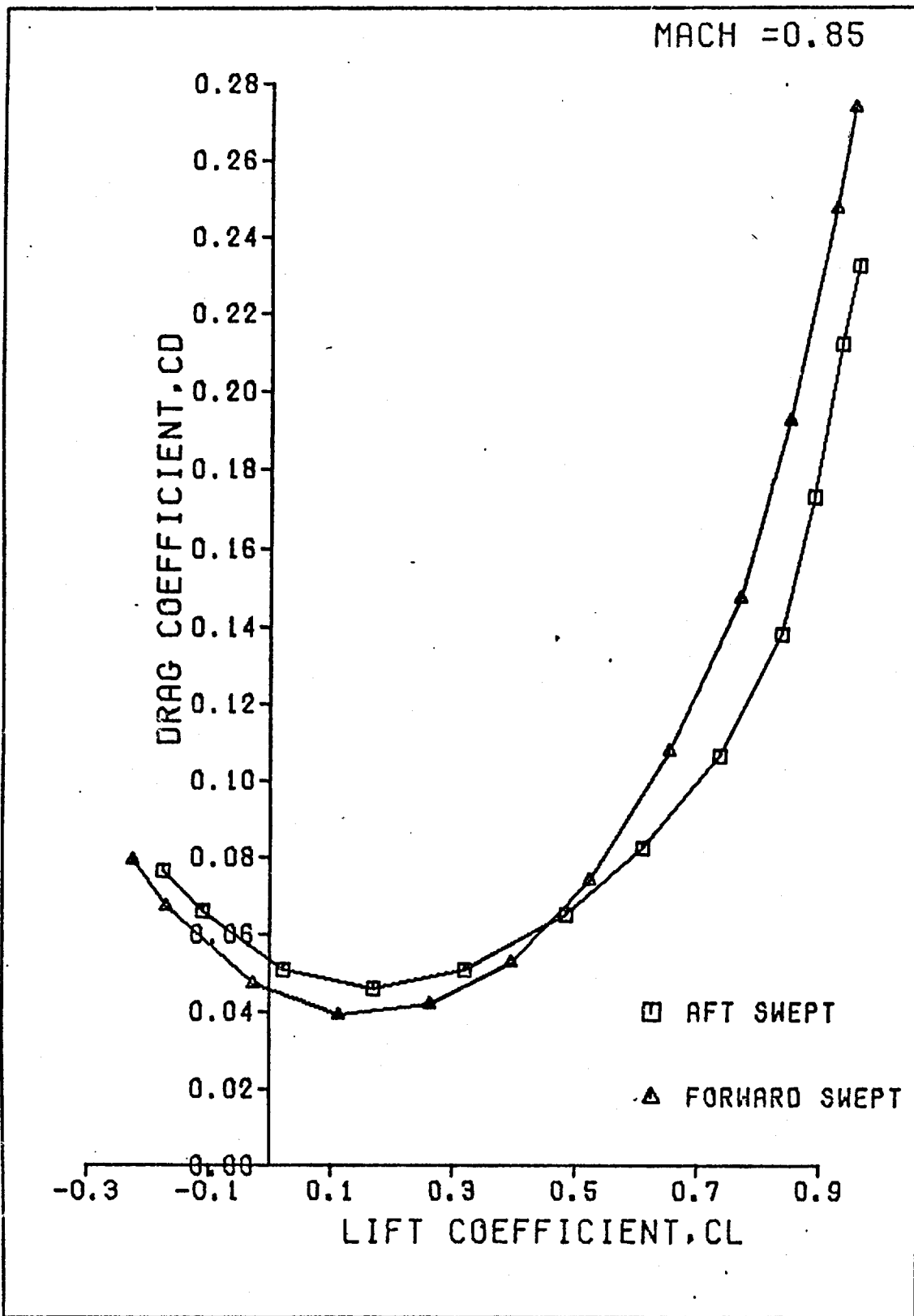


Figure 57.  $C_D$  vs  $C_L$  for  $M = 0.85$

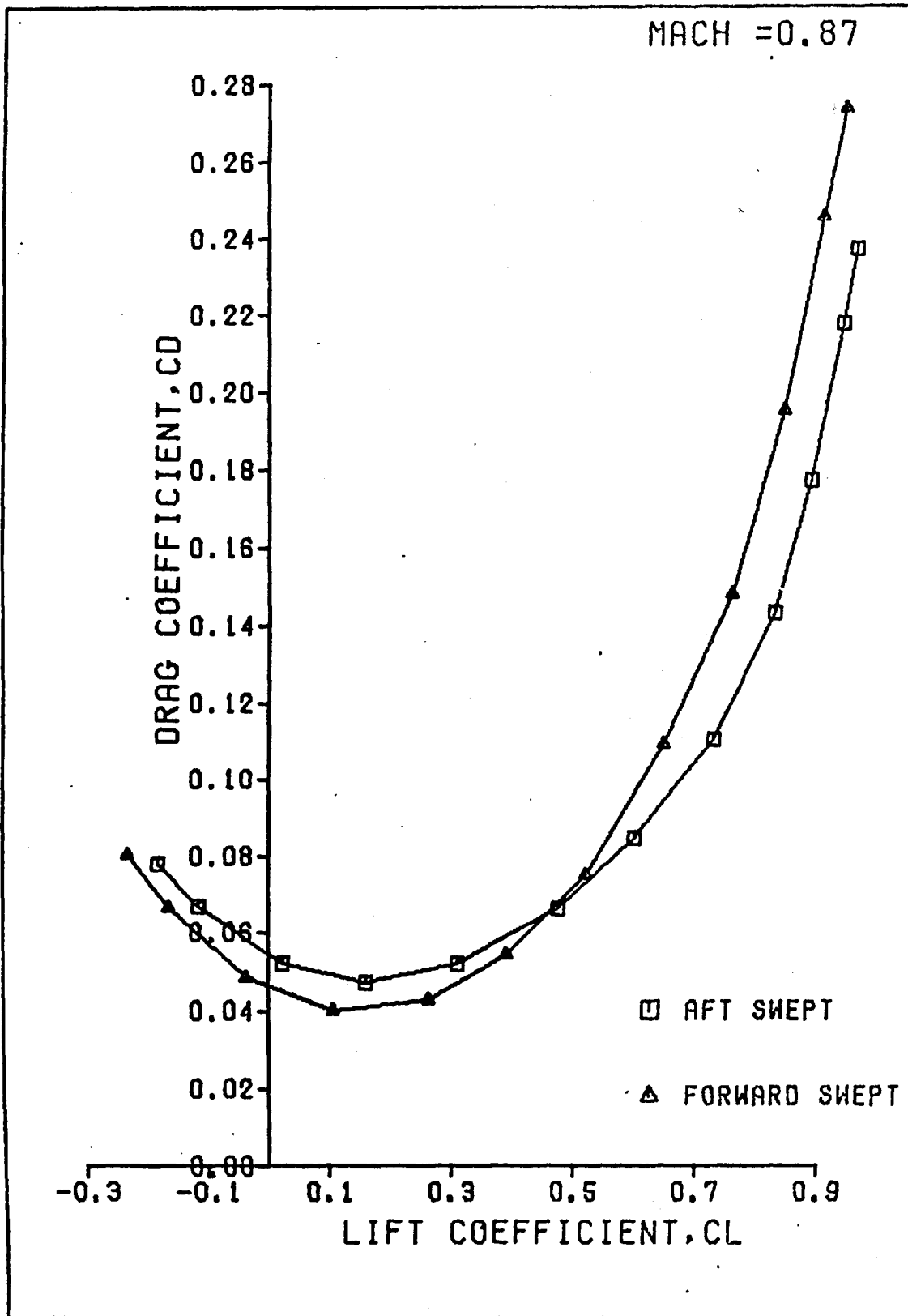


Figure 58.  $C_D$  vs  $C_L$  for  $M = 0.87$

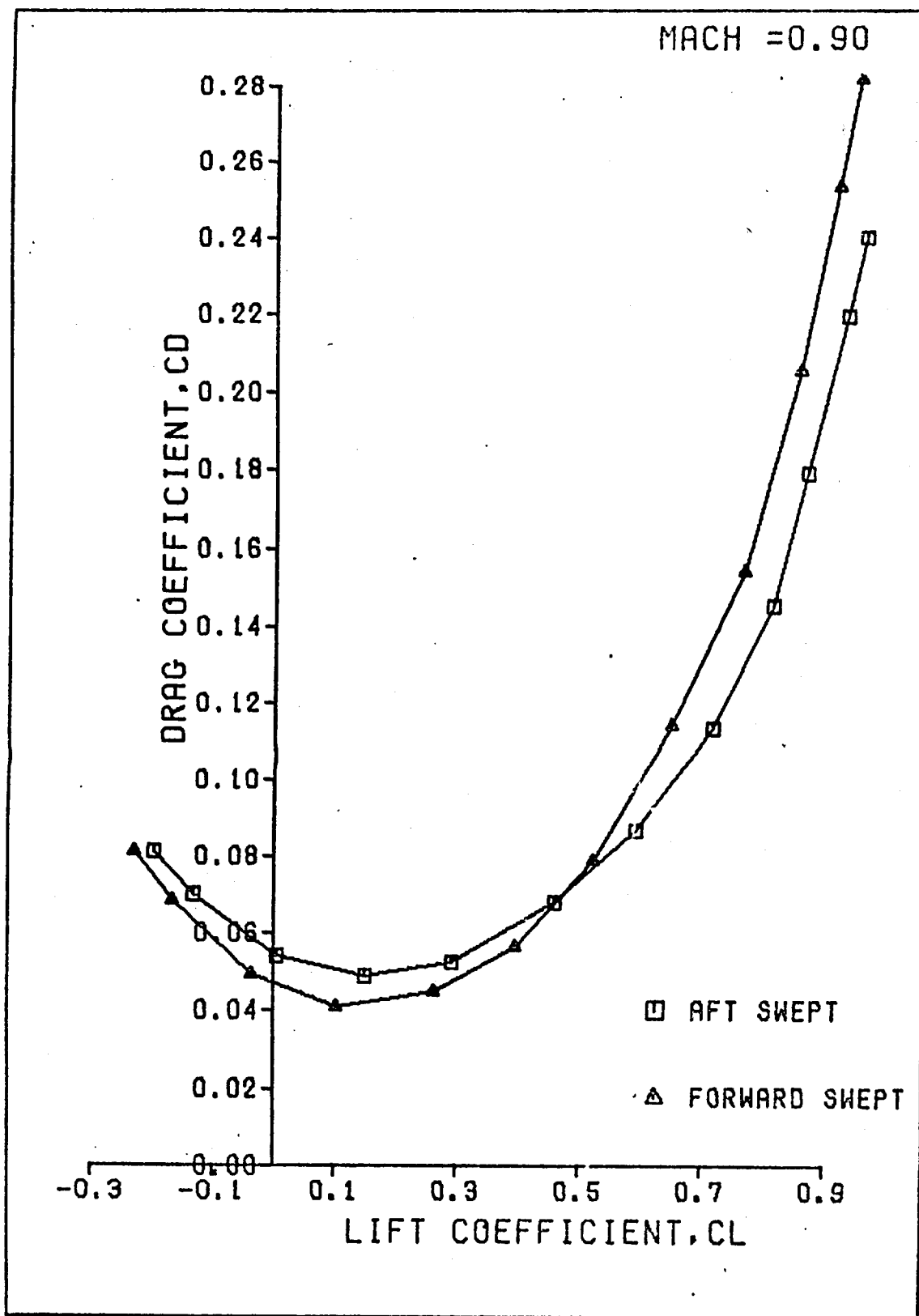


Figure 59.  $C_D$  vs  $C_L$  for  $M = 0.9$

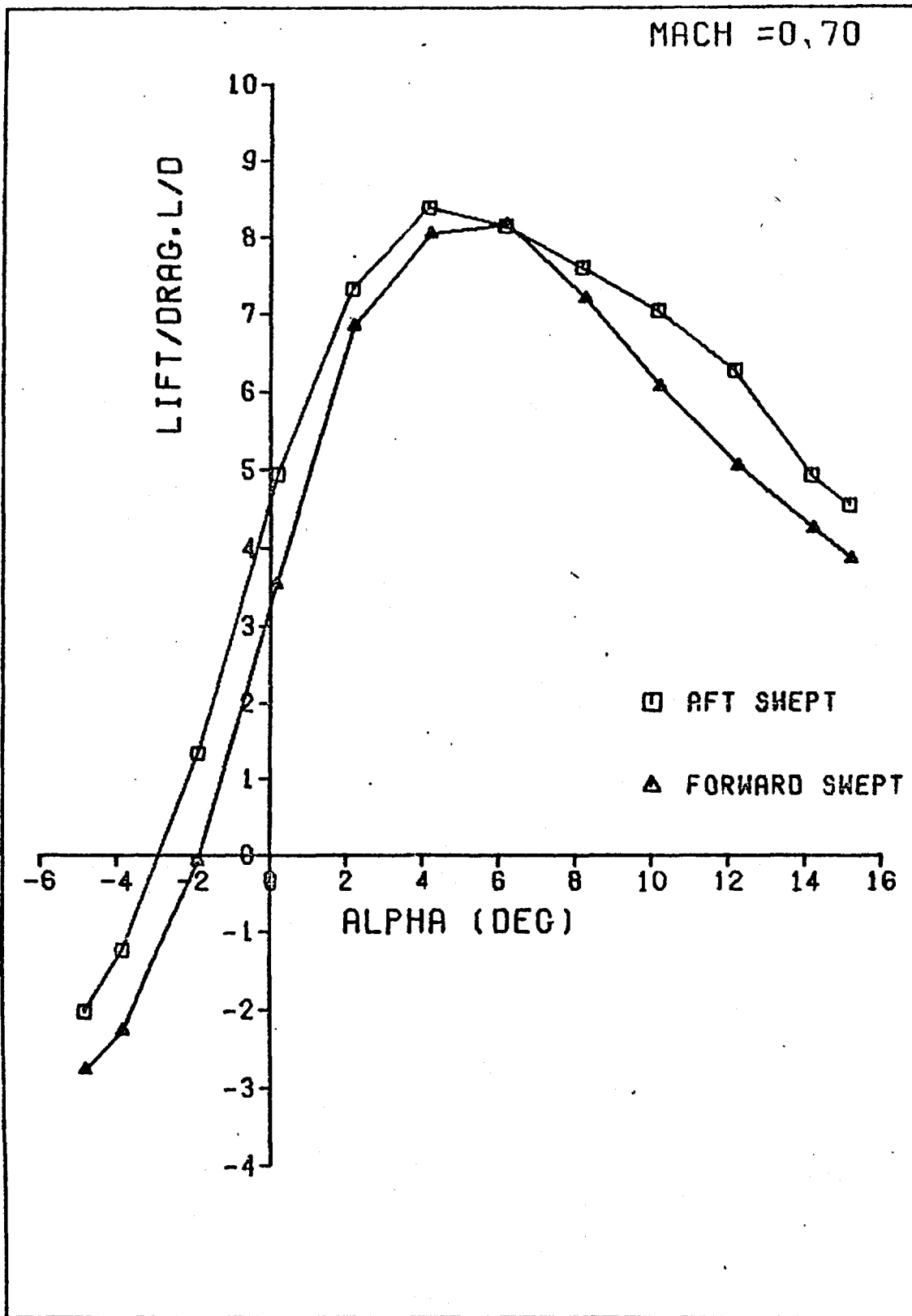


Figure 60. L/D vs  $\alpha$  for M = 0.7

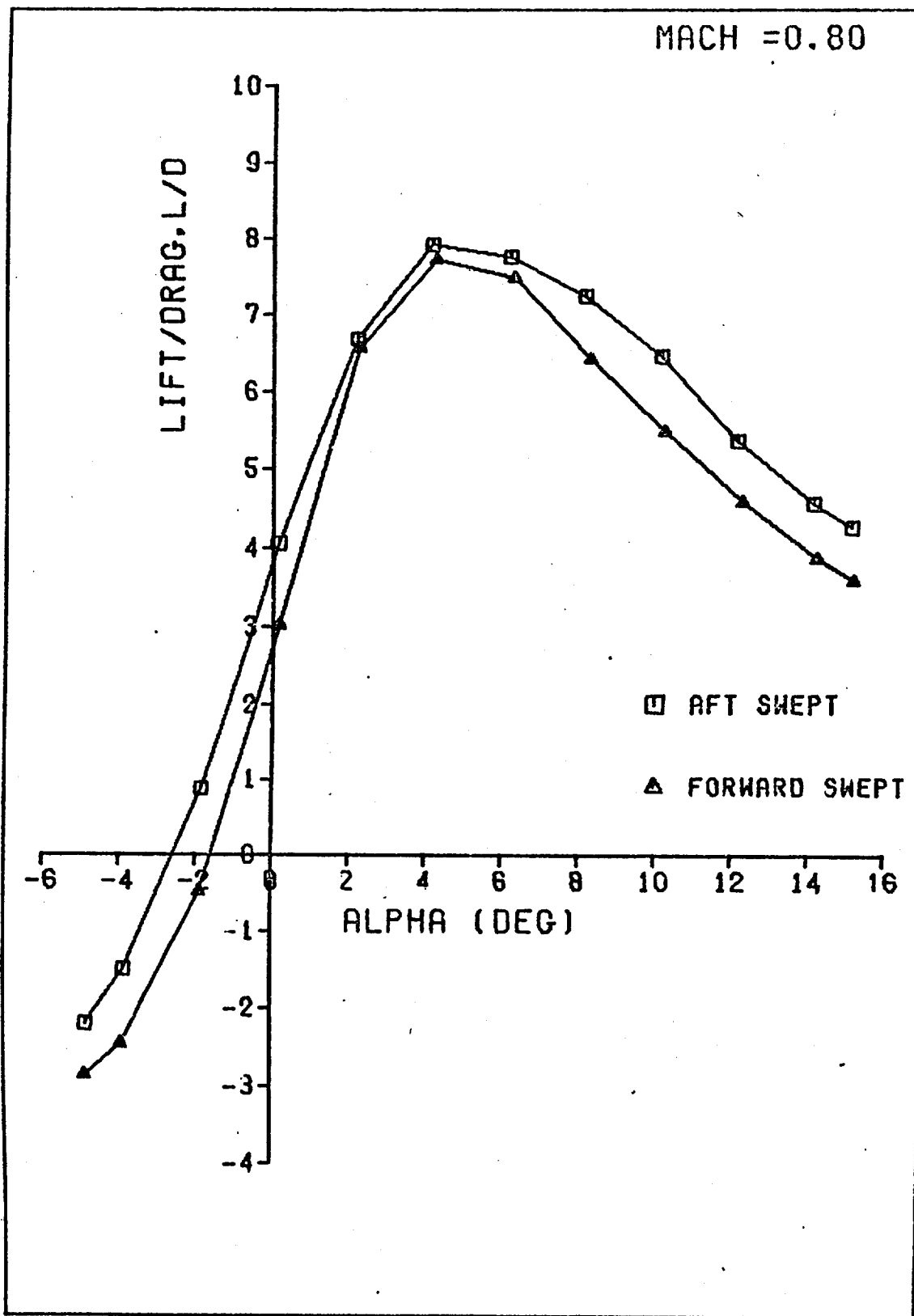


Figure 61. L/D vs  $\alpha$  for M = 0.8



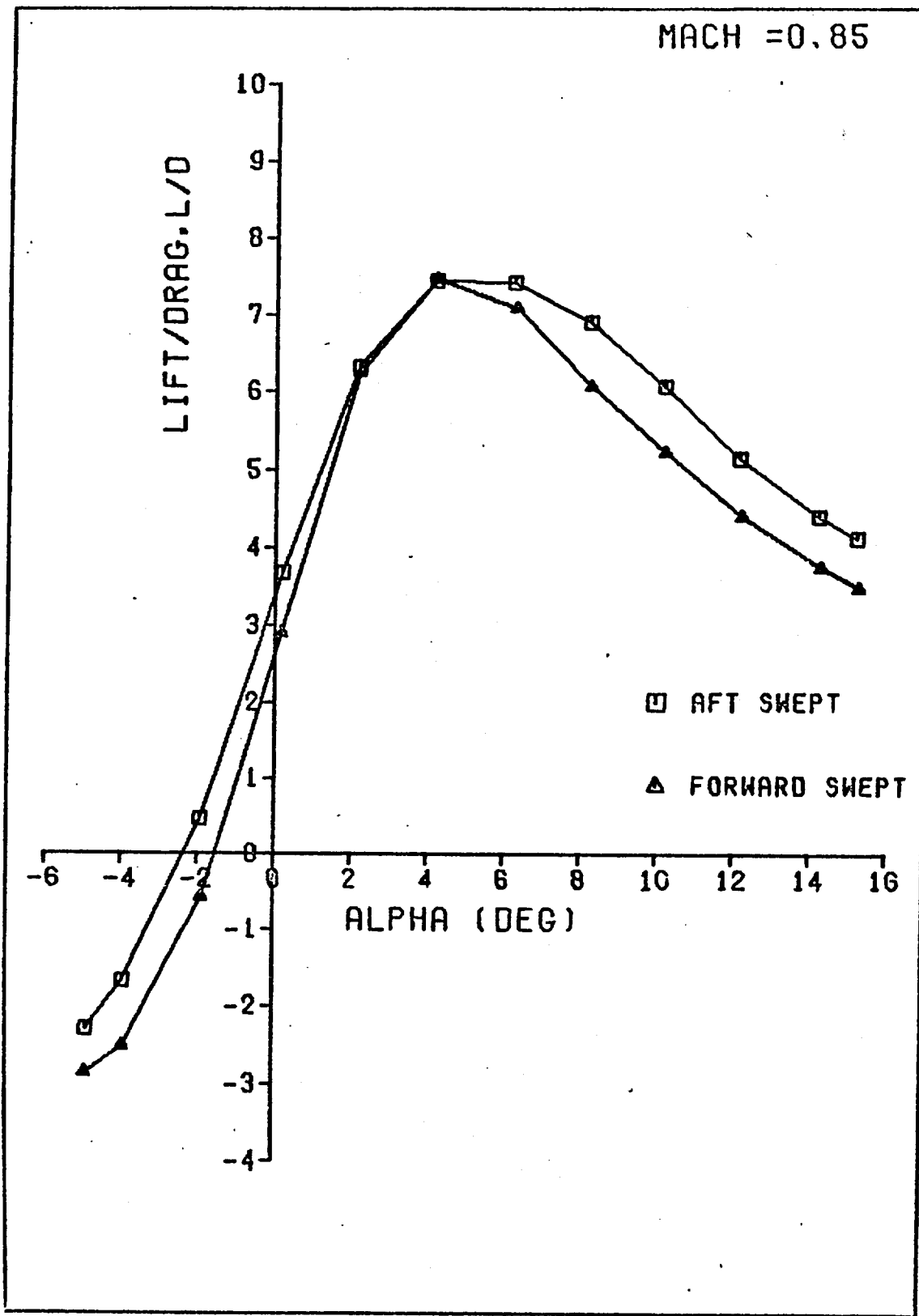


Figure 62. L/D vs  $\alpha$  for M = 0.85

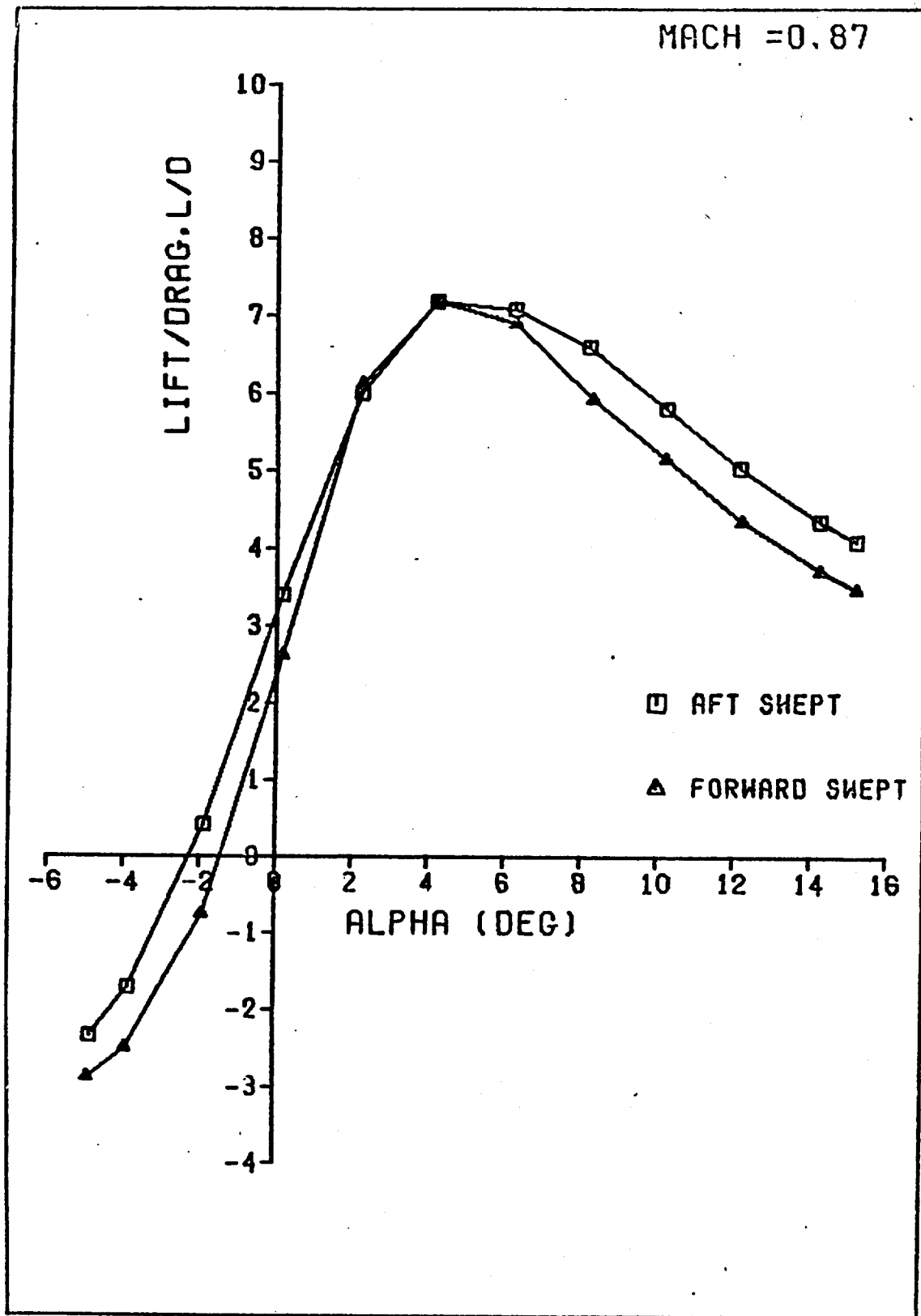


Figure 63. L/D vs  $\alpha$  for M = 0.87

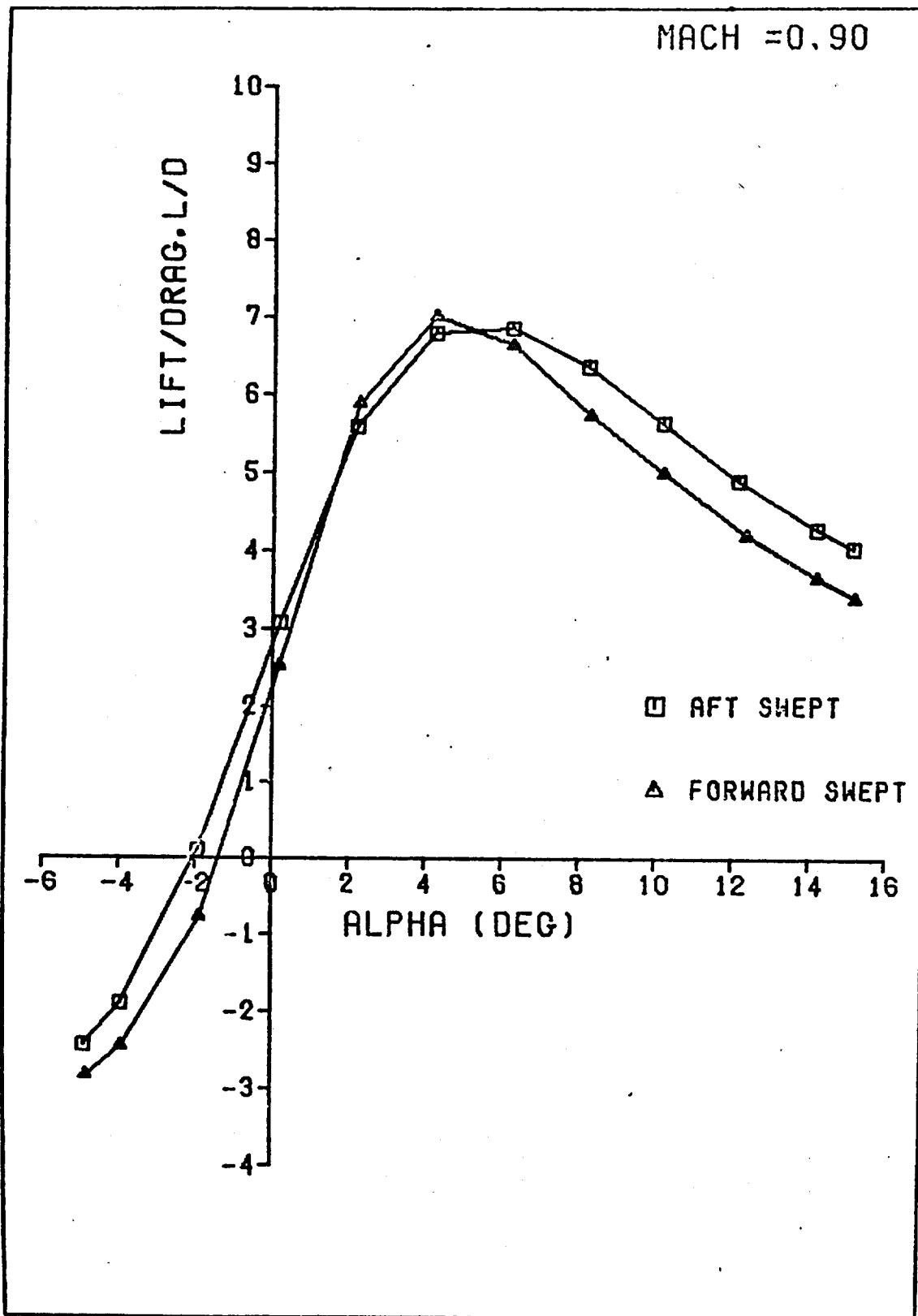


Figure 64. L/D vs  $\alpha$  for M = 0.9

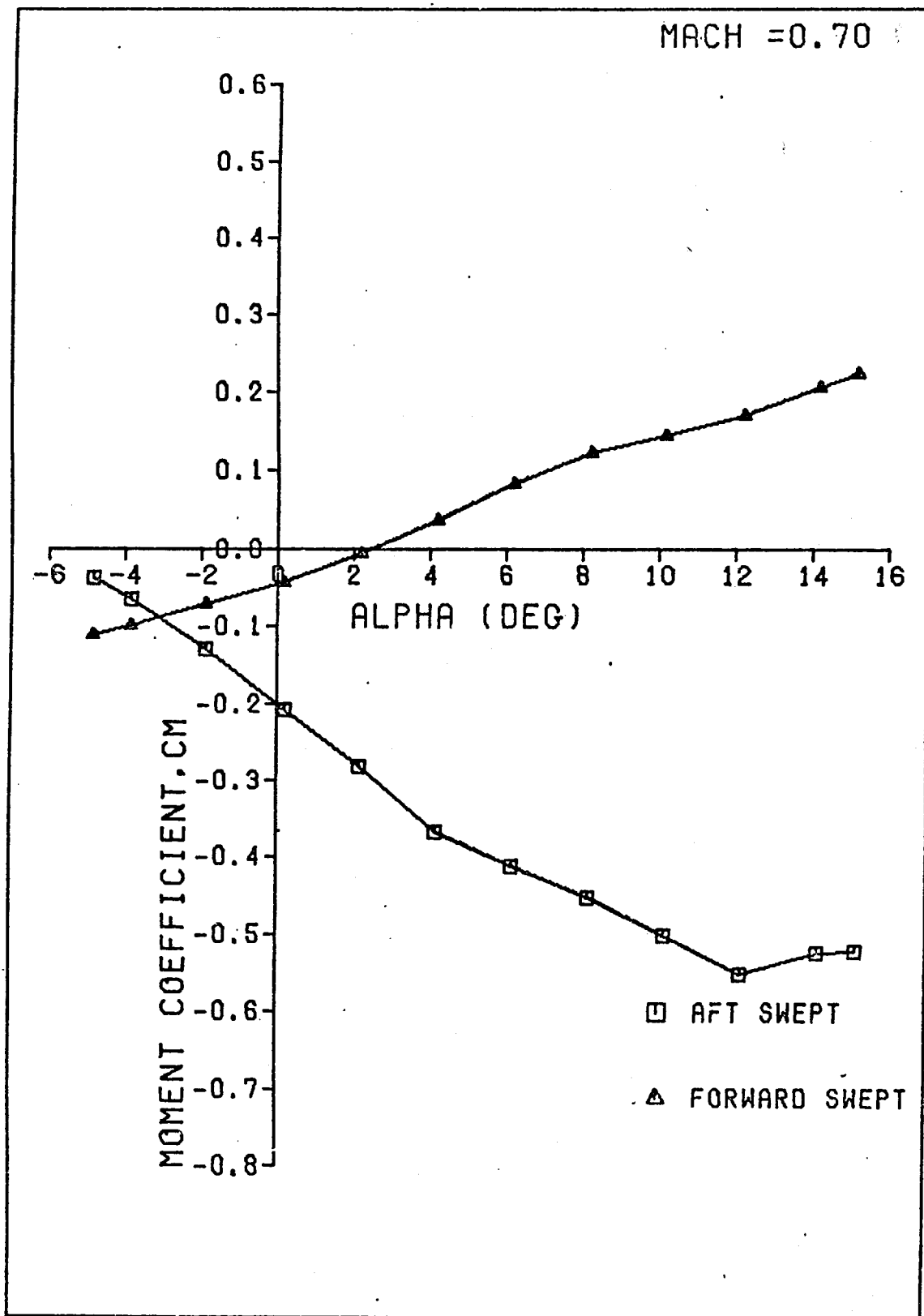


Figure 65.  $C_M$  vs  $\alpha$  for  $M = 0.7$

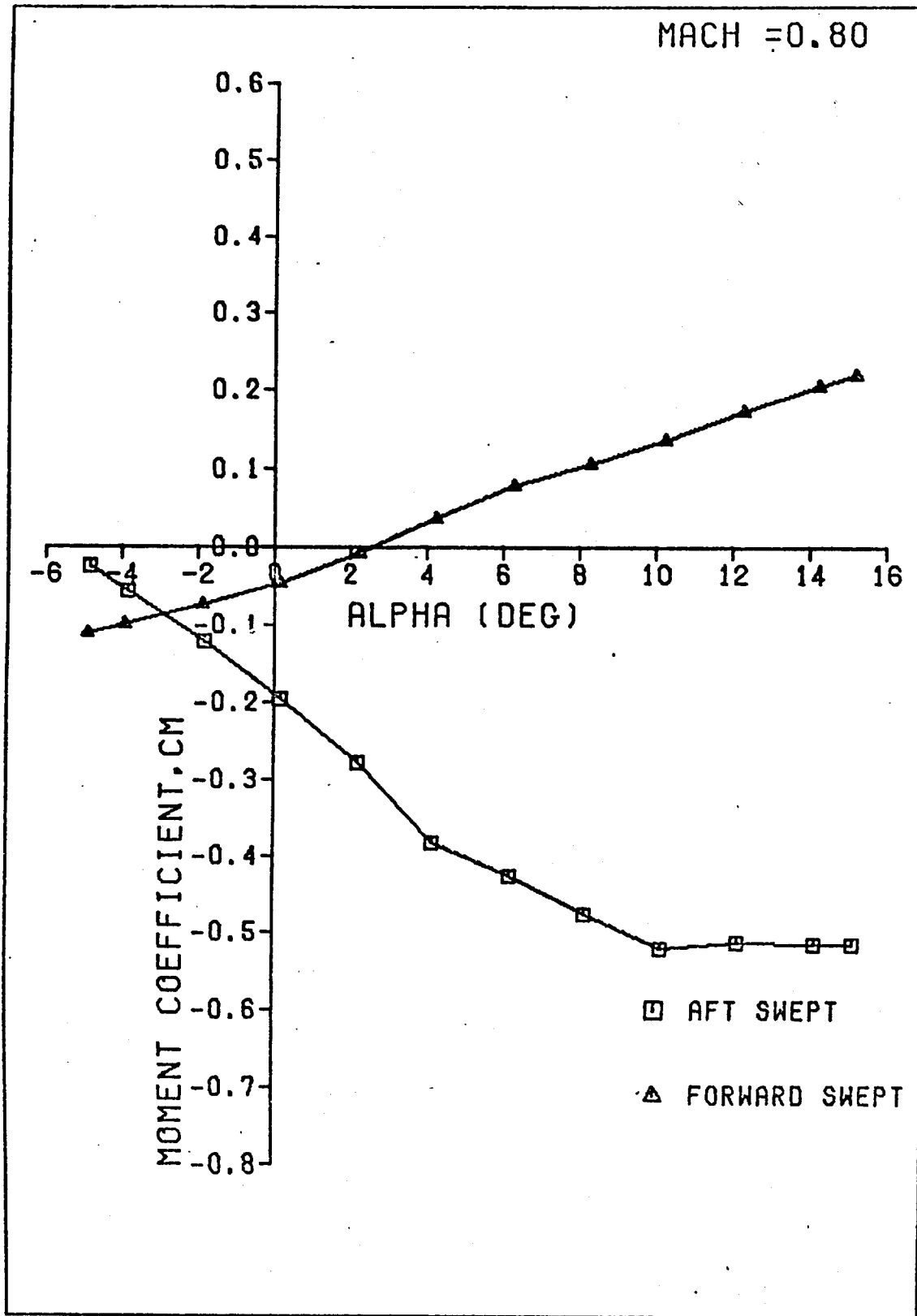


Figure 66.  $C_M$  vs  $\alpha$  for  $M = 0.8$

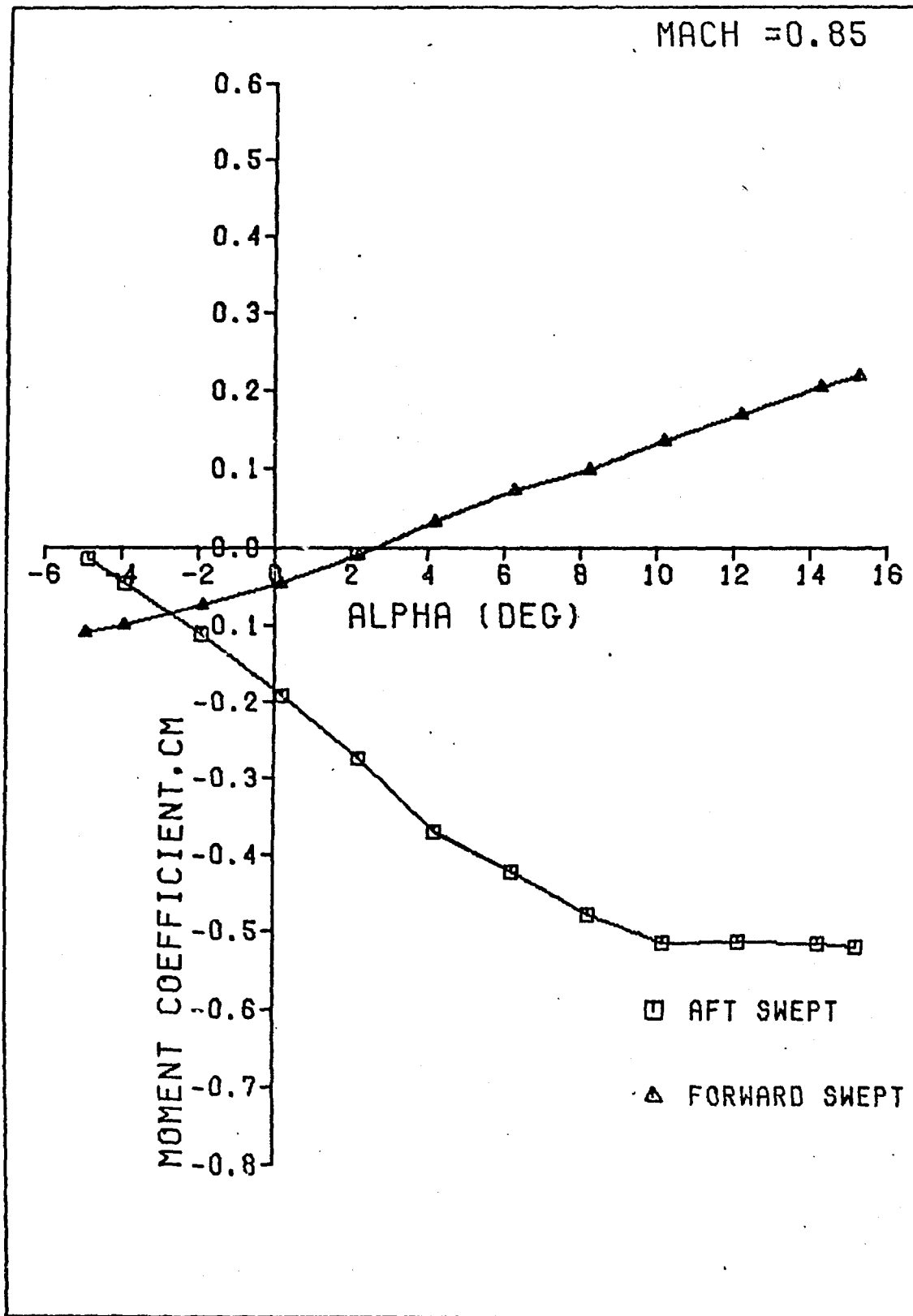


Figure 67.  $C_M$  vs  $\alpha$  for  $M = 0.85$

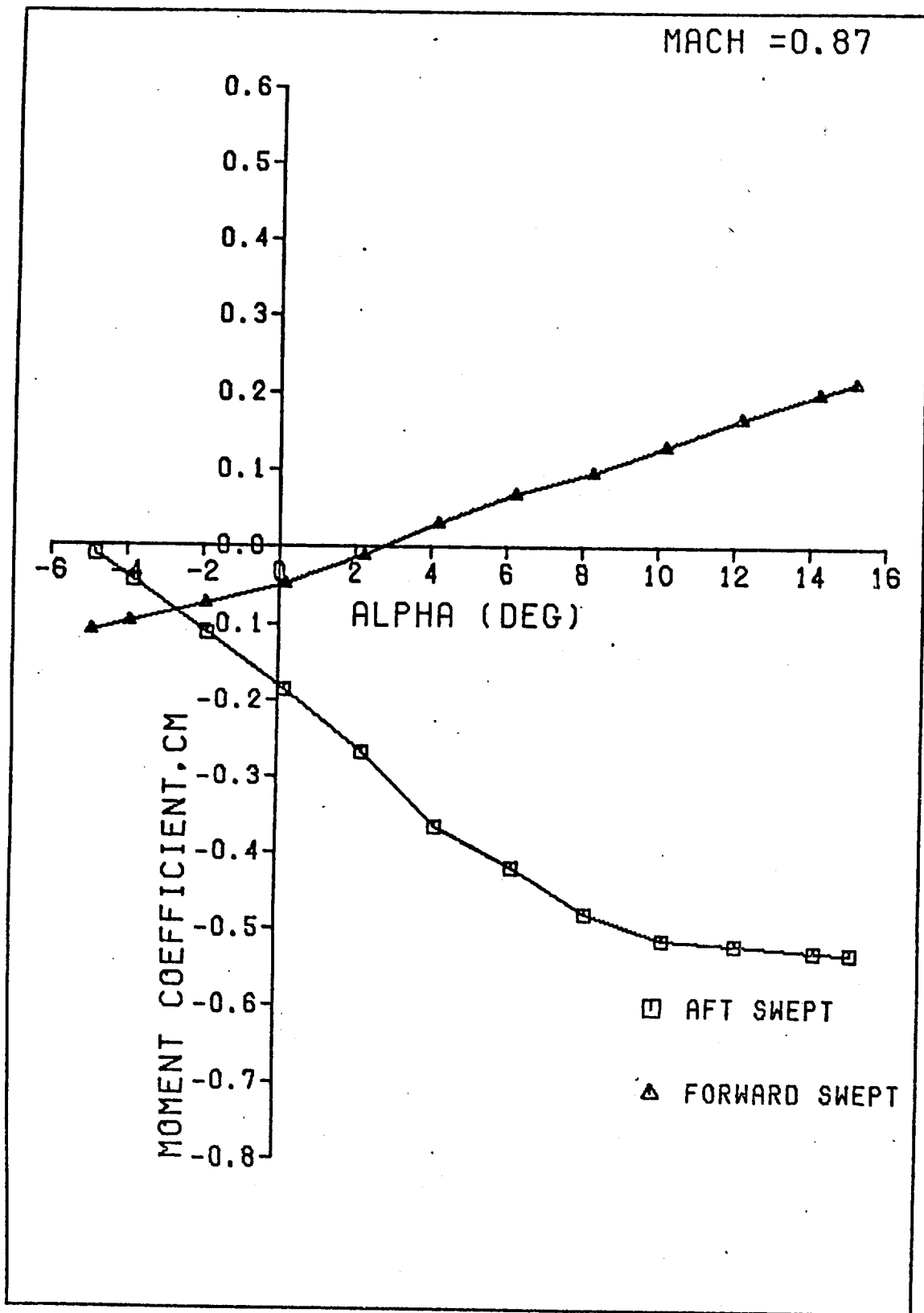


Figure 68.  $C_M$  vs  $\alpha$  for  $M = 0.87$

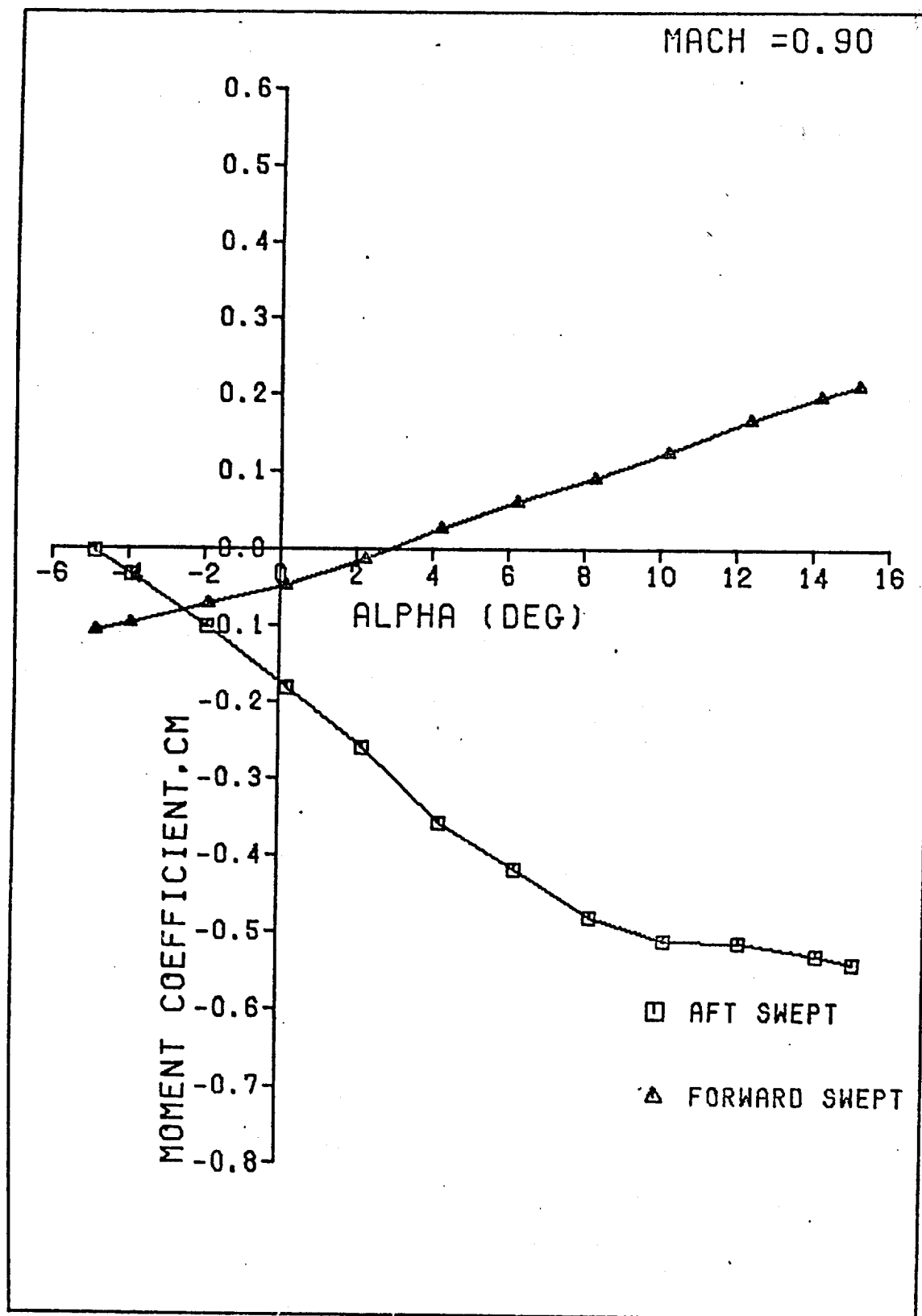


Figure 69.  $C_M$  vs  $\alpha$  for  $M = 0.9$



## VITA

Kenneth Lewis Sims was born in Birmingham, Alabama, in August, 1948. He graduated from the University of Alabama with a Bachelor of Science Degree in Aerospace Engineering in May, 1971. Upon completion of Undergraduate Pilot Training at Vance Air Force Base (AFB), Oklahoma, in May, 1972, he was assigned as a transport pilot at Charleston AFB, South Carolina. He progressed within three years to a crew commander and aircraft commander and during his last year of duty at Charleston AFB served as Squadron Operations Duty Officer. He entered the Air Force Institute of Technology in May, 1976.

Permanent Address: 2363 Rocky Ridge Road  
Birmingham, Alabama  
35216

This thesis typed by Mary H. Sims

UNCLASSIFIED

SECURITY CLASSIFICATION OF THIS PAGE (When Data Entered)

REPORT DOCUMENTATION PAGE		READ INSTRUCTIONS BEFORE COMPLETING FORM
1. REPORT NUMBER AFIT/GAE/AA/77D-14	2. GOVT ACCESSION NO.	3. RECIPIENT'S CATALOG NUMBER
4. TITLE (and Subtitle) AN AERODYNAMIC INVESTIGATION OF A FORWARD SWEEP WING		5. TYPE OF REPORT & PERIOD COVERED M.S. THESIS
		6. PERFORMING ORG. REPORT NUMBER
7. AUTHOR(s) KENNETH L. SIMS CAPTAIN USAF		8. CONTRACT OR GRANT NUMBER(s)
9. PERFORMING ORGANIZATION NAME AND ADDRESS AIR FORCE INSTITUTE OF TECHNOLOGY (AFIT/EN) WRIGHT-PATTERSON AFB, OHIO 45433		10. PROGRAM ELEMENT, PROJECT, TASK AREA & WORK UNIT NUMBERS Project 14760134
11. CONTROLLING OFFICE NAME AND ADDRESS AIR FORCE FLIGHT DYNAMICS LABORATORY (FXM) WRIGHT-PATTERSON AFB, OHIO 45433		12. REPORT DATE DECEMBER 1977
		13. NUMBER OF PAGES 112
14. MONITORING AGENCY NAME & ADDRESS (if different from Controlling Office)		15. SECURITY CLASS. (of this report) UNCLASSIFIED
		15a. DECLASSIFICATION/DOWNGRADING SCHEDULE
16. DISTRIBUTION STATEMENT (of this Report) Approved for public release; distribution unlimited.		
17. DISTRIBUTION STATEMENT (of the abstract entered in Block 20, if different from Report)		
18. SUPPLEMENTARY NOTES Approved for public release; IAW AFR 190-17  Jerral F. Guess, Captain USAF Director of Information		
19. KEY WORDS (Continue on reverse side if necessary and identify by block number) Swept Forward Wings Body-Wing Configurations Supercritical Wings Wind Tunnel Tests Woodward Unified Subsonic-Supersonic Aerodynamic Program		
20. ABSTRACT (Continue on reverse side if necessary and identify by block number) This study consisted of modeling and wind tunnel testing of a high speed, subsonic, low aspect ratio, forward swept wing with an advanced supercritical airfoil section for the purpose of determining its lift, drag, and pitching moment characteristics as compared to a similar aft swept wing. Tests were conducted at Mach numbers of 0.63 to 0.93 in the Air Force Flight Dynamics Laboratory's Trisomic Gasdynamic Facility located at Wright-Patterson Air Force Base, Ohio. Two wing configurations, forward		

DD FORM 1473 1 JAN 73 EDITION OF 1 NOV 65 IS OBSOLETE

UNCLASSIFIED  
SECURITY CLASSIFICATION OF THIS PAGE (When Data Entered)

UNCLASSIFIED

SECURITY CLASSIFICATION OF THIS PAGE(When Data Entered)

→ and aft swept, were tested and compared to computer predictions provided by the Unified Subsonic-Supersonic Program (Woodward's Version B). The results indicated that the forward swept wing was capable of higher useable angles of attack while maintaining a lower drag coefficient for angles of attack below eight degrees. Wind tunnel test results are presented in graphical and tabular form for use in future design studies of similar aerodynamic configurations. ↗

UNCLASSIFIED

SECURITY CLASSIFICATION OF THIS PAGE(When Data Entered)